



저작자표시-비영리-변경금지 2.0 대한민국

이용자는 아래의 조건을 따르는 경우에 한하여 자유롭게

- 이 저작물을 복제, 배포, 전송, 전시, 공연 및 방송할 수 있습니다.

다음과 같은 조건을 따라야 합니다:



저작자표시. 귀하는 원저작자를 표시하여야 합니다.



비영리. 귀하는 이 저작물을 영리 목적으로 이용할 수 없습니다.



변경금지. 귀하는 이 저작물을 개작, 변형 또는 가공할 수 없습니다.

- 귀하는, 이 저작물의 재이용이나 배포의 경우, 이 저작물에 적용된 이용허락조건을 명확하게 나타내어야 합니다.
- 저작권자로부터 별도의 허가를 받으면 이러한 조건들은 적용되지 않습니다.

저작권법에 따른 이용자의 권리는 위의 내용에 의하여 영향을 받지 않습니다.

이것은 [이용허락규약\(Legal Code\)](#)을 이해하기 쉽게 요약한 것입니다.

[Disclaimer](#)

공학박사학위논문

**데이터 기반 안전 영역 및
충돌 확률을 이용한 능동형 차로
변경 판단 및 제어 알고리즘 개발**

**Active Lane Change Decision and Control using
Data-driven Safety Boundary and
Collision Probability**

2021년 2월

서울대학교 대학원

기계항공공학부

채 홍 석

데이터 기반 안전 영역 및 충돌 확률을 이용한
능동형 차로 변경 판단 및 제어 알고리즘 개발

Active Lane Change Decision and Control using
Data-driven Safety Boundary and Collision Probability

지도교수 이 경 수

이 논문을 공학박사 학위논문으로 제출함

2020 년 10 월

서울대학교 대학원

기계항공공학부

채 홍 석

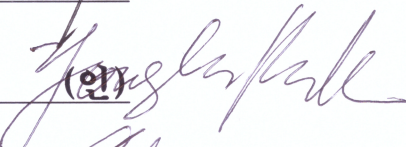
채홍석의 공학박사 학위논문을 인준함

2020 년 12 월

위 원 장 : 차 석 원 (인) 

부위원장 : 이 경 수 (인) 

위 원 : 이 동 준 (인) 

위 원 : 박 용 래 (인) 

위 원 : 유 송 민 (인) 

Abstract

Active Lane Change Decision and Control using Data-driven Safety Boundary and Collision Probability

CHAE Heungseok

Department of Mechanical and Aerospace Engineering

The Graduate School

Seoul National University

The traffic accidents caused by human error, such as distraction, drowsiness, or mistakes, account for 94 percent of all traffic accidents over last decades. Since safe driving is a goal of road-traffic-vehicle environments, major automakers develop driver assistance and active safety system. Recently, the majority of automotive makers have already commercialized active safety systems. Numerous kinds of research have attempted to integrate individual active safety systems for developing autonomous driving systems to enhance the safety and achieve zero fatalities. Moreover, in recent years, an interest of automotive industry is changed from the development of active safety to that of automated driving system capable of sensing surrounding environments and driving itself. Several projects have been conducted, and many others are still underway to evaluate the effects of automated driving in environmental, demographic, social, and economic aspects.

From a careful review of a considerable amount of literature, autonomous driving systems have been proven to increase the safety of traffic users, reduce traffic congestion, and improve driver convenience. Various methodologies have been employed to develop the core technology of autonomous vehicles, such as perception, motion planning, and control. However, the current state-of-the-art autonomous driving algorithms focus on the development of each

technology separately. Consequently, designing automated driving systems from an integrated perspective is not yet sufficiently considered.

This dissertation describes the design, implementation, and evaluation of an active lane change control algorithm for autonomous vehicles with human factor considerations. Lane changes need to be performed considering both driver acceptance and safety with surrounding vehicles. Therefore, autonomous driving systems need to be designed based on an analysis of human driving behavior. Based on the acquired driving data, safety indices are defined using rule based and learning based approaches. Also, collision probability has been employed to consider various uncertainties. A stochastic risk assessment-based lane change decision and control algorithm has been developed. The desired driving mode is decided to cope with all lane changes. To obtain desired reference and constraints, motion planning for lane changes has been designed taking driving data based safety indices into account. A stochastic MPC with constraints has been adopted to determine vehicle control inputs: the steering angle and the longitudinal acceleration. The proposed algorithm has been developed to implement the autonomous vehicle in consideration with diverse uncertainties, light calculation and sensor limitation.

The effectiveness of the proposed automated driving algorithm has been evaluated via test-data based simulations and vehicle tests. Diverse simulations have been proceeded to show performance improvement compared to other algorithms through monte-calro simulation. The proposed active lane change algorithm has been successfully implemented on an autonomous vehicle and evaluated via real-world driving tests. Safe and comfortable lane changes have been demonstrated using our autonomous test vehicle in diverse road environments.

Keywords: Autonomous driving vehicle, Human driving data, Stochastic prediction, Risk Assessment, Intention inference, Recurrent neural network, Decision-making, Lane change decision, Motion planning, Virtual vehicle, Model predictive control, Active lane change.

Student Number: 2015-20754

List of Figures

Figure 2.1. The overall structure of the autonomous driving system.	14
Figure 2.2. The overall structure of the autonomous driving system.	15
Figure 2.3. System overview of the proposed algorithm for autonomous driving system.	17
Figure 2.4. Configuration of sensors, controllers, and actuators for the first autonomous vehicle.	18
Figure 2.5. Configuration of sensors, controllers, and actuators for the second autonomous vehicle.	19
Figure 2.6. Configuration of sensors, controllers, and actuators for the third autonomous vehicle.	19
Figure 3.1. Overall architecture of stochastic motion prediction.	20
Figure 3.2. Moving object classification criteria in urban roads.	21
Figure 3.3. The results of the other two perception modules using LiDAR.	22
Figure 3.4. Moving object classification criteria in urban roads.	23
Figure 3.5. Moving object classification criteria in urban roads.	24
Figure 3.6. Perception range limitation.	26
Figure 3.7. A concept of virtual vehicles for safe motion planning in a lane change situation.	26
Figure 3.8. Diagram of the lateral dynamics model.	31
Figure 3.9. Architecture of stochastic prediction.	32
Figure 3.10. Uncertainty propagation as prediction step progresses.	33
Figure 3.11. Conceptual diagram of adaptive uncertainty propagation.	35
Figure 3.12. Concept of two prediction model.	38
Figure 3.13. Calculation time of EKF-based prediction model.	39
Figure 3.14. Calculation time comparison of data-driven models and EKF- based model.	39
Figure 4.1. Overall architecture of stochastic risk assessment.	41
Figure 4.2. Concept of safety distances.	42
Figure 4.3. Steady-state following data collected from 125 driver test data and the linear regression.	44
Figure 4.4. Highway Driving Data Acquisition Route.	47
Figure 4.5. Driving data in highway lane change situation.	48

Figure 4.6. Urban Driving Data Acquisition Route.....	50
Figure 4.7. Driving data in urban lane change situation.	51
Figure 4.8. The concept of the traffic pressure.....	56
Figure 4.9. Problems by constant parameters of lane change safety distance.	57
Figure 4.10. The acceleration in vehicle where no tendency is found.	59
Figure 4.11. Classification of yield & non-yield cases.....	60
Figure 4.12. Diagram of the proposed LSTM-RNN for yield intention inference.....	64
Figure 4.13. Variables for yield intention inference of lane change.....	65
Figure 4.14. Comparison of LSTM-RNN learning results for input set selection.	66
Figure 4.15. Unselected network candidates who have progressed learning.	67
Figure 4.16. The proposed network selection for yield intention inference...	68
Figure 4.17. The proposed network architecture for yield intention inference.	68
Figure 4.18. The lane change safety distance based on the yield intention....	70
Figure 4.19. Collision situation.	71
Figure 4.20. Procedure and concept of conventional collision probability. ...	73
Figure 4.21. Reachable set of ego vehicle.....	76
Figure 4.22. Reachable set of surrounding vehicles.....	77
Figure 4.23. Estimation examples of the proposed collision probability.	78
Figure 4.24. Conceptual diagram for estimated collision probability at each step in prediction horizon.....	78
Figure 5.1. Reasons of lane change.	80
Figure 5.2. Overall architecture of decision-making.....	81
Figure 5.3. Flow chart of driving mode decision for lane change.....	82
Figure 5.4. A Concept of lane change availability check.	83
Figure 5.5. Virtual vehicle creation on only available lane.	83
Figure 5.6. Space candidate for lane change based on safety distance.	84
Figure 5.7. Acceleration candidates of ego vehicle prediction for searching the lane change space.....	85
Figure 5.8. Concept of main path.	88
Figure 5.9. Overtaking situation.....	88
Figure 5.10. A concept of lane change possibility based on safety distance. .	92

Figure 5.11. Driving mode decision based on lane change possibility.....	94
Figure 5.12. Situations where the lane change is impossible in the MLC sections.....	95
Figure 6.1. Overall architecture of motion planning and control.	98
Figure 6.2. Reference and bound of longitudinal motion planning.....	99
Figure 6.3. Preceding vehicle in lane keeping driving.	100
Figure 6.4. Risky vehicles based on collision probability.	101
Figure 6.5. Overtaking is possible, but the ego vehicle is forever stopped..	103
Figure 6.6. Desired motion planning for side vehicles.....	104
Figure 6.7. Final motion planning based on driving mode and lane crossing.	106
Figure 6.8. Reference velocity in prediction horizon.	107
Figure 6.9. Lateral motion planning based on driving mode.	110
Figure 6.10. Lane change motion planning of lane change maneuver.	111
Figure 7.1. Configuration of multi-vehicle simulation tool.	116
Figure 7.2. Control response analysis.	118
Figure 7.3. Difficult situation to decide lane change demand.	121
Figure 7.4. Concept of supervised learning for overtaking decision.....	122
Figure 7.5. Two case about one episode.....	123
Figure 7.6. Schematic of supervised learning for overtaking decision.	124
Figure 7.7. Validation simulation initial vehicle disposition.....	125
Figure 7.8. Simulation results.	128
Figure 7.9. The initial condition of the simulation.	130
Figure 7.10. Simulation results.	132
Figure 7.11. The initial condition of the simulation.	133
Figure 7.12. One case in monte-carlo simulation.....	135
Figure 7.13. Comparison of base and proposed algorithms in monte-carlo simulation.....	137
Figure 7.14. Comparison of proactive and proposed algorithms in monte-carlo simulation.....	138
Figure 7.15. Simulation environment.....	139
Figure 7.16. Driving situation of one case among monte-calro simulation.	141
Figure 7.17. Results of one case among monte-calro simulation.....	142
Figure 7.18. Accumulated results of monte-calro simulation.	144

Figure 7.19. Initial conditions of lane change simulation in congested traffic.	145
Figure 7.20. Lateral position related with yield intention of side vehicles. .	146
Figure 7.21. Lane change completed time in congested traffic.....	148
Figure 7.22. Clearance between ego vehicle and rear vehicle when finishing lane change in congested traffic.	148
Figure 7.23. Three vehicles relation of test scenario.....	150
Figure 7.24. Four snap shots of each test scenarios.	153
Figure 7.25. Test results of scenario 3.....	155
Figure 7.26. Vehicle test environment.....	156
Figure 7.27. Snapshots in on-ramp (MLC).	161
Figure 7.28. Test results in on-ramp (MLC).....	163
Figure 7.29. Snapshots in off-ramp (MLC).....	164
Figure 7.30. Test results in off-ramp (MLC).....	166
Figure 7.31. Snapshots in general road section (DLC: overtaking).	167
Figure 7.32. Test results in general road section (DLC: overtaking).	169
Figure 7.33. Vehicle test results: cumulative test data.....	172
Figure 7.34. Vehicle test environment.....	173
Figure 7.35. Vehicle test snapshots: the selected one overtaking situation. .	175
Figure 7.36. Vehicle test results: the selected one overtaking situation.	178
Figure 7.37. Vehicle test results: cumulative test data.....	180
Figure 7.38. Vehicle test environment.....	181
Figure 7.39. High definition map of autonomous driving test bed in Seoul.	182
Figure 7.40. Complex urban road which is vehicle test environment.	183
Figure 7.41. All path and main path on the high definition map.....	183
Figure 7.42. Vehicle test snapshots: the MLC situation.	187
Figure 7.43. Vehicle test results: the MLC situation.	189
Figure 7.44. Vehicle test snapshots: the DLC situation.....	190
Figure 7.45. Vehicle test results: the DLC situation.....	192
Figure 7.46. Test bed for autonomous vehicles at Siheung Campus, Seoul National University.	193
Figure 7.47. Interactive lane change vehicle test environment.	194
Figure 7.48. Two situation of interactive lane change vehicle test.....	195
Figure 7.49. Vehicle test snapshots: the first situation.	197

Figure 7.50. Vehicle test results: the first situation.	199
Figure 7.51. Vehicle test snapshots: the second situation.....	201
Figure 7.52. Vehicle test results: the second situation.....	203

Contents

Chapter 1 Introduction	1
1.1. Background and Motivation	1
1.2. Previous Researches	4
1.3. Thesis Objectives	8
1.4. Thesis Outline	12
Chapter 2 Overview of Autonomous Driving System	14
Chapter 3 Stochastic Motion Prediction	20
3.1. Vehicle Classification.....	21
3.2. Virtual Vehicle Generation for Perception Limit	25
3.3. Vehicle Model	28
3.4. Prediction Model.....	32
3.4.1. Prediction of ego vehicle.....	34
3.4.2. Prediction of surrounding vehicle	36
Chapter 4 Stochastic Risk Assessment.....	40
4.1. Safety Distance based on Human Driving Data	42
4.1.1. Lane Keeping Safety Distance based on Driving Data	43
4.1.2. Lane Change Safety Distance based on Highway Driving Data	45
4.1.3. Lane Change Safety Distance based on Urban Driving Data	50
4.1.4. Kinematic Analysis of Lane Change Safety Distance and Stochastic Prediction based Safety Distance	53
4.2. Lane Change Yield Inference using LSTM-based RNN	55
4.2.1. Dataset Selection	60
4.2.2. Network Architecture	62

4.2.3. Yield Intention Inference based Safety Distance	69
4.3. Collision Probability based on Stochastic Particle	71
4.3.1. Conventional Collision Probability	72
4.3.2. Proposed Collision Probability to select target for safety control.....	75
Chapter 5 Decision-Making	80
5.1. Lane Change Availability Check and Target Space Decision .	83
5.2. Lane Change Demand Check.....	87
5.3. Lane Change Possibility Check and Traffic Pressure Mode for Interactive Lane Change.....	92
5.4. Limit Mode Decision by Road End	95
Chapter 6 Motion Planning and Control	98
6.1. Longitudinal Motion Planning and Control.....	99
6.2. Lateral Motion Planning and Control	109
Chapter 7 Performance Evaluation	115
7.1. Simulation Test	115
7.1.1. Simulation Environment.....	116
7.1.2. Overtaking simulation for decision-making evaluation .	119
7.1.3. Overtaking simulation to evaluate the effectiveness of virtual vehicle.....	129
7.1.4. Simulation about cut-in vehicle safety to evaluate the stochastic risk assessment and the predictive control.....	133
7.1.5. Merging simulation in on-ramp to evaluate MLC.....	139
7.1.6. Interactive lane change simulation in congested traffic to evaluate the yield intention inference.....	145
7.2. Vehicle Test	149
7.2.1. Self-directed Test using First Vehicle Platform	150

7.2.2. Highway DLC and MLC Test using First Vehicle Platform	156
7.2.3. Highway Overtaking Test for DLC using Second Vehicle Platform.....	173
7.2.4. Urban DLC and MLC Test using Third Vehicle Platform	181
7.2.5. Self-directed Interactive Lane Change Test using Second Vehicle Platform	193
Chapter 8 Conclusion & Future Works	204
8.1. Conclusion	204
8.2. Future Works.....	207
Bibliography.....	208
Abstract in Korean	217

Chapter 1 Introduction

1.1. Background and Motivation

According to a report from Volvo Cars, nearly 90% of accidents occur due to human error [Trucks,'13]. Particularly, many traffic accidents have occurred with the increase of the traffic participants on the roads. Of all traffic accidents, 85.2% of traffic accidents have been caused by human factors [KOSIS,'18]. The human factors that affect the traffic accidents are inattention, inexperience, old age, drowsiness, overestimation of capabilities, speeding, or indecent driving behavior. [Petridou,'00]. Especially, lane change maneuvers have resulted in various vehicle accidents due to inaccurate perception of surrounding environments, neglectful driving, or illegal maneuvers. Currently, automakers consider autonomous driving as a mainstream entity, because it helps to improve safety, comfort, and convenience [Eskandarian,'12]. The development of autonomous driving has been spurred by improvements in sensors, actuators, processors, communications, and other technologies for autonomous vehicles.

Recently, the interests of automotive researches have been expanding from passive safety systems to active safety systems with advances in sensing and processing technologies. Recently, the majority of automotive makers have already commercialized active safety systems, such as Adaptive Cruise Control (ACC), Lane Keeping Assist System (LKAS), Lane Change Assist (LCA),

Forward Collision Mitigation (FCM), Automated Parking Assist (APA) and Blind Spot Intervention (BSI). Numerous kinds of research have attempted to integrate individual active safety systems for developing autonomous driving systems to enhance the safety and achieve zero fatalities [Bishop,'00].

A number of projects have been and are ongoing to evaluate the effects of autonomous driving in environmental, demographic, social, and economic aspects. For example, the European project “AdaptIVe,” which comprises a consortium of 29 partners, develops various automated driving functions and defines specific evaluation methodologies. This project demonstrates autonomous driving in a complex traffic environment which considers the full range of automation levels from 0 to 4 [Etemad,'17]. In addition, “CityMobil2” successfully integrates driverless intelligent vehicles in nine other environments throughout Europe. However, this project used separate roads that prohibit the entrance of other vehicles [Alessandrini,'14]. In Japan, the “Automated Driving System Research Project” began on May 2014, which focuses on the development and verification of autonomous driving systems and next-generation urban transport [Yamamoto,'15].

From a careful review of a considerable amount of extant literature, autonomous driving systems have been proven to increase the safety of traffic users, reduce traffic congestion, and improve driver convenience. Various methodologies have been employed to develop the core technology of autonomous driving, such as localization, perception, motion planning, and control. However, the current state-of-the-art autonomous driving algorithms focus on the development of each technology separately. Consequently,

designing autonomous driving systems from an integrated perspective is not yet sufficiently considered.

Autonomous driving systems should be acceptable to drivers and passengers. Therefore, these systems need to be similar to the normal driving operation of human drivers [Okuda,'14, Van Waterschoot,'09, Lindgren,'06]. In lane change driving, the ego vehicle characteristic has already been studied extensively. The ego vehicle means the vehicle which the autonomous driving system is applied to. Surrounding vehicles mean the every vehicles except the ego vehicle. Lane change trajectory prediction models have been described using human databases [Yao,'13, Nishiwaki,'08]. Acceleration and jerk used for lane changes were presented in some literature [Wan,'11, Toledo,'03, Ahmed,'99]. Lane change time was researched in some studies [Toledo,'07b, Finnegan,'90]. In addition to the ego vehicle characteristic, the relationship with the surrounding vehicles is so important in lane changes. This is because the lane change is the interactive task with an ego vehicle and surrounding vehicles.

Therefore, we focus on developing autonomous driving systems from an integrated perspective. Also, we focus on designing autonomous driving systems to be acceptable to drivers and passengers based on human driving data. The proposed motion planning and control algorithm is compatible with various localization and perception modules, while considering the driver's driving characteristics. This methodology realizes autonomous driving in diverse road environments.

1.2. Previous Researches

An autonomous vehicle is an integrated system consisting of five categories: localization, perception, decision-making, motion planning, and control [Suganuma,'12, Suganuma,'14]. Among these categories, this study focuses on decision-making, motion planning, and control for active lane change maneuver. In addition to the categories, prediction module is needed. As this study aims to implement autonomous driving based on driver data, it is also important to study driving data in a lane change situation. In conclusion, previous studies have been investigated on the following items: lane change driving data, prediction, decision-making, motion planning and control.

Several previous studies analyzed and utilized driver characteristics of the relationship with surrounding vehicles for lane change driving. A lane change assist system has been presented that selects three simple driving modes based on driver data and grid maps [Do,'17]. A lane change model has been proposed considering gaps between vehicles above a target lane for lane change [Butakov,'15]. Learning-based models were used in both studies. Such models could be accurate, flexible, and adjustable if properly trained with accurate data. However, these models might lack intuitive meaning or physical meaning for their parameters, Moreover, since models cannot be rebuilt without data, these models are difficult to actually use in other studies.

Actual drivers usually drive in anticipation of the near future. Diverse prediction methods have been utilized for autonomous driving applications. A

prediction model has been presented based on a fuzzy rule and finite-state machines [Hülnhagen,'10]. Vehicle trajectory has been predicted by building various situation models [Otto,'12]. Because deterministic prediction methods have limits, probabilistic prediction methods have been developed to augment robustness [Althoff,'09, Kim,'14]. Also, advanced probabilistic prediction algorithms have been devised utilizing data-driven approaches. Inverse reinforcement learning has been employed to predict interactive motions considering discrete and continuous driving decisions [Sun,'18]. The multi-modal probabilistic model could consider behavior intention based on deep neural networks [Hu,'19]. Long short-term memory-based recurrent neural networks have been utilized for interactive prediction in multi-lane turn intersections [Jeong,'20a]. Data-driven probabilistic prediction models considering interactive behavior are powerful in complex situations, such as ramp-merging, roundabout, and multi-lane turn intersections.

A variety of research has attempted to solve the lane change decision-making problem. For lane change decision problems, fuzzy logic has been utilized [Naranjo,'08, Perez,'11, Basjaruddin,'15]. Fuzzy logic has the merit of considering various aspects of lane change maneuver. However, these studies have only considered the ideal situation, where the surrounding vehicles are at a constant speed. Also, these studies have solved the problem of lane change only one vehicle. Reinforcement learning has been employed to plan lane change maneuvers [Ngai,'11, Li,'15]. The algorithm has been trained on the lane change problem through repeated simulation. The learned algorithm has shown

good lane change performance. However, it is only verified by simulation, and the approach lacks verification of generality and safety.

For the active lane change model, the various behaviors of the ego vehicle and surrounding vehicles should be considered. The motion planning algorithms for the active lane change have been researched in previous studies. Deterministic approaches have been utilized by formulating optimization problems [Shiller,'98, Feng,'06, Ferguson,'08, McNaughton,'11]. The approaches are simple and efficient, but could not consider diverse uncertainties which occur in lane change situations. A Markov Decision Process (MDP) and a Partially Observable Markov Decision Process (POMDP) have been employed to plan an optimal lane change policy [Brechtel,'11, Ulbrich,'13, Ulbrich,'15]. MDP and POMDP are able to cope with uncertain system behaviors. However, these methods have problems in implementing the vehicle due to heavy computation loads.

A model predictive control (MPC) framework constitutes an attractive method and is extensively used for autonomous driving. The MPC method employs a dynamic vehicle model to predict future states, and calculates an optimal control input trajectory sequence for tracking state reference while satisfying constraints [Mayne,'00, Anderson,'10]. MPC has been utilized for an active steering controller [Falcone,'07]. For an autonomous vehicle control algorithm, a robust MPC has been used which is more robust, but possesses the weakness of being too conservative [Mayne,'05]. A lane change assistance system has been presented utilizing a scenario MPC [Schildbach,'15]. Although the scenario MPC complements shortcomings of robust MPC, all scenarios are

difficult to consider. It necessitates vast amounts of data. A stochastic MPC (SMPC) has been described based on the chance-constraints optimization problem for autonomous driving [Gray,'13]. Previous studies have verified an autonomous driving algorithm adopting SMPC in only simulation and simple vehicle tests [Gray,'13, Suh,'18].

In most of these researches for motion planning of autonomous driving, the current state-of-the-art autonomous driving algorithms focused on the development of each function separately. In other words, the previous researches developed the prediction, decision-making, motion planning, and control, respectively, rather than the integrated perspective of considering the interdependence between each function.

Therefore, in this research, we focus on developing a motion planning algorithm for autonomous vehicle in diverse lane change environment based on stochastic risk assessment with vehicle motion prediction, motion planner with driving mode decision and model predictive control.

1.3. Thesis Objectives

From a careful review of a considerable amount of extant literature, autonomous driving systems have been proven to increase the safety of traffic users, reduce traffic congestion, and improve driver convenience. Therefore, we focus on developing a motion planning algorithm for autonomous lane change control, while considering the driver's driving characteristics. In other words, the proposed algorithm predicts the behavior of traffic participants, assesses collision risk, plans and controls the motion like human drivers. This approach improves safety by considering the driver acceptance based on human driving data.

This study aims the lane change algorithm with driver acceptance. Driving data in lane change situations were examined for driver acceptance. The driving data-based risk assessment have been developed with kinematic analysis about safety performance. Both rule based and learning based approaches were used for risk assessment. By inferring lane change yield intention of surrounding vehicles, a more human-like risk assessment has been conducted. To improve safety within near future, stochastic predictions are employed with considering sensor noise, model uncertainty and prediction uncertainty. In particular, the lane change is greatly affected by the changing states between the vehicles. To reflect this characteristic, the stochastic prediction-based risk assessment are proposed by the stochastic predictions and the risk assessment. The risk assessment is time-varying by states of vehicles. The decision and the motion

planning are conducted based on the stochastic prediction-based risk assessment. These have the advantage of efficiency in calculation.

In this dissertation, we argue that it is crucial to pursue vehicle implementation as well as lane change performance. For vehicle implementation, it is important to consider efficient calculation and limitation of the vehicle. We propose efficient decision-making and motion planning based on stochastic prediction and risk assessment. To improve safety within the near future, stochastic predictions are employed that consider sensor noise, model uncertainty, and prediction uncertainty. An extended Kalman filter (EKF) based probabilistic model is adopted in this dissertation. Learning-based probabilistic models show a powerful prediction performance. However, data-driven prediction models require heavier computation than the EKF-based model. Also, it is efficient to train on the data of the perception module that is actually used. Additionally, learning-based prediction techniques generally need historical information. This approach is vulnerable to effects such as object emergence, object disappearance, and false alarm, which frequently occur in perception modules of actual autonomous vehicles. A particle filter-based generic vehicle tracking framework could solve this problem [Li,'18]. However, this framework adds additional computation and needs to be tuned for the perception module to be used in this study. Since the target environment in this study is a simpler overtaking situation than ramp-merging, roundabouts, and intersections, the EKF-based prediction model was adopted in consideration of the trade-off relationship between calculation load and performance.

Because all vehicles cannot be equipped with vehicle to vehicle (V2V) communications at present, autonomous vehicles should perceive the surrounding environment based on local sensors. Social perception has been devised to deal with local sensor limits [Afolabi,'18, Sun,'19]. The perceived vehicle information could be used to infer the area beyond the blind spot or sensor limit. This approach enables rational behavior planning by inferring targets beyond perceived vehicles. It is powerful, especially in environments such as intersections and crosswalks. However, a vehicle that suddenly emerges outside the perception range is important in an overtaking situation. Also, inference for each perceived vehicle increases the calculation load, and social perception is affected by issues of the perception module. Therefore, a more efficient and feasible approach is required for the overtaking problem. In this dissertation, virtual targets are devised to cope with the limitation of cognitive range. The concept of a “virtual target” has been used as a virtual preceding vehicle for path following [Bibuli,'10, Rucco,'15]. This concept is adopted to solve the lane change problem in this study. Virtual targets are very efficient for vehicle implementation. Virtual targets do not burden the computation and are not affected by perception module issues.

In this dissertation, we present the autonomous lane change algorithm containing prediction, risk assessment, decision-making, motion planning, and control modules. This study deals with issues for vehicle implementation such as cognitive range and computation load than existing relevant works. The main contribution of this study is to develop a simple, but performance guaranteed and feasible lane change algorithm. In the decision-making part, driving mode

and target space are determined for the lane change. The decision-making part is divided into three stages: availability, demand, and possibility of lane change. According to the driving mode, the appropriate motion is planned based on perceived vehicles and virtual targets. The SMPC calculates control input for tracking the desired motion. The proposed algorithm could achieve driver acceptance, efficient calculations, overcoming of perception limit, and consideration of diverse uncertainties. The performance of the proposed system has been investigated repeatedly through real-world driving tests in diverse lane change situations. The proposed algorithm is compared with the base algorithm through simulation. And, the performance of the proposed system has been investigated repeatedly through real-world driving tests.

1.4. Thesis Outline

This dissertation is structured in the following manner. Overall architecture of the proposed motion planning algorithm for urban autonomous driving is described in Chapter 2. In Chapter 3, a stochastic motion prediction algorithm is introduced. The vehicle motions for ego vehicle and surrounding vehicles are predicted based on model predictive control framework and rule based approach. The prediction is advantageous for vehicle implementation due to calculation efficiency. Virtual vehicles are adopted to overcome perception limitation. Safety performance has been improved by reflecting various uncertainties. In Chapter 4, stochastic risk assessment is introduced based on prediction. Safety distance and collision probability are derived to assess risk. The safety distance is derived based on human driving data. The model-based and learning-based approaches are employed to make safety distance for driver acceptance. By inferring lane change yield intention of surrounding vehicles, a more human-like safety distance has been devised. Collision probability has been used to assess risk for diverse uncertainties. In Chapter 5, decision-making is introduced. Driving mode decision has been proposed that the autonomous vehicle can cope with the various lane change situations. In Chapter 6, motion planning and control is introduced. Proper motions are planned for active lane change and interactive lane change based on driving mode. Stochastic model predictive controllers are tracking desired motion with vehicle model and constraints. Chapter 7 shows performance evaluation which is composed of the

simulation test and vehicle test. The performance and effectiveness of the proposed algorithm has been showed through diverse simulation tests. Comparisons with other algorithms show the performance improvement of the proposed algorithm. Vehicle tests have been conducted in various environments. Therefore, the vehicle implementation represents feasible, repetitive and stable performance of the proposed algorithm. Then, the conclusion, which includes the summary and contribution of the proposed algorithm, and future works, is presented in Chapter 8.

Chapter 2 Overview of Autonomous Driving System

The autonomous driving is integrated system from multiple modules. Multiple modules can be broadly classified into four modules: localization, perception, planning, and control [Suganuma,'12, Suganuma,'14]. The overall structure of the autonomous driving system is described in Figure 2.1, which represents the description of each module. It is important to develop a module that is compatible with other modules.

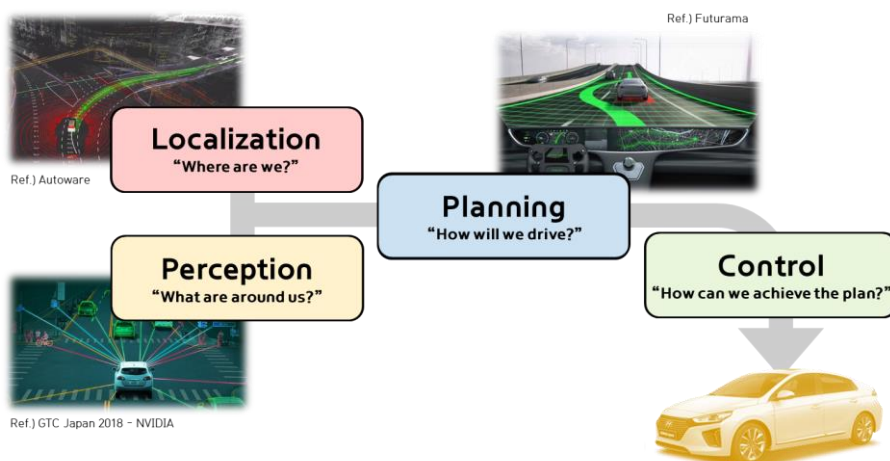


Figure 2.1. The overall structure of the autonomous driving system.

Each module has the following features as described in Figure 2.2. First, diverse sensor information comes in as input to the autonomous driving system.

These information is first processed in localization and perception modules, which are optimized for sensor configuration. Then, planning module, which determines how to drive, is optimized for target driving environment. Finally, control module, which determines final control inputs of the vehicle, is optimized for vehicle configuration.

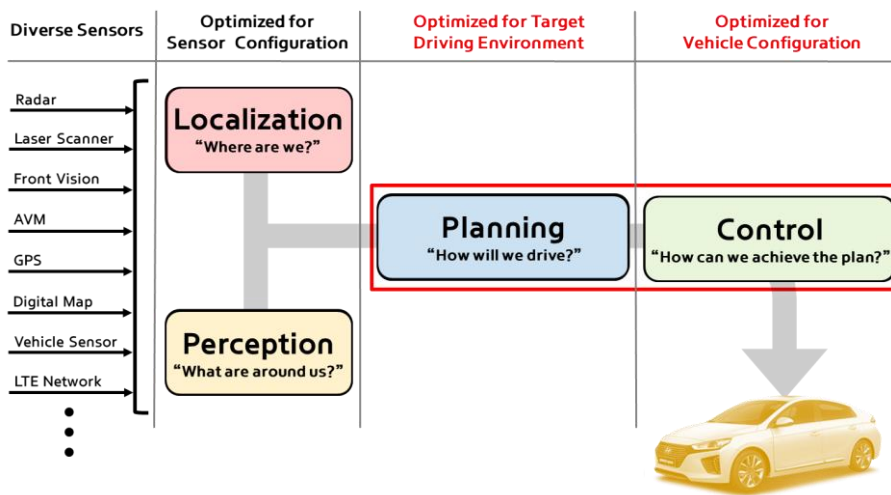


Figure 2.2. The overall structure of the autonomous driving system.

In this research, we focus on developing planning and control modules for autonomous driving. This is the red box in Figure 2.2. The overall architecture of the proposed algorithm is described in Figure 2.3, which has a 4-layers, stochastic prediction, risk assessment, decision-making, and motion planning & motion control. The proposed algorithm uses information from upper modules: localization and perception. Upper modules uses information from equipped various sensors. Localization module provides states of the ego

vehicle including the current position on the map. Perception module provides states of static and dynamic obstacles located in the vicinity of the ego vehicle. The proposed algorithm is compatible with alteration of upper modules.

The first layer of the proposed algorithm is stochastic prediction, which predicts future states of ego vehicle and surrounding vehicles. Static and dynamic obstacles are classified as surrounding vehicles. And virtual vehicles are created considering the perception limit in the local sensor. Then, considering diverse uncertainties, the future behavior of the ego vehicle and surrounding vehicles is predicted. Uncertainties are caused by diverse factors such as model uncertainty, sensor noise, actuator delay, localization uncertainty and perception uncertainty. The second layer of the proposed algorithm is risk assessment, which evaluates the collision risk between ego vehicle and surrounding vehicles using predicted states of vehicles. To consider driver acceptance, lane change yield intention and safety distance based on human driving data have been developed. In addition, collision probability has been developed to reflect the potential risk posed by various uncertainties. The third layer of the proposed algorithm is decision-making, which decides whether to perform lane keeping or lane change. The driving mode is determined in consideration of surrounding vehicles and the road environment. In addition, space for lane change is also explored. This makes active lane change possible. The last layer of the proposed algorithm is motion planning and motion control, which plan the desired motion of the ego vehicle and determine the final control input to track desired motion. It is divided into longitudinal and lateral motions. The final control input for longitudinal motion is longitudinal acceleration. The

final control input for lateral motion is steering angle.

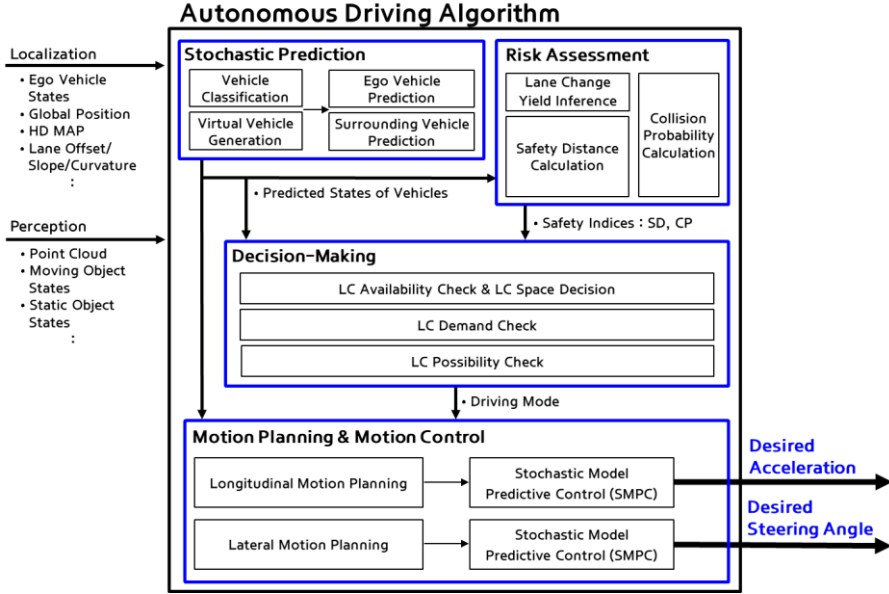


Figure 2.3. System overview of the proposed algorithm for autonomous driving system.

Since the proposed algorithm is compatible with the alternation of upper modules, it has been implemented with several vehicles equipped with diverse sensor configurations. In this dissertation, the proposed algorithm is applied to three vehicles with different upper modules. The first implemented vehicles are shown in Figure 2.4. In this vehicle, commercial differential GPS/INS platform is used for localization module. 2D LiDAR and radar sensor fusion is employed for perception module [Lee,'19]. The second implemented vehicles are shown in Figure 2.5. In this vehicle, AVM and vision cameras form is used for

localization module [Kim,'16]. Commercial LiDAR processor is employed for perception module. The third implemented vehicles are shown in Figure 2.6. In this vehicle, commercial differential GPS/INS platform is used for localization module. Geometric model-free approach is employed for perception module [Lee,'20].

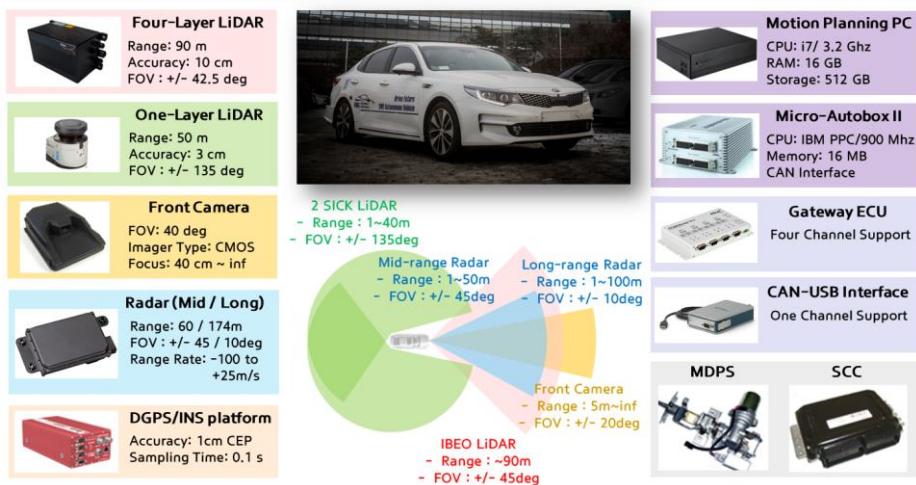


Figure 2.4. Configuration of sensors, controllers, and actuators for the first autonomous vehicle.



Figure 2.5. Configuration of sensors, controllers, and actuators for the second autonomous vehicle.

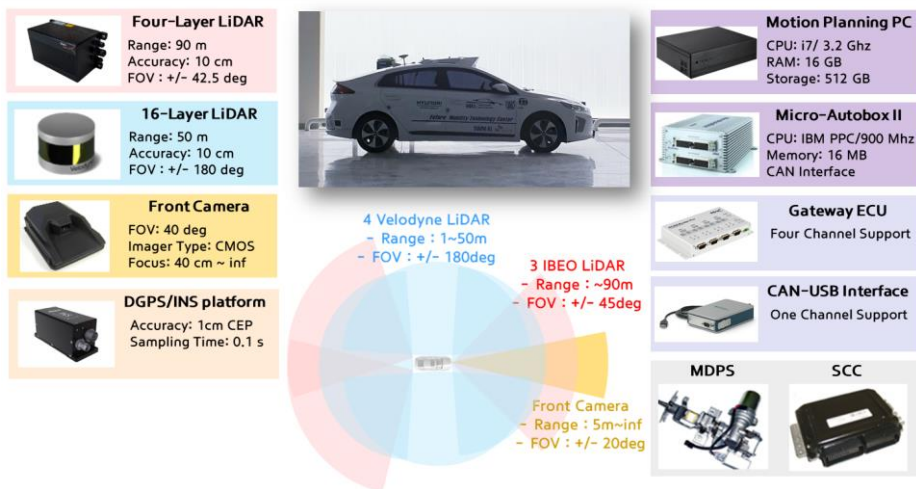


Figure 2.6. Configuration of sensors, controllers, and actuators for the third autonomous vehicle.

Chapter 3 Stochastic Motion Prediction

The prediction is commonly used in autonomous driving, because autonomous vehicles operate in a reciprocal manner with the surrounding environment. The prediction is especially important because the lane change is greatly influenced by the changing states between the vehicles. In this chapter, a vehicle and a prediction model are introduced concerning both the ego vehicle and the surrounding vehicle. Prior to prediction, it is necessary to classify vehicles. Then, virtual vehicles are created to correspond to the sensor limit. Figure 3.1 shows the overall architecture of stochastic motion prediction.

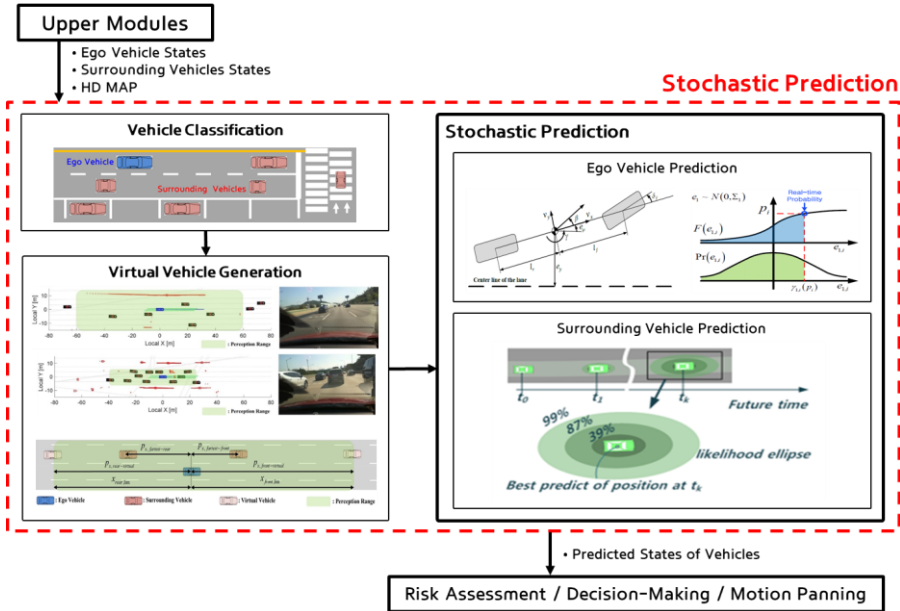


Figure 3.1. Overall architecture of stochastic motion prediction.

3.1. Vehicle Classification

Before prediction, classification of surrounding vehicles is necessary. There are various traffic participant on road. On highways, there are usually vehicle and obstacle. In urban roads, there are more various traffic participant such as vehicle, cyclist, pedestrian, motorcycle and obstacle. Figure 3.2 shows various traffic participant in urban roads.

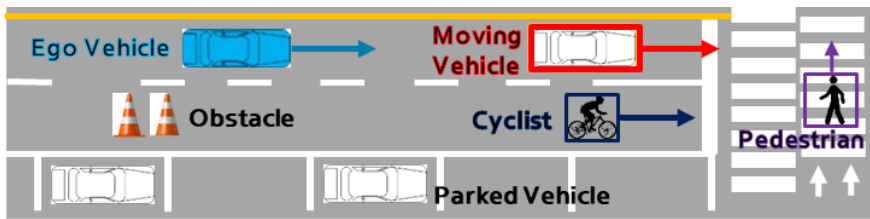
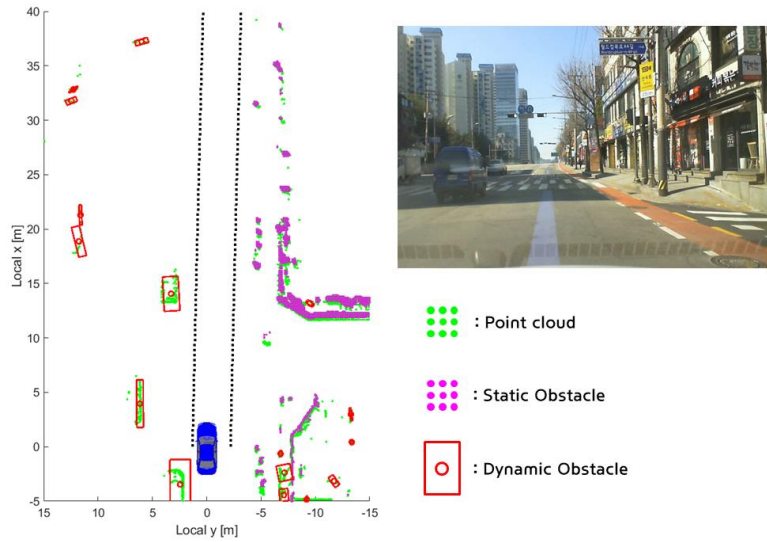


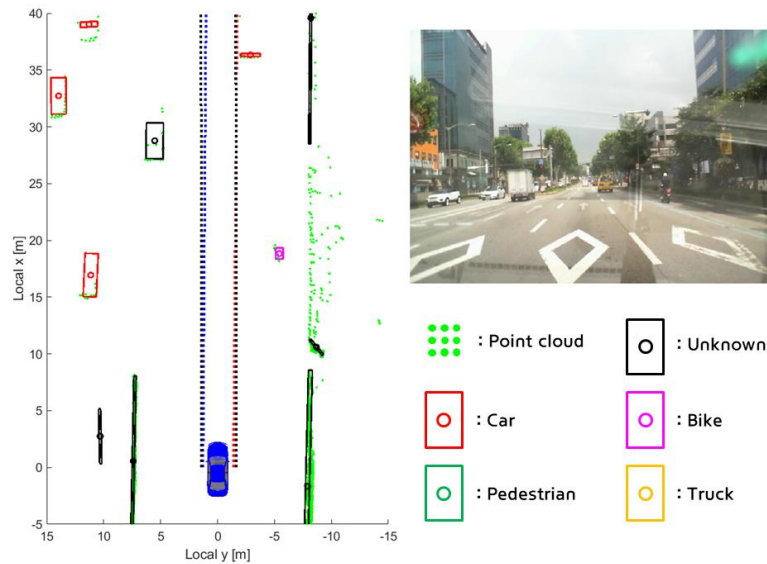
Figure 3.2. Moving object classification criteria in urban roads.

Basically, the perception modules essentially give the states of the surrounding vehicles (relative position, speed, heading, etc.). However, various perception modules have different reliability of each state according to the sensor and the perception module. In addition, perception modules have different classification level of various traffic participant. The results of the other two perception modules are shown in Figure 3.3. Both perception modules use only LiDAR sensors. The former distinguishes between static and dynamic obstacles [Lee,'20]. While the latter classifies objects in detail. However, since the latter uses only LiDAR, not vision, the ability to classify

objects is limited [Gao,'18].



(a) Geometric model-free approach



(b) Commercial LiDAR processor

Figure 3.3. The results of the other two perception modules using LiDAR.

In this research, all obstacles are considered surrounding vehicles as shown Figure 3.4. This approach makes the proposed algorithm compatible with various perception modules. In addition, the overall structure of the algorithm is simplified. It also reduces the computational burden. However, this approach is problematic because it considers non-vehicle objects, as vehicles. In particular, the prediction of cyclist, motorcycle and pedestrian is incorrect. The main issue in this study is lane keeping and lane change so the problem was excluded.

In this way, the proposed algorithm considers all traffic participants as surrounding vehicles. The information required for the proposed algorithm is the states of surrounding vehicle and the space it occupies. States are essential for prediction of surrounding vehicles. The occupied space is employed to define the safety envelope to prevent collision.

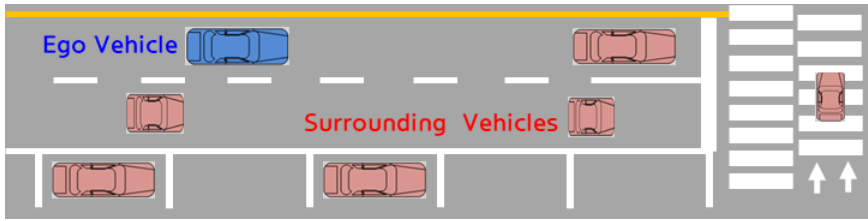


Figure 3.4. Moving object classification criteria in urban roads.

In order to perform lane keeping and lane change, the surrounding vehicles could be divided into three categories: in-lane, left lane and right lane. The proposed algorithm performs target selection using a high-definition map and absolute position of ego vehicle. Relative position of surrounding vehicles are

transformed to absolute position by coordinate transformation on the basis of the absolute position of the ego vehicle, which is provided by the localization module. Based on the high-definition map, the surrounding vehicles are classified into three categories as shown in Figure 3.5. We make predictions with interest only for vehicles in three categories, which helps to reduce the calculation time. In particular, it has a great effect on perception modules with many false positive detections.

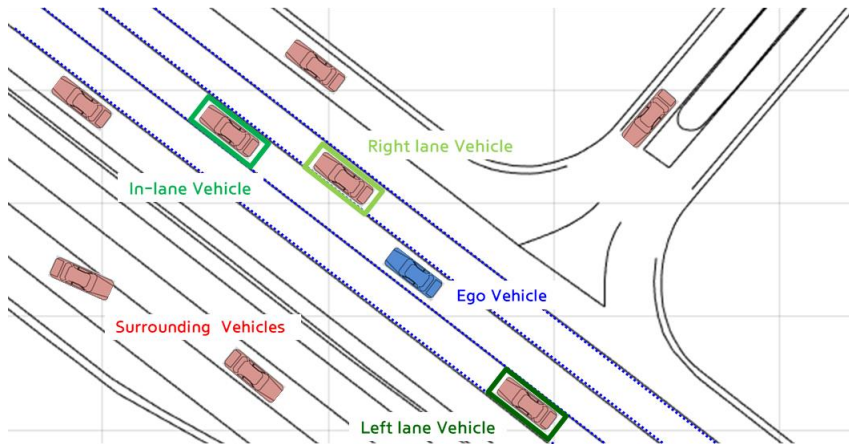
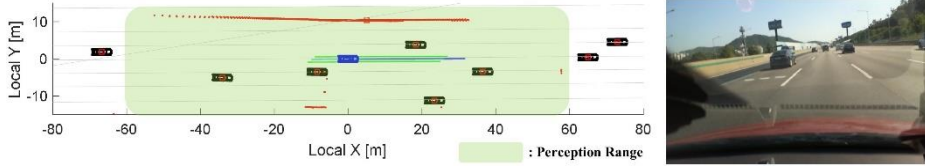


Figure 3.5. Moving object classification criteria in urban roads.

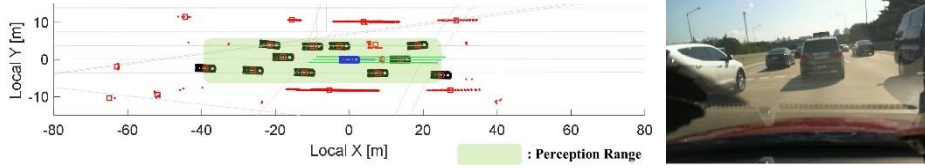
3.2. Virtual Vehicle Generation for Perception Limit

Since the current road is a mixed environment of normal vehicles and autonomous vehicles, all vehicles cannot be equipped with V2V. Therefore, autonomous vehicles perceive the surrounding environment based on local sensors. Inevitably, autonomous vehicles have a cognitive range limit. The perception range is influenced by blind spots as well as the sensor limits.

Subject to perception limit analysis is the vehicle equipped with the best perception module among the three vehicles presented in Chapter 2. The cognitive range of limitations for two reasons is shown in Figure 3.6. An autonomous vehicle recognized the surrounding environment. The autonomous vehicle was equipped with six 2D-LiDARs and a LiDAR processor. The blue vehicle is an autonomous vehicle. Red points represent point clouds measured by LiDAR sensors. Red vehicles represent the surrounding vehicles recognized by the LiDAR processor. Although the point clouds of a vehicle 60 m ahead were detected, the perception module did not identify the vehicle in Figure 3.6. (a). Therefore, the limit of the perception module to stably recognize vehicles was 60 m. Figure 3.6.(b) shows a situation in which the perception module cannot detect vehicles closer than 60 m. This is because of the blind spot caused by congested traffic.



(a) Reason 1: Sensor limit.



(b) Reason 2: Blind spot in congested traffic.

Figure 3.6. Perception range limitation.

In lane change situations, interactions with side vehicles are important. When the ego vehicle conducts lane change, side vehicles might suddenly appear from outside of the perception range. In this study, the concept of virtual targets has been developed to cope with the limitation of cognitive range. The concept of virtual targets is shown in Figure 3.7. Since it is assumed that vehicles always exist at the perception limit, the virtual target can conduct decision-making and motion planning, considering the perception limit.

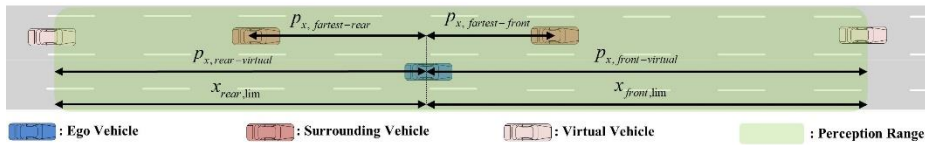


Figure 3.7. A concept of virtual vehicles for safe motion planning in a lane change situation.

In the case of the open space, virtual targets are located on the sensor limit. In congested traffic, the virtual targets are located in front of and behind the recognized vehicles at the farthest distance. The velocity of the ego vehicle is used as a condition for distinguishing two cases. The threshold velocity is designed assuming that the vehicles travel with the general time gap (τ_k) in the recognition range [Moon,'08]. The threshold velocity is as follows:

$$v_{vir,th} = (x_{rlim} + x_{flim}) / \tau_k \quad (3.1)$$

where subscript vir,th is the threshold for distinguishing the two cases; the subscript $rlim$ is the limit of rear sensor range (-60 m); and the subscript $flim$ is the limit of front sensor range (60 m).

The position of virtual targets is decided in two cases and is as follows:

$$x_{rvir} = \begin{cases} x_{rlim} & \text{if } v_e > v_{vir,th} \\ x_{rear} & \text{otherwise} \end{cases} \quad (3.2)$$

$$\text{s.t. } x_{rear} = \max[x_{rlim}, x_{rst} - \tau_k \cdot v_e]$$

$$x_{fvir} = \begin{cases} x_{flim} & \text{if } v_e > v_{vir,th} \\ x_{front} & \text{otherwise} \end{cases} \quad (3.3)$$

$$\text{s.t. } x_{front} = \max[x_{flim}, x_{fst} + \tau_k \cdot v_e]$$

where t represents the current time; subscript $rvir$ and $fvir$ mean rear (resp. front) virtual target; subscript rst and fst mean the rearmost (resp. the foremost) virtual target on the target lane.

Since it is risky to assume that a fast vehicle is in the rear and a slow vehicle is in front, the velocity of virtual targets is set as follows:

$$v_{rvir} = \min[v_{set}, v_e] \quad (3.4)$$

$$v_{fvir} = v_e \quad (3.5)$$

3.3. Vehicle Model

Since a vehicle is the controlled system plant for autonomous driving, the controlled model needs to reflect the real vehicle dynamic properties. There is a trade-off between simple and detailed models. The vehicle model for the ego vehicle is derived for a predictive control approach. The predictive control approach used in this study needs numerous optimization procedures. Therefore, decoupled control architecture is adopted in this dissertation. The decoupled control architecture has an advantage for computational efficiency. Table 1 represents the average calculation time of SMPC using a coupled model in [Carvalho,'14] and SMPC using the decouple control architecture. Even if two controllers using longitudinal and lateral models are operated sequentially, the approach of decouple control architecture has more than twice the computation time advantage over the coupled model based controller.

Table 1. Average calculation time of SMPC according to vehicle models

Vehicle Model	Calculation Time [ms]
Coupled Model	0.66085
Decoupled Lateral Model	0.18519
Decoupled Longitudinal Model	0.08971

The architecture also could consider the coupling dynamics, which the lateral

motions are affected by the longitudinal velocity. The longitudinal velocity is involved in the state space model of the lateral dynamics. The longitudinal velocity changes with time and prediction step. Therefore, the longitudinal and the lateral vehicle dynamics models are used separately.

The longitudinal dynamics model is designed to decide the desired longitudinal acceleration. Both the longitudinal dynamics and the actuator delay model are considered. The actuator's dynamics is adopted according to the first order delay model [Rajamani,'11]. The state-space model of the longitudinal dynamics could be written as:

$$\begin{aligned} \dot{\bar{x}}_{lon} &= A_{lon}\bar{x}_{lon} + B_{lon}u_{lon} \\ \text{s.t. } A_{lon} &= \begin{bmatrix} 0 & 1 & 0 \\ 0 & 0 & 1 \\ 0 & 0 & -1/\tau_a \end{bmatrix}, B_{lon} = \begin{bmatrix} 0 \\ 0 \\ 1/\tau_a \end{bmatrix} \end{aligned} \quad (3.6)$$

where $\bar{x}_{lon} = [p \quad v \quad a]^T$ and $u_{lon} = a_{des}$ are state and input, respectively; a is longitudinal acceleration input, which is determined in the prediction time horizon by the control part; and τ_a represents the actuator delay of longitudinal acceleration.

The lateral dynamics model is designed by combining the bicycle model and error dynamics with a central path of the lane [Falcone,'07, Enache,'09]. Figure 3.8 presents the lateral dynamics model. The state-space model of the lateral dynamics could be written as:

$$\begin{aligned}
\dot{\bar{x}}_{lat} &= A_{lat} \bar{x}_{lat} + B_{lat} u_{lat} + F_{lat} \rho \\
\text{s.t. } A_{lat} &= \begin{bmatrix} \frac{2C_f + 2C_r}{-mv} & \frac{2C_f l_f - 2C_r l_r}{-mv} & 0 & 0 \\ \frac{2C_f l_f - 2C_r l_r}{-I_z} & \frac{2C_f l_f^2 + 2C_r l_r^2}{-I_z v} & 0 & 0 \\ 0 & 1 & 0 & 0 \\ v & 0 & v & 0 \end{bmatrix}, \\
B_{lat} &= \begin{bmatrix} \frac{2C_f}{mv_x} \\ \frac{2C_f l_f}{I_z} \\ 0 \\ 0 \end{bmatrix}, \quad F_{lat} = \begin{bmatrix} 0 \\ 0 \\ -v_x \\ 0 \end{bmatrix}
\end{aligned} \tag{3.7}$$

where $\bar{x}_{lat} = [\beta \quad \gamma \quad e_\psi \quad e_y]^T$, $u_{lat} = \delta_f$ and ρ denotes state, input, and disturbance, respectively; β is the tire-slip angle; γ is the yaw rate; e_ψ denotes the orientation error of the vehicle with respect to the center-line of the lane; e_y denotes the lateral position error with respect to the center-line of the lane; δ_f denotes the desired steering angle, which is determined in the prediction time horizon by the control part; ρ is the road curvature, C_f and C_r are stiffness coefficient of the front (resp. rear) tire, l_f and l_r are distances between the front (resp. rear) axle and the center of gravity, and m is an inertia of the vehicle around its yaw angle.

The tire stiffness is not constant because the target maneuver requires high speed lane changing. Since the driving range of this study is mild driving ($a_y < 0.2g$), a steady-state tire model is appropriate. Lateral tire force is in the linear tire region. In this context, the lateral tire stiffness is almost unchanged, so the effect on variable speed could be neglected.

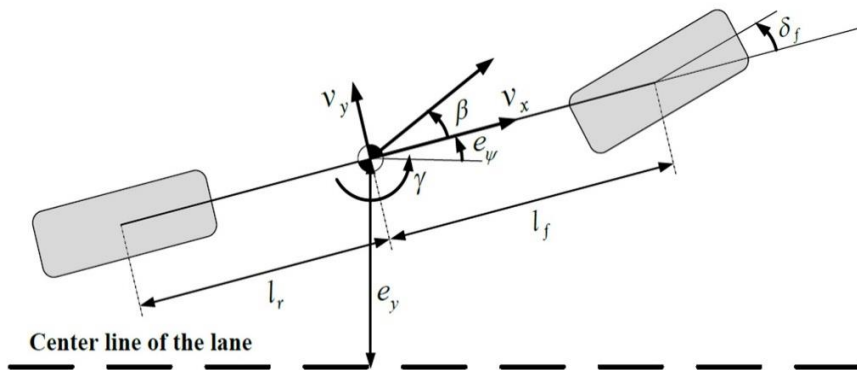


Figure 3.8. Diagram of the lateral dynamics model.

3.4. Prediction Model

The appropriate prediction contributes to decision-making, motion planning, and control of autonomous driving. To enhance safety, given the potential behavior of surrounding vehicles, it is essential to predict the ego vehicle and the surrounding vehicles. The prediction model used in this dissertation is shown in Figure 3.9.

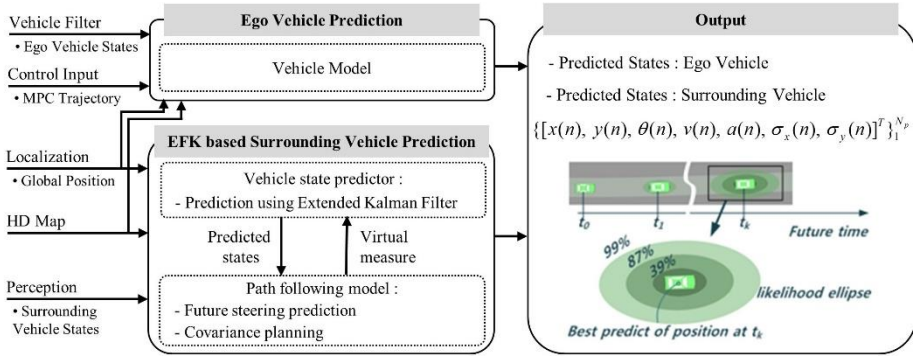


Figure 3.9. Architecture of stochastic prediction.

In an actual environment, diverse disturbance always exists due to reasons such as model uncertainties, sensor noises and actuator delays. Therefore, a stochastic uncertainty is considered to reflect disturbance effects. By the stochastic predictions of the ego vehicle and the surrounding vehicle, the standard deviation of position states could be reflected. As the model error or estimation error increases, the standard deviation increases. Also, prediction step is propagated, the standard deviation increases. Figure 3.10 shows

uncertainty propagation of both ego vehicle and surrounding vehicle. This could enhance the safety, which is harmed by various uncertainties.

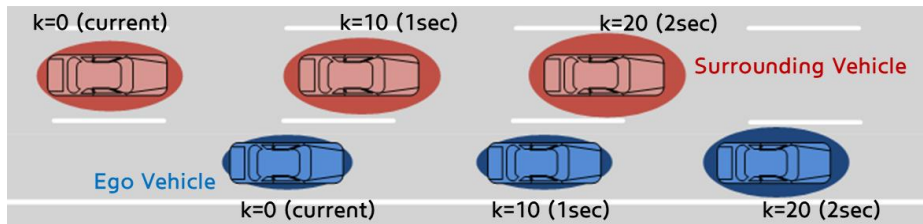


Figure 3.10. Uncertainty propagation as prediction step progresses.

3.4.1. Prediction of ego vehicle

For the prediction of the ego vehicle, the decoupled vehicle model is applied to the control input trajectory calculated by SMPC. The predicted model of the ego vehicle is discretized as:

$$\begin{aligned}\bar{x}_{lon}(n+1) &= A_{lon}\bar{x}_{lon}(n) + B_{lon}u_{lon}(n) \\ \bar{x}_{lat}(n+1) &= A_{lat}(n)\bar{x}_{lat}(n) + B_{lat}(n)u_{lat}(n) + F_{lat}\rho\end{aligned}\quad (3.8)$$

where n is the prediction step. The prediction horizon is 2 s, and the prediction sampling time (t_{sam}) is 0.1 s. This means that the prediction sample is 20 ($n=0, \dots, 19$).

The model error analysis of the ego vehicle is needed to reflect uncertainties. The additive stochastic disturbance of the linear dynamic model is defined using experimental data. The one-step prediction of the model is compared with the measured data and can be written as:

$$\begin{aligned}e_{lon}(n) &= \bar{x}_{lon}(n+1) - A_{lon}\bar{x}_{lon}(n) - B_{lon}u_{lon}(n) \\ e_{lat}(n) &= \bar{x}_{lat}(n+1) - A_{lat}(n)\bar{x}_{lat}(n) - B_{lat}(n)u_{lat}(n) - F_{lat}\rho\end{aligned}\quad (3.9)$$

where e represents the error with the prediction and the measurement.

Error is calculated under various circumstances, such as acceleration, deceleration, lane change, and lane keeping. The disturbance covariance is derived and can be denoted as:

$$\begin{aligned}\Sigma_{w,lon} &= diag(0.05, 0.2, 0.05) \\ \Sigma_{w,lat} &= diag(0.01, 0.01, 0.02, 0.05)\end{aligned}\quad (3.10)$$

where Σ_w represents the error with the prediction and the measurement.

e could be propagated based on Σ_w , which is derived from a disturbance analysis with various situations [Suh,'18]. Since consideration of error using only disturbance analysis cannot reflect the present status of the subject vehicle,

real-time error needs to be addressed. Moreover, real-time error, which reflects the present vehicle motion, cannot be obtained in the general n -th step, except for the first step. This is because the vehicle sensors and exterior sensors have only present information. Therefore, the dissertation adopts the uncertainties concept using the closed-loop paradigm [Gray,'13] and adaptive uncertainty propagation as shown in Figure 3.11 [Suh,'17, Suh,'18]. The final outputs from the adaptive uncertainty propagation are uncertainties of the position states as: the longitudinal position standard deviation (σ_{p_x}) and the lateral position standard deviation (σ_{e_y}). Uncertainties of the position states are propagated as prediction steps.

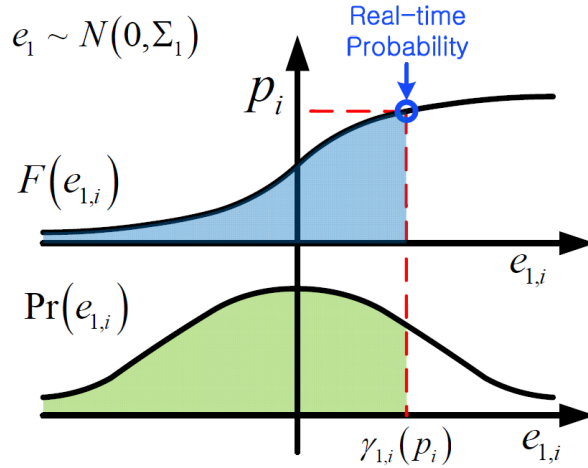


Figure 3.11. Conceptual diagram of adaptive uncertainty propagation.

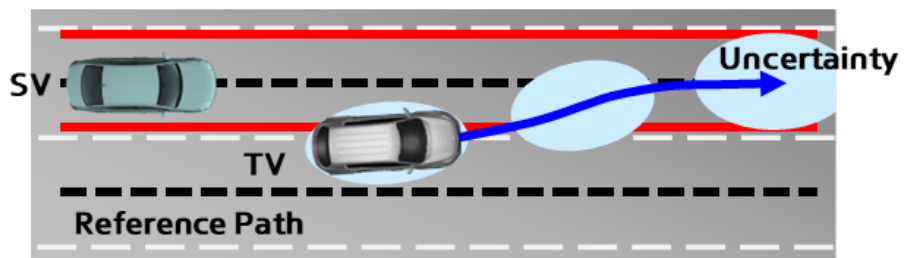
3.4.2. Prediction of surrounding vehicle

It is essential to predict future states of the surrounding environment, to enhance safety given the potential behavior of surrounding vehicles. Other stochastic prediction model is employed about the surrounding vehicles. A probabilistic prediction model is adopted for the prediction of the surrounding vehicles. The prediction uses the states which are estimated in the perception module. The prediction model is based on the probabilistic movement characteristics of the surrounding vehicles. In a vehicle state predictor, the vehicle's reasonable position and its error covariance are predicted by EKF using the desired yaw rate generated by the path-following model as the virtual measurement [Kim,'14]. Therefore, the error covariance is propagated according to the prediction step by EKF. The initial covariance matrix used in the prediction utilizes the covariance matrix of the estimation result. The final outputs from the probabilistic prediction model are shown in Figure 3.9 and as follows: the relative longitudinal position from ego vehicle (x), the relative lateral position from ego vehicle (y), the yaw angle (θ), the longitudinal velocity (v), the longitudinal acceleration (a), the longitudinal position standard deviation (σ_x), and the lateral position standard deviation (σ_y). Like the prediction of the ego vehicle, the prediction horizon is 2 s and the prediction sampling time is 0.1 s.

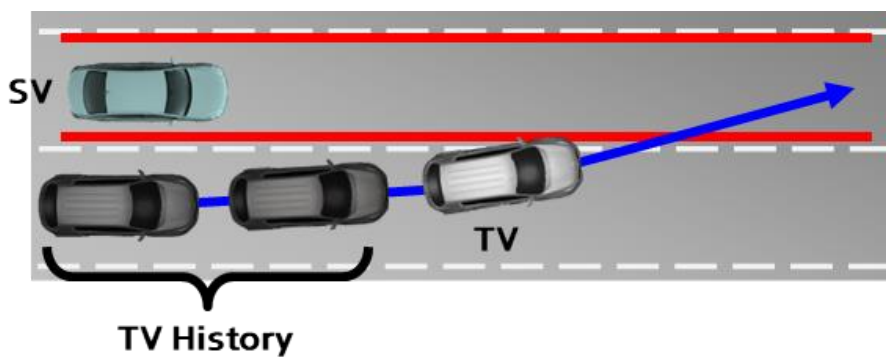
There are probabilistic prediction methods that could perform better than EKF-based prediction [Sun,'18, Hu,'19, Jeong,'20a, Jeong,'20b]. Figure 3.12 represents concepts of EKF-based prediction and RNN-based prediction. The EFK-based approach conducts prediction of lateral motion based on the

assumption of lane keeping. And, the EKF-based approach conducts prediction of longitudinal motion based on the assumption of decayed acceleration. The RNN-based approach predicts the motion of surrounding vehicle using the learning model. And, the RNN-based approach conducts integrated prediction of lateral and longitudinal motions based on observation history.

However, in this dissertation, the EKF-based probabilistic prediction model is adopted in consideration of vehicle implementation. The computation power is important for the algorithm implementation of the vehicle. Figure 3.13 shows the calculation time of the EKF-based prediction model. The total data included 6574 steps. The relative value is important because the absolute value of the computation time depends on the CPU performance. As the number of vehicles to be predicted increases, the calculation time increases. The calculation time of the EKF-based model is compared with other data-driven prediction models. These predictors were learned from the data of the perception module used in this study [Jeong,'20a, Jeong,'20b]. One is the RNN-based method, which predicts behavior through the accumulated trajectory of the target vehicle [Jeong,'20a]. The other is a predictor, which combines RNN and EKF methods to reduce the computational load [Jeong,'20b]. The predictor determines the target lane of the vehicle through the accumulated trajectory and predicts behavior to the target lane-based EKF method. Figure 3.14 shows the relative computational ratio of the two models over the EKF-based model. Both techniques need about 480- and 60-times more computation than the EKF-based model, respectively. Heavy computation makes implementation difficult because overtaking requires predicting multiple vehicles.



(a) EFK-based prediction model.



(b) RNN-based prediction model.

Figure 3.12. Concept of two prediction model.

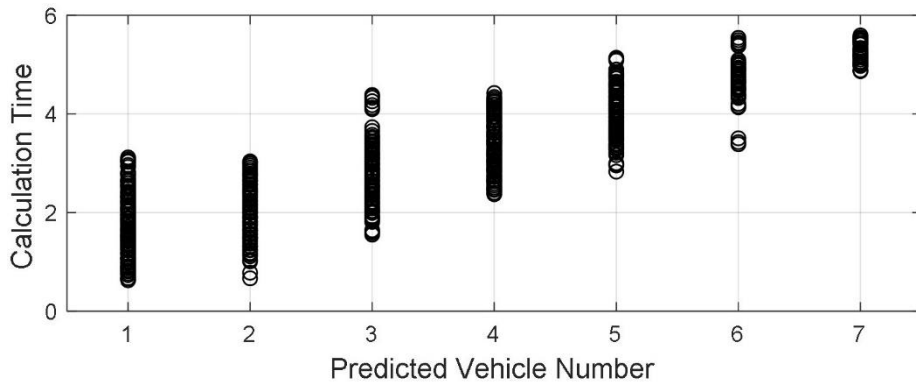


Figure 3.13. Calculation time of EKF-based prediction model.

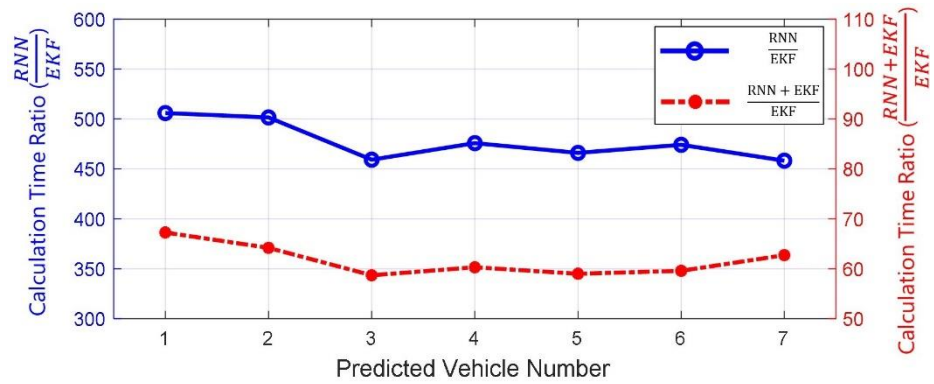


Figure 3.14. Calculation time comparison of data-driven models and EKF-based model.

Chapter 4 Stochastic Risk Assessment

Appropriate risk assessment is important as securing safety from the surrounding obstacles is the top priority of autonomous vehicles. Various indices have been proposed to express risk with surrounding vehicles: clearance (c), time gap (TG), time to collision (TTC), warning index (x), and margin to collision (MTC). These are indices that take into account physical collisions related to time and brake [Lee,'15]. In addition, there are probabilistic risk assessment that considers the potential behavior of vehicles such as collision probability [Kim,'17]. Probabilistic approaches have focused their research on development of new concept of risk index and elaboration of estimation and prediction steps with consideration of uncertainties.

Previous risk assessment approaches are insufficient to reflect driver data characteristics. In this dissertation, human driving data are analyzed to derive characteristics of human drivers. We defined the safety distance and reflected driver characteristics to the distance. Especially, studies on the safety index in lane change situations are insufficient. Excessive safety consideration reduces the possibility of lane changes. On the other hand, mild safety consideration increases the collision risk. The dissertation proposes safety distances as safety indices, which better express the lane change situation based on the driving data. And the collision risk analysis for the proposed safety distance was conducted.

The lane change safety distance was derived in the highway and urban

environments. And the lane change yield intention has been developed to complement each other's characteristics in these two environments. This intention is essential for interactive lane change at low speed, the most difficult situation in lane change. The intention inference module has been developed by learning approach based on data in congested traffic. Finally, proposed yield intention is used to complement the lane change safety distance.

Reflecting uncertainties as well as driver characteristics is important for proper risk assessment. In this study, uncertainties is reflected in the proposed safety distance. This enables the safety distance, which is safer as uncertainties grows. In addition, a new collision probability was proposed by modifying the previously developed collision probability [Kim,'17]. Figure 4.1 shows the overall architecture of stochastic risk assessment.

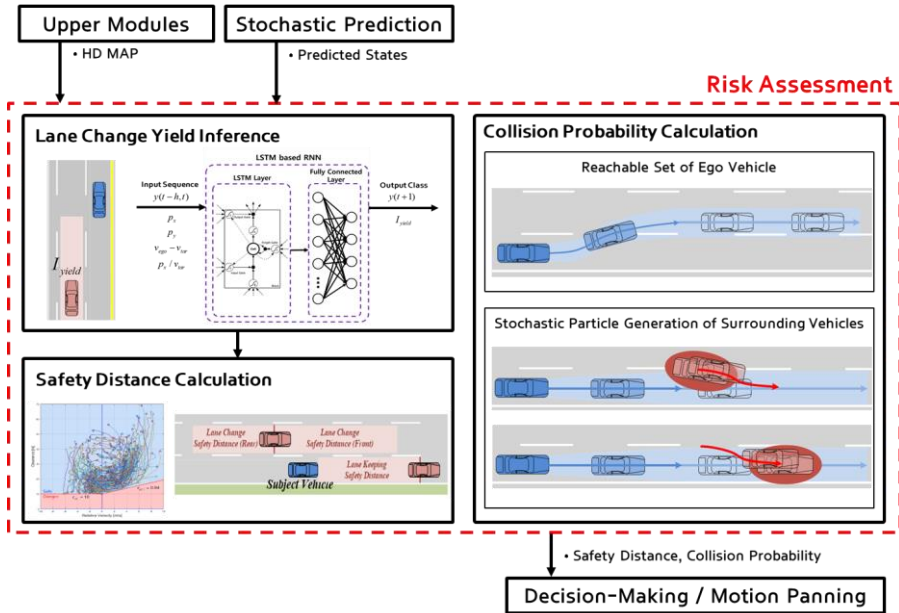
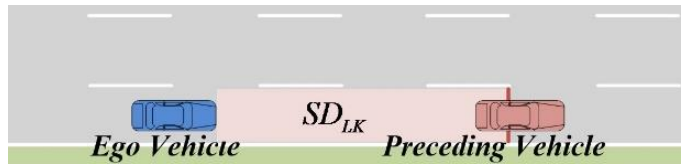


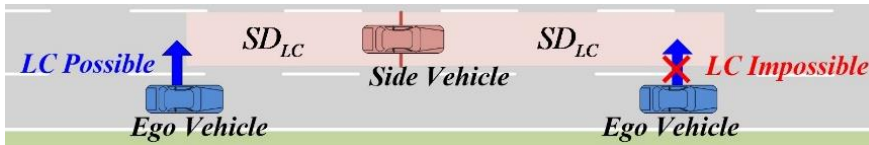
Figure 4.1. Overall architecture of stochastic risk assessment.

4.1. Safety Distance based on Human Driving Data

The safety with surrounding vehicles could be represented by safety distances as shown in Figure 4.2. In lane keeping situations, the ego vehicle drives to keep a certain distance away with a preceding vehicle. The certain distance is defined as a safe distance in lane keeping situations (SD_{LK}). Meanwhile, vehicles located in the side lane are important in lane change situation. These vehicles are called as the side vehicles. A lane change maneuver is permitted when the distance with the ego vehicle and the side vehicle is larger than a certain distance. The certain distance is defined as a safe distance on lane change situations (SD_{LC}).



(a) In the lane keeping situation.



(b) In the lane change situation.

Figure 4.2. Concept of safety distances.

4.1.1. Lane Keeping Safety Distance based on Driving Data

SD_{LK} is developed based on previous studies. In previous studies, the steady-state distance maintained by the ego vehicle when following the preceding vehicle has been investigated. Constant time-gap (CTG) policy and constant clearance policy have received the most attention in spacing policies for following a preceding vehicle [Moon,'08, Sayer,'97]. As a result of analyzing actual driver data, SD_{LK} could be well represented by a first-order regression in respect of velocity [Moon,'08]. Therefore, SD_{LK} is defined by a linear coefficient of velocity and a zero-velocity clearance as:

$$SD_{LK} = v_{ego} \cdot \tau_{LK} + c_{LK} \quad (4.1)$$

where subscript *ego* means the ego vehicle, v is the longitudinal velocity; τ_{LK} is the linear coefficient of lane keeping; and c_{LK} is the zero-speed clearance of lane keeping.

Figure 4.3 shows all the steady-state data collected from 125 drivers and a linear regression on a speed-clearance domain. The zero-speed clearance, c_0 , and the linear coefficient, τ , were 1.98m and 1.36s, respectively. The parameters of SD_{LK} are determined by previous research based on driving data [Moon,'08].

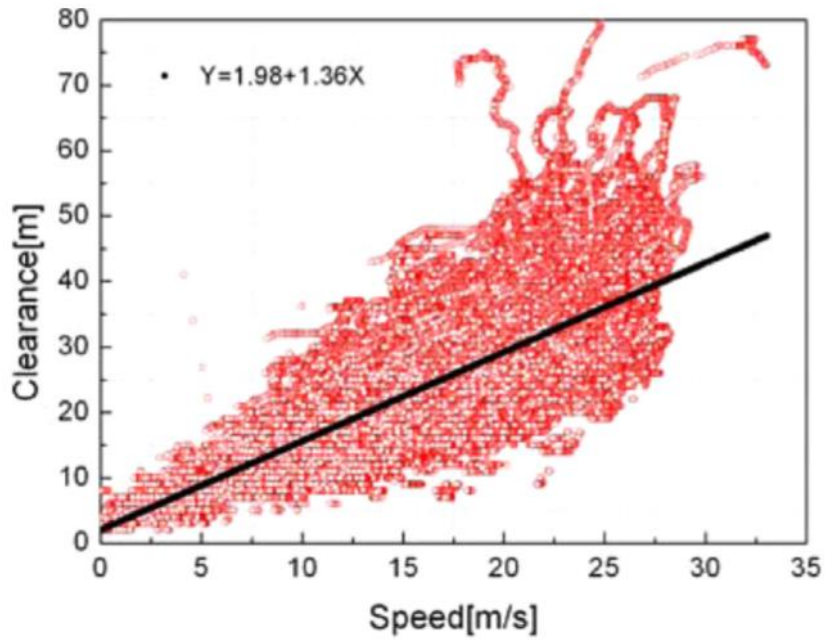


Figure 4.3. Steady-state following data collected from 125 driver test data and the linear regression.

Table 2. Parameters of the lane keeping safe distance based on human driving data in preceding vehicle following situation

Symbol	Value	Symbol	Value
τ_{LK}	1.36 [s]	c_{LK}	4 [m]

4.1.2. Lane Change Safety Distance based on Highway Driving Data

Unlike lane keeping situations, the relative velocity between the ego vehicle and the side vehicle is very important in lane change situations [Do,'17]. A larger distance is required when the velocity of the rear vehicle is faster than that of the front vehicle. In this case, the distance about the relative velocity has to be added to the safety distance. In the opposite case, only a minimum clearance needs to be considered. Therefore, SD_{LC} is determined depending on whether the ego vehicle is forward or behind the side vehicle. SD_{LC} is the sum of the relative velocity term and the minimum clearance term. The minimum clearance varies by the velocity of rear vehicle. SD_{LC} is defined as:

$$SD_{LC} = \begin{cases} \max[(v_{ego} - v_{side}), 0] \cdot \tau_{LC,1} + \max[v_{ego} \cdot \tau_{LC,2}, c_{LC}], & \text{if } x_{side} > 0 \\ \max[(v_{side} - v_{ego}), 0] \cdot \tau_{LC,1} + \max[v_{side} \cdot \tau_{LC,2}, c_{LC}], & \text{otherwise} \end{cases} \quad (4.2)$$

where subscript *side* means the vehicle on the side lane; x is the longitudinal relative position from the ego vehicle; $\tau_{LC,1}$ is the time gap for the relative velocity of lane change; $\tau_{LC,2}$ is the time gap for the minimum clearance of lane change; and c_{LC} is the minimum clearance of lane change.

In the lane change situation, there was no study that calculated the safety distance based on the human driving data, so lane changing driving data was collected and analyzed. Driving data has been collected using two test vehicle described in Chapter 2. In highway, first platform is utilized for collection of driving data. In urban, second platform is utilized for collection of driving data. The test vehicles are used for both collecting data and implementing the proposed algorithm. On the highway, lane change driving has been performed

at a speed of 60 km/h to 120 km/h. On the urban roads, lane change driving has been performed at a speed of 0 km/h to 60 km/h.

First, the description of the highway driving data is as follows. The total driving distance is approximately 1500 km on highways for measuring data. Driving data was collected on a total of 6 highways with 12 drivers. The travelled roads are 3, 4 or 5 lanes. For data accuracy, data collection was conducted in well-appointed roads on a clear day. Driving roads are shown in Figure 4.4.

Figure 4.5 shows highway driving data in lane change situations where the ego vehicle changes lane to the front or rear of the side vehicle. Because first autonomous vehicle platform was used in urban driving, a sensor fusion algorithm, which uses radars and LiDARs, is adopted for detection and tracking of surrounding vehicles. The position and the velocity are estimated by the sensor fusion algorithm. One connected line represents one case of the lane change. Both ends of the each line are labelled with circles and crosses, which indicate start and end of lane change, respectively. Since the data is represented by lines from the start to the end of the lane change, Figure 4.5 presents the velocity changes of the ego vehicle and the side vehicles. This means interactions in the case of a lane change. The interactions express the safety control between the ego vehicle and the side vehicle during lane change maneuvers.

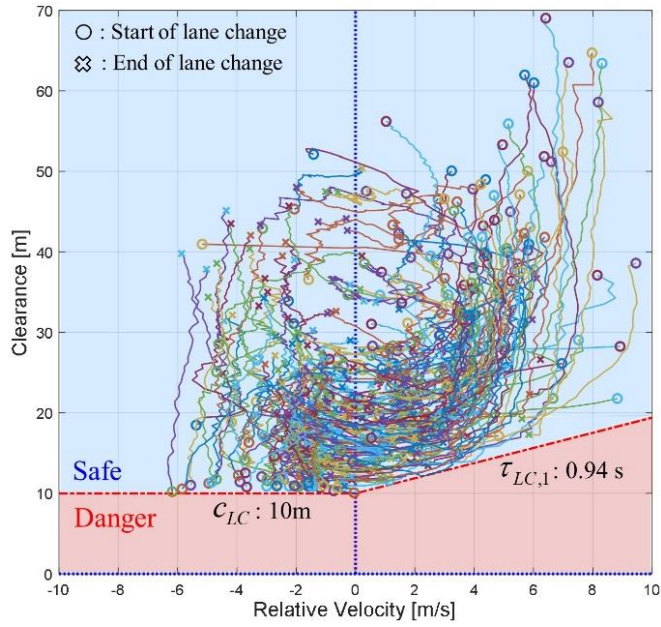


(a) Iljik-Jonam-Anhyeon junction.

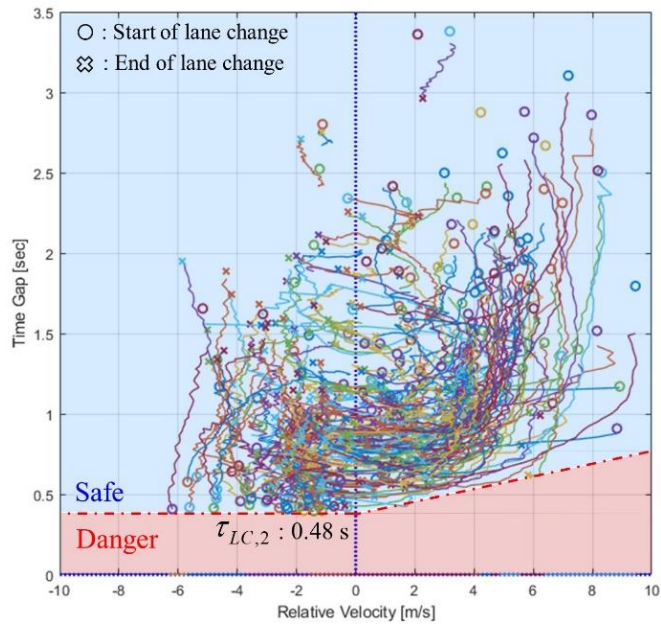


(b) The second Seoul-Incheon linking highway.

Figure 4.4. Highway Driving Data Acquisition Route.



(a) Relative velocity to clearance.



(b) Relative velocity to time gap.

Figure 4.5. Driving data in highway lane change situation.

The above driving data is employed for deciding parameters of SD_{LC} . From the driving data, c_{LC} could be set to 10 [m] in Figure 4.5 (a). $\tau_{LC,1}$ could be set to 0.94 [s] by slope of the right half plane in Figure 4.5 (a). $\tau_{LC,2}$ could be set to 0.48 [s] in Figure 4.5 (b). The parameters should be set conservatively for driver acceptance and collision avoidance. Therefore, the parameters are decided with a little margin from the boundary of the driving data. Table 3 presents the determined parameters.

Table 3. Parameters of the lane change safe distance based human driving data on highway driving

Symbol	Value	Symbol	Value
$\tau_{LC,1}$	1 [s]	$\tau_{LC,2}$	0.5 [s]
c_{LC}	12 [m]		

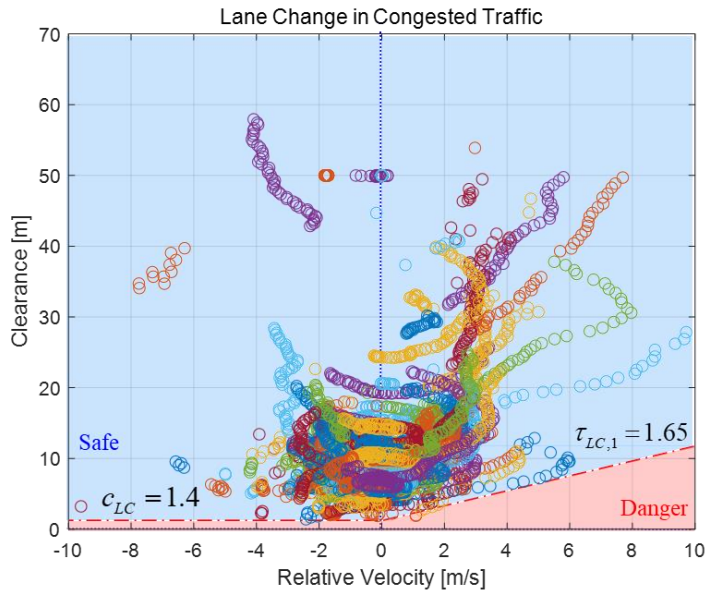
4.1.3. Lane Change Safety Distance based on Urban Driving Data

Second, the description of the urban driving data is as follows. The total driving distance is approximately 150 km on urban roads for measuring data. Driving data was collected on diverse urban roads with 12 drivers. The travelled roads are 2, 3 or 4 lanes. For data accuracy, data collection was conducted in well-appointed roads on a clear day. Driving roads are shown in Figure 4.6.

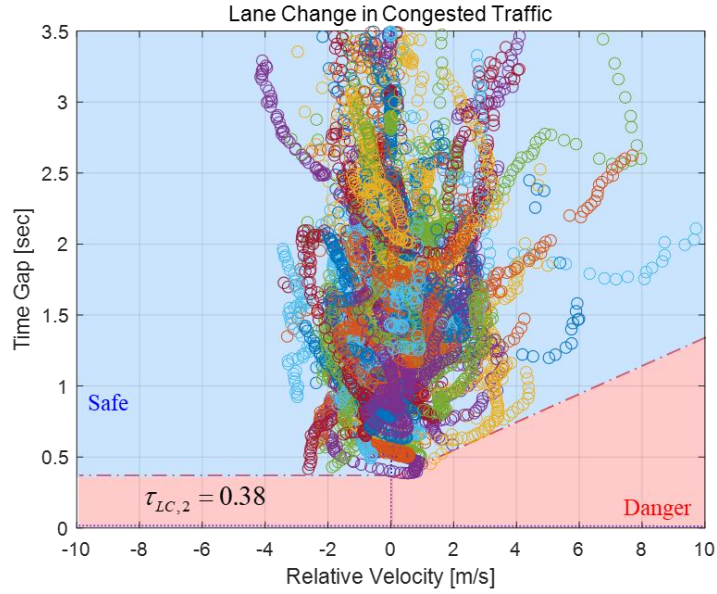


Figure 4.6. Urban Driving Data Acquisition Route.

Figure 4.7 shows urban driving data in lane change situations where the ego vehicle changes lane to the front or rear of the side vehicle. Because second autonomous vehicle platform was used in urban driving, commercial LiDAR processor is adopted for detection and tracking of surrounding vehicles. The position and the velocity are estimated by the commercial LiDAR processor. In urban roads, lane change under 60 km/h was carried out, and lane changes were mainly performed in a congested traffic situation.



(a) Relative velocity to clearance.



(b) Relative velocity to time gap.

Figure 4.7. Driving data in urban lane change situation.

The above driving data is employed for deciding parameters of SD_{LC} . From the driving data, c_{LC} could be set to 1.4 [m] in Figure 4.7 (a). $\tau_{LC,1}$ could be set to 1.65 [s] by slope of the right half plane in Figure 4.7 (a). $\tau_{LC,2}$ could be set to 0.38 [s] in Figure 4.7 (b). The parameters should be set conservatively for driver acceptance and collision avoidance. Therefore, the parameters are decided with a little margin from the boundary of the driving data. Table 4 presents the determined parameters.

Table 4. Parameters of the lane change safe distance based human driving data on urban driving

Symbol	Value	Symbol	Value
$\tau_{LC,1}$	1.65 [s]	$\tau_{LC,2}$	0.4 [s]
c_{LC}	1.4 [m]		

4.1.4. Kinematic Analysis of Lane Change Safety Distance and Stochastic Prediction based Safety Distance

Since the proposed SD_{LC} is derived by the driving data, kinematic analysis is need. In a lane change situation in which the rear vehicle is faster than the front vehicle, the rear vehicle needs to decelerate for collision avoidance. As $\tau_{LC,1}$ is a term about the relative velocity, the term is associated with collision avoidance. On the other hand, $\tau_{LC,2}$ and c_{LC} are terms which represent the marginal safety. Therefore, $\tau_{LC,1}$ is examined for investigation about collision avoidance. Since $\tau_{LC,1}$ based on highway driving data is smaller, we analyzed the safety level based on highway driving data. The analysis situation is when the slow ego vehicle changes lane and the fast side vehicle is approaching from the rear. As the rear vehicle responds and decelerates, the remaining distance is as follows:

$$D_{CA} = (v_{side} - v_{ego}) \cdot t_{CA} - (v_{side} - v_{ego})^2 / (2a_{CA}) \quad (4.3)$$

where t_{CA} is response delay of the rear vehicle; a_{CA} is deceleration of the rear vehicle; and two values are set as 0.3 [s] and -4 [m/s²], respectively [Ising,'12].

In this situation, the safety distance about $\tau_{LC,1}$ is as follows:

$$SD_{LC,CA} = (v_{ego} - v_{side}) \cdot \tau_{LC,1} \quad (4.4)$$

If Eqn. (3) equals Eqn. (4), the relative velocity is derived as follows:

$$v_{side} - v_{ego} = (\tau_{LC,1} - t_{resp}) \cdot (2a_{decel}) \quad (4.5)$$

The relative speed means the maximum velocity difference at which the collision could be avoided. The maximum velocity difference is 20.16 [km/h].

Since this velocity difference is sufficiently large and the marginal safety distance also exists, the proposed SD_{LC} is appropriate about both the driver acceptance and the safety.

Through these processes, we proposed the safety distances considering both driver acceptance and collision safety. In addition to this, uncertainties must be considered for more advanced autonomous driving. In fact, there are various uncertainties for implementation of an autonomous vehicle. In Chapter 3.4 described above, the stochastic predictions are presented reflecting various uncertainties. By the stochastic predictions of the ego vehicle and the surrounding vehicle, the safety distances could reflect the standard deviation of position states. As the model error or estimation error increases, the safety distance increases. Also, prediction step is propagated, the safety distance increases. The proposed prediction models involve uncertainty propagation of both ego vehicle and surrounding vehicle. This could enhance the safety, which is harmed by various uncertainties. The driving data based safety distances (equations (4.1), (4.2)) can be rewritten as the stochastic prediction based safety distances (equations. (4.6), (4.7)).

$$SD_{LK}(n) = v_{ego}(n) \cdot \tau_{LK} + c_{LK} + \sigma_{p_x}(n) + \sigma_{x,preceding}(n) \quad (4.6)$$

$$SD_{LC}(n) = \begin{cases} SD_{LC,1}(n), & \text{if } x_{side}(n) > 0 \\ SD_{LC,2}(n), & \text{otherwise} \end{cases}$$

$$SD_{LC,1}(n) = \max\left[(v_{ego}(n) - v_{side}(n)), 0\right] \cdot \tau_{LC,1} + \max\left[v_{ego}(n) \cdot \tau_{LC,2}, c_{LC}\right] + \sigma_{p_x}(n) + \sigma_{x,side}(n) \quad (4.7)$$

$$SD_{LC,2}(n) = \max\left[(v_{side}(n) - v_{ego}(n)), 0\right] \cdot \tau_{LC,1} + \max\left[v_{side}(n) \cdot \tau_{LC,2}, c_{LC}\right] + \sigma_{p_x}(n) + \sigma_{x,side}(n)$$

4.2. Lane Change Yield Inference using LSTM-based RNN

In this research, the safety distance for lane change was calculated based on driver data. Driving data in highway and urban roads was analyzed. The high-speed lane change is performed in highway driving data. The low-speed lane change is performed in urban driving data. Basically, the safety distance based on highway driving data is good to improve safety performance. This is because it adopts a safer distance than the urban situation. However, when using only a safe distance based on highway data, the following problems exist. As shown in Figure 4.8, in a congested traffic situation, there is no space for a lane change due to overlapping safety distances. In this case, it is necessary to make space by transmitting the intention to change with the appropriate lane. There are two ways to transmit the intention for lane change. The first is to activate the turn signal. This is a basic method that is always performed when a lane change demand is activated. The second is to convey the intention for lane change through slight lateral behavior. To transmit the intention for lane change to the side rear vehicle on target lane, the ego vehicle can drive a little closer to the target lane. This lateral behavior is referred to as ‘traffic pressure’ in this research.

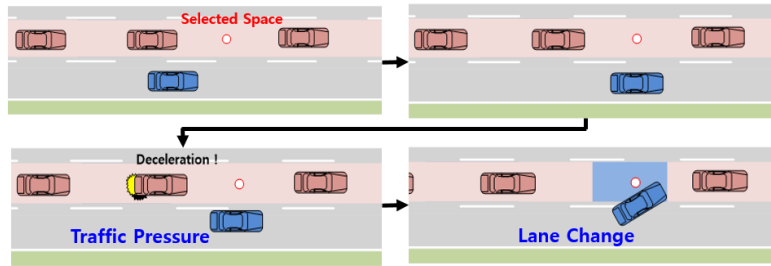
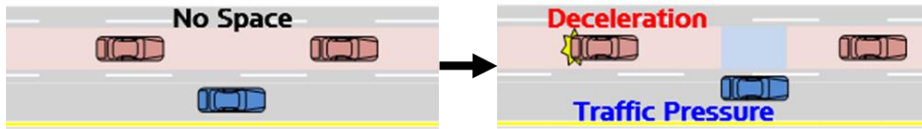
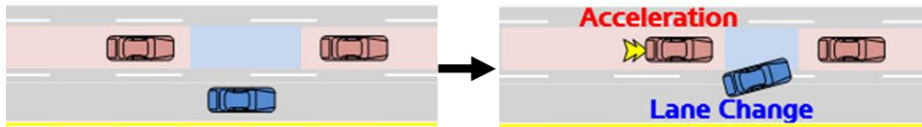


Figure 4.8. The concept of the traffic pressure.

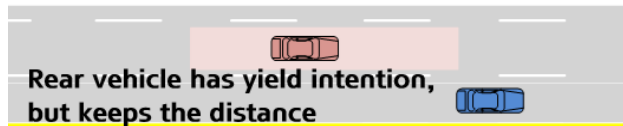
When the intention is transmitted to side rear vehicle, the side rear vehicle with a yield intention secures space for the ego vehicle through deceleration. At this time, if the safe distance based on highway data is used, it is too conservative. It takes too long until the ego vehicle judges that there is space for lane change as shown Figure 4.9 (a). This problem could be solved by using the safety distance based on urban data, but the safety distance based on urban data is inherently dangerous because it is not too conservative as shown Figure 4.9 (b). Another problem with the constant safe distance is follows. As shown in Figure 4.9 (c), a side rear vehicle with the yield intention could maintain a constant distance on the boundary of safety distance. In this case, the driving mode decision for lane change may cause chattering phenomenon. In addition, it could be judged that it is impossible to change the lane even if the side rear vehicle have yield intention.



(a) Highway parameters: too conservative in congested traffic.



(b) Urban parameters: too progressive in congested traffic.



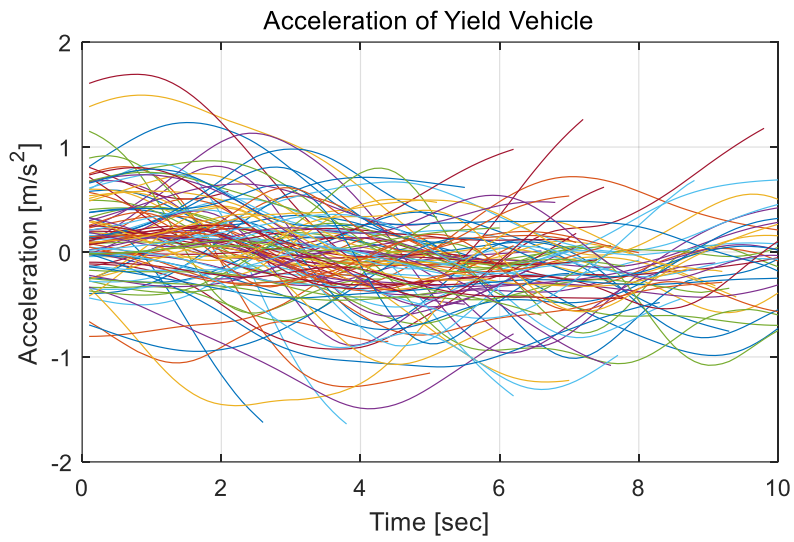
(c) Vehicle with the yield intention could maintain a constant distance.

Figure 4.9. Problems by constant parameters of lane change safety distance.

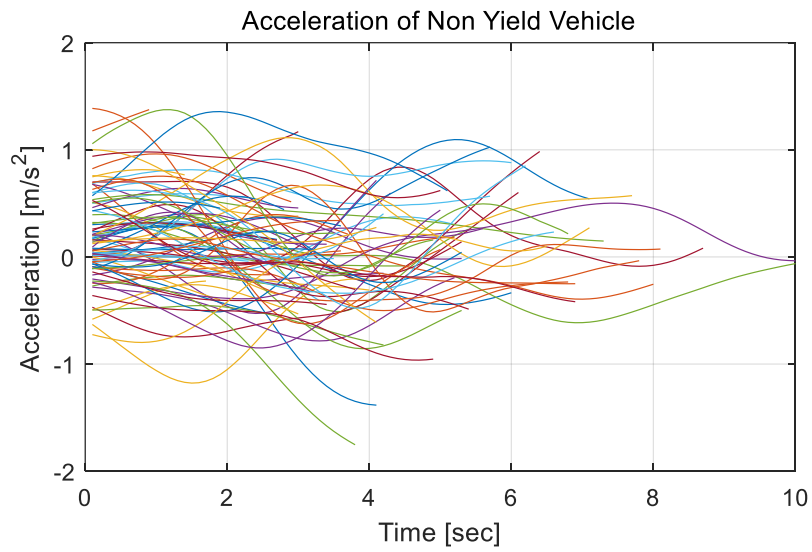
Therefore, this study introduces the concept of lane change yield intention in order to supplement the safety distance. The yield intention in the lane change situation has not been studied much, but several yield intentions have been developed for the autonomous driving. Previously, the yield intention has been researched on unsignalized intersection and merging sections. All of these studies have treated the collision-based yield intention related to longitudinal behavior. The lane change yield intention in this study is the collision-based intention related to more complex longitudinal and lateral integration behavior. Also, previous studies use the trend of acceleration or velocity change for the yield intention inference. Figure 4.10 shows a situation where acceleration is used for yield intention inference. It is impossible to infer intention solely from

acceleration or velocity tendencies. In particular, it is not V2V communication in an actual situation, but it estimates the state of surrounding vehicles using a local sensor. In this situation, it is almost impossible to accurately estimate the acceleration, so there is a problem in inferring the yield intention by methods in previous researches.

In the study, lane change driving data on urban roads was used to make the yield intention inference model. The driving data of the urban situation is a low speed situation of 60 km/h or less. Most of the data is under congested traffic. It is difficult to use rule-based method to make the yield intention inference model. This is because lane change in congested traffic is a complex situation related to longitudinal and lateral integration behavior. As a results, a learning-based approach has been adopted rather than a rule-based approach to make the yield intention inference model. And SD_{LC} is supplemented based on the inferred yield intention.



(a) Acceleration of yield vehicle.



(b) Acceleration of non-yield vehicle.

Figure 4.10. The acceleration in vehicle where no tendency is found.

4.2.1. Dataset Selection

We used the collected data for urban lane change distance. We collected the data on surrounding vehicle tracks from second autonomous vehicle platform which adopts commercial LiDAR processor for detection and tracking of surrounding vehicles. The data collection environment is described in Chapter 4.1.3. The data was collected in a low speed situation of less than 60kph on the urban roads, and most are data of congested traffic.

In Chapter 4.1.3, only data that successfully changed lanes are presented, but data that failed to change lanes is also required for inferring yield intention. The driver transmitted the intention of lane change to the side-rear vehicle through the turn signals and appropriate traffic pressure. The case where the lane change was successful means that the side-rear vehicle had yield intention. On the other hand, the case where the lane change was failed means that the side-rear vehicle did not have yield intention. Figure 4.11 represents the classification of yield & non-yield cases.

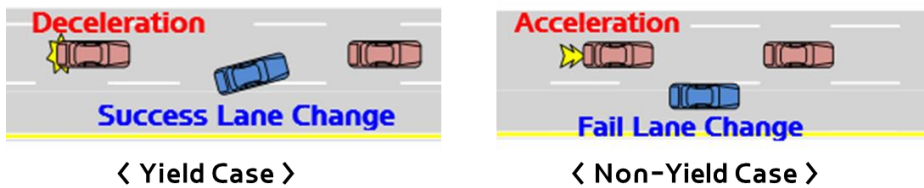


Figure 4.11. Classification of yield & non-yield cases.

In conclusion, yield intention data was collected for the side-rear vehicle. The moment when there was a request to change lanes was labeled through the

turn signal information. Finally, the following data was collected and used for learning. Dataset for training and validation is illustrated in Table 5.

Table 5. Dataset for Training and Validation

	<i>Y+N</i>	<i>Yield</i>	<i>Non-Yield</i>
<i>Total</i>	<i>9357</i>	<i>6830</i>	<i>2527</i>
<i>Training</i>	<i>8166</i>	<i>5986</i>	<i>2180</i>
<i>Validation</i>	<i>1000</i>	<i>740</i>	<i>260</i>
<i>Test</i>	<i>191</i>	<i>104</i>	<i>87</i>

4.2.2. Network Architecture

Yield intention is continuous based on the interaction of vehicles; in other words, the intention of the vehicle depends on the sequential previous interactions. Previous motion can be measured using the perception module on ego vehicle, but it is difficult to infer surrounding vehicle's driver intention based on rules. Particularly on interactive lane change in congested traffic, it is difficult to apply conventional maneuver-based approaches to infer driver intention. Therefore, we propose a data-driven approach to infer lane change intention based on previous interactions of the ego vehicle and the side rear vehicle. The intention inference module based on LSTM-RNN architecture that we propose in this work used only information collected from the perception module on an ego vehicle.

An RNN is an artificial neural network that is appropriate for use with sequential data such as speech or text recognition written in natural language. In addition, RNNs can be used with time series data, where the pattern of the data depends on the time flow. The recurrence in RNNs allows for modeling the correlations between consecutive data points in a sequence. This feature is realized by having the same network for each time step and passing activations to a successor [Goodfellow,'16].

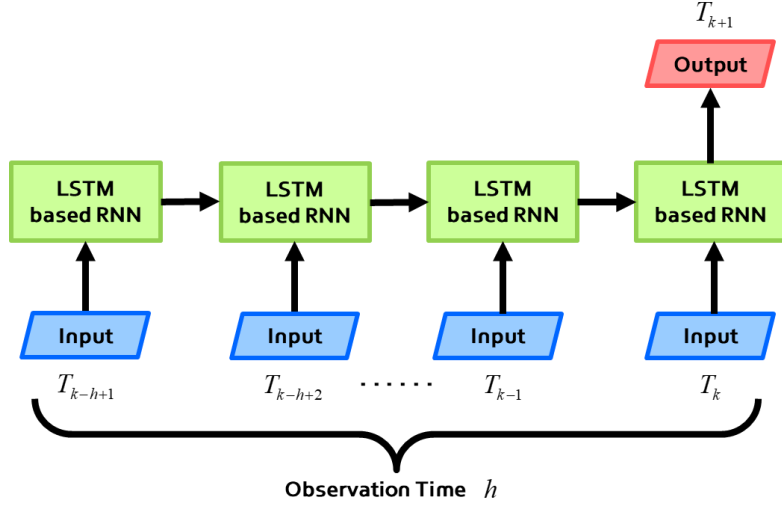
The RNN can contain feedback loops, which allows activations to flow interactively in the loop. This feature allows for processing the sequences of inputs by persisting the activations over multiple steps. In other words, the network can memorize the previous information and predict the future after specific steps by applying the same network iteratively. Figure 4.12 (a) depicts

the structure of the RNN used in this study for an observation horizon h . As the figure shows, the activations in each step are passed to the same network of the next time step and updated with new input data. This means that one set of weights of the RNN is repeated over the prediction horizon by matching the formats of the input sequences and output class.

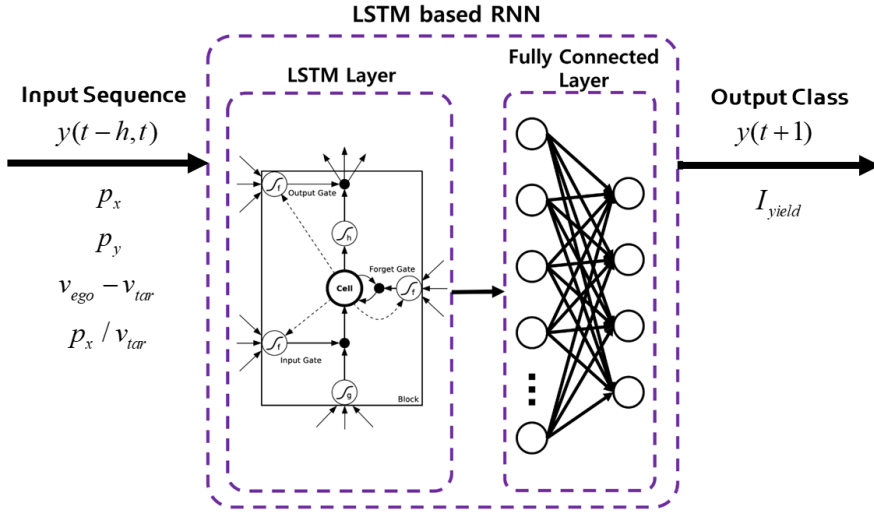
The inference step using the proposed RNN is conceptually expressed in Figure 4.12 (b) with LSTM used as a network cell. LSTM can avoid the vanishing gradient problem by making the error flow backward through unlimited numbers of virtual layers. This property prevents the error from increasing or decaying over time, which would make the network train inappropriately [Hochreiter,'97].

Before searching the optimal network configuration, inputs need to be decided. Yield intentions can basically be inferred from the longitudinal behavior of the side-rear vehicle [Dong,'17, Wei,'13]. However, it is possible to consider the lateral behavior as the characteristic interaction appears in the congested traffic lane change. Variables for inference are shown in Figure 4.13. We defined input candidates containing meaning of variables for inference as follows:

$$\begin{aligned}
 p_x &= p_{x,ego} - p_{x,tar} \\
 p_y &= p_{y,ego} - p_{y,tar} \\
 v_{rel} &= v_{ego} - v_{tar} \\
 TG_{tar} &= p_x / v_{tar}
 \end{aligned} \tag{4.8}$$



(a) Diagram representing the proposed RNN of observation time h .



(b) Conceptual diagram of the LSTM-RNN inference module.

Figure 4.12. Diagram of the proposed LSTM-RNN for yield intention inference.

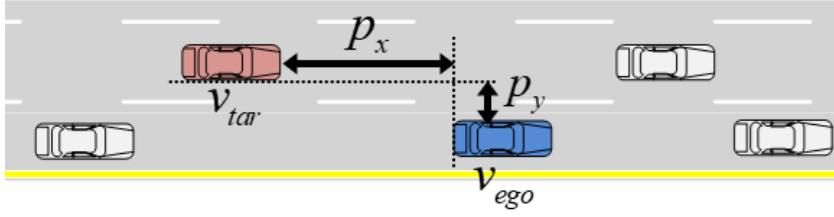
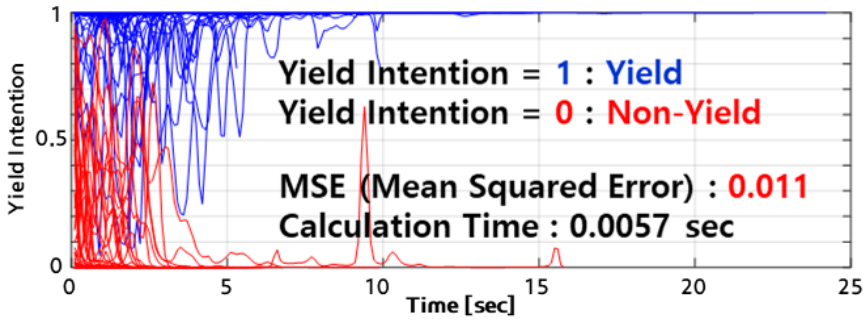


Figure 4.13. Variables for yield intention inference of lane change.

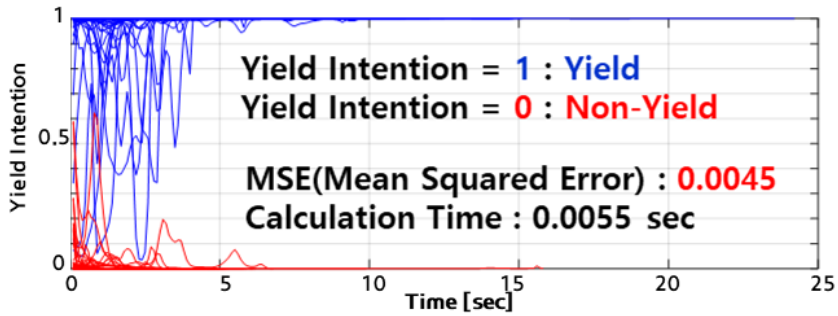
A comparison has been made between inputs considering only the longitudinal elements and inputs considering the longitudinal and lateral elements. In the former, we defined p_x , v_{rel} and TG_{tar} as inputs for learning. In the latter, we defined p_x , p_y , v_{rel} and TG_{tar} as inputs for learning. The comparison result is represented in Figure 4.14. For the same LSTM-based RNN network architecture, 4 inputs considering longitudinal and lateral motions show better performance than 3 inputs considering only longitudinal motions. In the network with 4 inputs, both mean square error (MSE) and calculation time are smaller. In conclusion, when inferring yield intention, it is good to consider lateral motions as well.

We determined the optimal network configuration by comparing the several network configurations. In general, when searching for an optimal network, error is defined and the network with the smallest error is selected. However, the network of this study cannot define error as the network is for yield intention inference. Therefore, the optimal network has been determined by considering the following factors: the purpose of yield intention inference, the MSE and calculation time. Networks that are too data-biased do not match the intention inference. Therefore, a network with a low MSE and well suited to the purpose

of intention inference is selected. And since the network should be implemented to the actual vehicle, it was also considered whether it has an appropriate calculation time. Network candidates who have progressed several learning are as shown in Figure 4.15. The finally selected network learning result is shown in Figure 4.16.

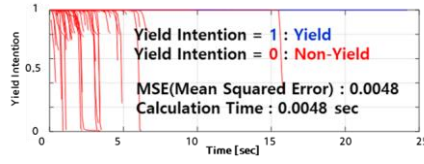


(a) Learning result of network with three inputs (p_x , v_{rel} , TG_{tar}).

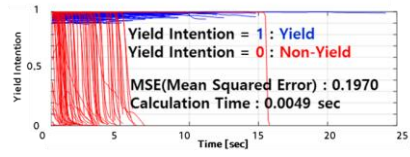


(b) Learning result of network with four inputs (p_x , p_y , v_{rel} , TG_{tar}).

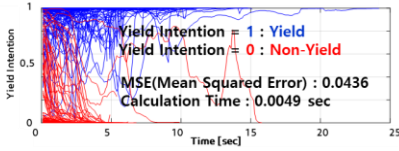
Figure 4.14. Comparison of LSTM-RNN learning results for input set selection.



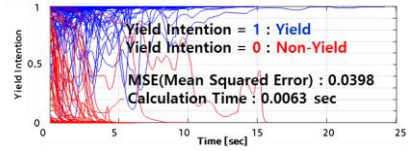
(a) Unselected Candidate 1



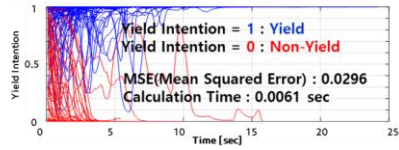
(b) Unselected Candidate 2



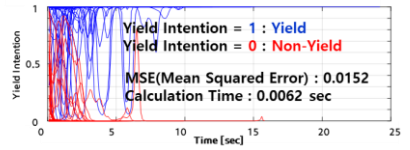
(c) Unselected Candidate 3



(d) Unselected Candidate 4



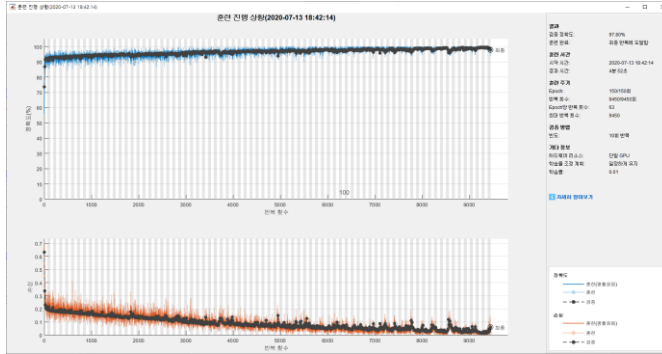
(e) Unselected Candidate 5



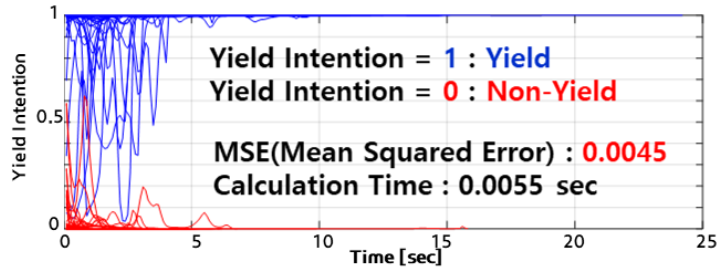
(f) Unselected Candidate 6

Figure 4.15. Unselected network candidates who have progressed learning.

The proposed network architecture is represented in Figure 4.17. Sequential four inputs are used for the network. Observation horizon is 2 seconds and sampling time is 0.1 seconds. The network two LSTM layers with drop-out, one fully connected layer and one softmax layer. Softmax layer makes the yield intention a probability value between 0 and 1.



(a) Learning process of final selected network.



(b) Learning result of final selected network.

Figure 4.16. The proposed network selection for yield intention inference.

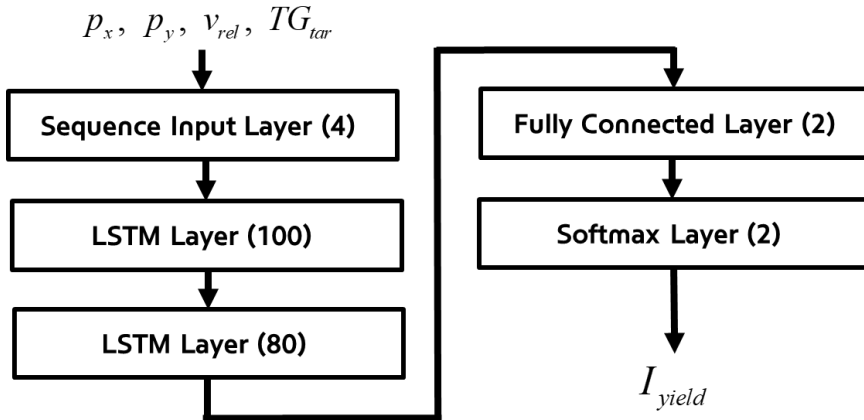


Figure 4.17. The proposed network architecture for yield intention inference.

4.2.3. Yield Intention Inference based Safety Distance

Yield intention developed in this study is used to complement the lane change safety distance. There is a limit to using yield intention alone. Since yield intention is expressed as a probability, it is not meaningful to use it in decision-making, motion planning and control for autonomous vehicles. Therefore, this intention is used as the weight for the two parameters of the lane change safety distance presented in this study.

In this study, the lane change safety distance is derived based on driver data. Data collection was conducted in two environments. One is based on data acquired from the highway as described in Chapter 4.1.2. The other is based on data acquired from the urban roads as described in Chapter 4.1.3. In the former, lane changes were made at 60~120 km/h, and the latter were a lane changes at 0~60 km/h. Therefore, the former is named the progressive lane change distance and the latter is named the conservative lane change distance. Two kinds of parameters are complemented with the yield intention as shown Figure 4.18. Two kinds of parameters are arranged in Table 6. The proposed lane change safety distance based yield intention is as follows:

$$\begin{aligned}
 SD_{LC} &= \begin{cases} \max[(v_{ego} - v_{side}), 0] \cdot \tau_{LC,1} + \max[v_{ego} \cdot \tau_{LC,2}, c_{LC}], & \text{if } x_{side} > 0 \\ \max[(v_{side} - v_{ego}), 0] \cdot \tau_{LC,1} + \max[v_{side} \cdot \tau_{LC,2}, c_{LC}], & \text{otherwise} \end{cases} \quad (4.9) \\
 s.t. \quad \tau_{LC,1} &= I_{yield} \cdot \tau_{LC,1,p} + (1 - I_{yield}) \cdot \tau_{LC,1,c} \\
 \tau_{LC,2} &= I_{yield} \cdot \tau_{LC,2,p} + (1 - I_{yield}) \cdot \tau_{LC,2,c} \\
 c_{LC} &= I_{yield} \cdot c_{LC,p} + (1 - I_{yield}) \cdot c_{LC,c}
 \end{aligned}$$

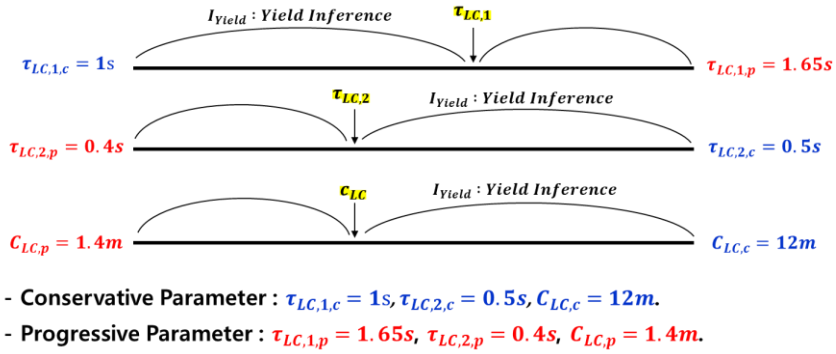


Figure 4.18. The lane change safety distance based on the yield intention.

Table 6. Parameters of the lane change safe distance based human driving data on highway and urban driving

Symbol	Value	Symbol	Value
$\tau_{LC,1,c}$	1 [s]	$\tau_{LC,1,p}$	1.65 [s]
$\tau_{LC,2,c}$	0.5 [s]	$\tau_{LC,2,p}$	0.4 [s]
$c_{LC,c}$	12 [m]	$c_{LC,p}$	1.4 [m]

4.3. Collision Probability based on Stochastic Particle

The most important purpose of autonomous vehicles is collision avoidance. The risk of collision will have to be assessed continuously. Therefore, it is necessary to assess an appropriate collision by using the motion prediction information of the ego vehicle and surrounding vehicle. When predicting collisions of vehicles, the size of the vehicle must be considered. Figure 4.19 shows a situation of vehicle collision. As a result of considering the future behavior of the ego vehicle, a collision does not occur for the A vehicle, but a collision for the B vehicle. Therefore, it is sufficient to proceed with the control to prevent collision only for the B vehicle. If the control for preventing collision is also performed for the A vehicle, the unnecessary deceleration is too frequent. However, it is not ideal as the above in an actual autonomous driving situation. There are several uncertainties in predicting correct collision. Therefore, it is necessary to assess collision risks considering various uncertainties. Since the stochastic prediction is conducted considering various uncertainties in this study, it is necessary to fully utilize this prediction information.

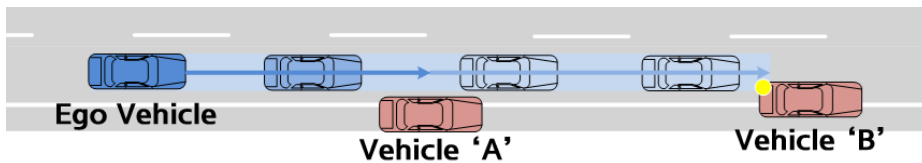


Figure 4.19. Collision situation.

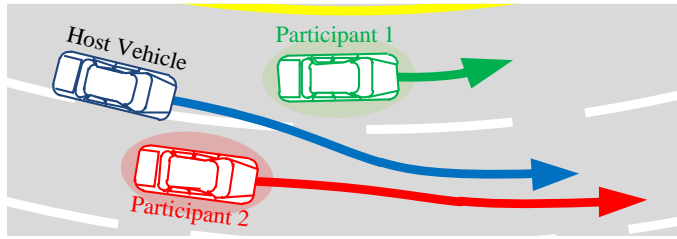
4.3.1. Conventional Collision Probability

The collision probability has been developed to express the risk of collision between vehicles [Kim,'17]. This probability reflects the stochastic motions of vehicles generated by various uncertainties. In this previous study, the ego vehicle is the host vehicle and surrounding vehicles are traffic participant. The concepts of probabilistic collision risk are summarized and presented in Figure 4.20. As the beginning of the collision probability estimation, we randomly generate a given number N state vectors based on the given initial probability density function from the prediction algorithm. The parameter N could be chosen by a designer as a trade-off between computational effort and collision probability approximation accuracy. The state vectors are called particles and denoted as:

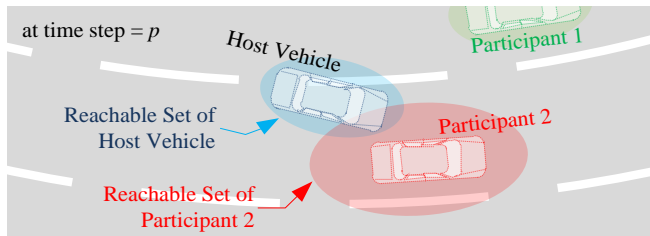
$$\mathbf{x}_n^i[p] = \begin{bmatrix} \hat{\mathbf{x}}_{host}[p] \\ \hat{\mathbf{x}}_n[p] \end{bmatrix} + \left(\sqrt{\begin{bmatrix} \hat{\mathbf{P}}_{host}[p] & \\ & \hat{\mathbf{P}}_n[p] \end{bmatrix}} \right) \cdot \tilde{\mathbf{r}}^i \quad (i=1, \dots, N) \quad (4.10)$$

where the subscript p is the predictive time step; $\hat{\mathbf{x}}_{host}$ is the predicted position and orientation state vector of the host vehicle; $\hat{\mathbf{x}}_n$ is the predicted pose state vector of n -th traffic participant; $\hat{\mathbf{P}}$ denotes the appropriate size of the covariance matrix of each predicted state; $\tilde{\mathbf{r}}$ is a white noise random vector of the proper size.

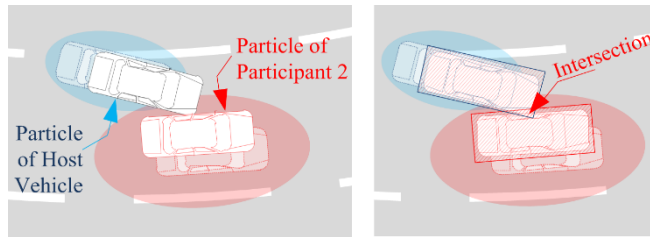
For every possible pair of ego and one of traffic participants, we investigate whether the vehicle bodies of the traffic participant can intersect the ego vehicle at each predicted time step. To determine the body intersection, a body-shaped diagram is introduced. Algorithm 1 shows a pseudo code of the algorithm.



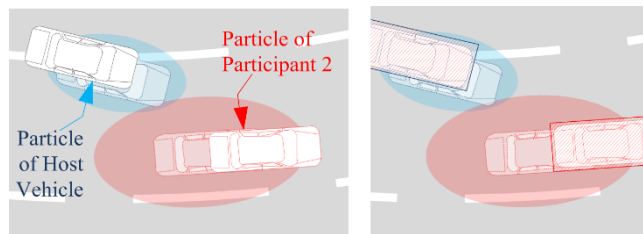
(a) Environment description: road, host vehicle, and multi-traffic-participant.



(b) Prediction of multi-traffic pose and their covariance at predictive time step, p . Reachable set of each participant as stochastic distribution.



(c) A collision case example of the generated N particles and its two vehicle-body-shaped-polygons. Intersection between two polygons.



(d) A non-collision case example of the generated N particles and its two vehicle-body-shaped-polygons.

Figure 4.20. Procedure and concept of conventional collision probability.

Algorithm 1 : Conventional Collision Probability Calculation

- 1: Inputs: Predicted states and its covariance within a pre-defined prediction horizon for the ego vehicle and all tracked surrounding vehicles
 - 2: for all tracked surrounding vehicles, $n = 1, \dots, N_{target}$
 - 3: for every predictive time step, $p = 0, \dots, N_p$
 - 4: Initialize collision count with participant n at predictive time step p, $C.P.cnt_n^i = 0$
 - 5: From the given predicted state and covariance, randomly generate N particles, $\mathbf{x}_n^i[p]$
 - 6: for every particle, $i = 1, \dots, N$
 - 7: Generate two vehicle-body-shaped-polygons
 - 8: Check if the vehicle bodies can be possibly intersected
 - 9: if intersection is detected, $C.P.cnt_n^i = C.P.cnt_n^i + 1$
 - 10: else, $C.P.cnt_n^i = C.P.cnt_n^i$
 - 11: Approximate collision probability with participant n at predictive time step p
 - 12:
$$C.P._n^i = C.P.cnt_n^i / N$$
 - 13: end
 - 14: end
 - 15: end
-

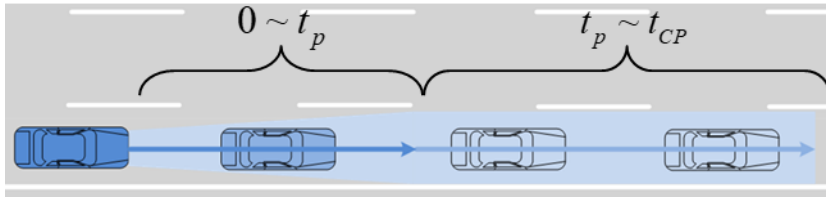
4.3.2. Proposed Collision Probability to select target for safety control

The conventional collision probability is suitable for risk assessment, but there is a problem in reflecting the probability in the actual autonomous driving control. Since there is no physical meaning of this probability, it is ambiguous to keep the autonomous vehicle within a certain probability value. Because of the problem of the conventional collision probability, the safety distance based on driving data is used directly in decision-making and motion planning of autonomous driving in this study. Meanwhile, the collision probability is used for checking whether the surrounding vehicle is targeted for safety control. Therefore, the conventional collision probability was modified to develop a proposed collision probability to meet this strategy.

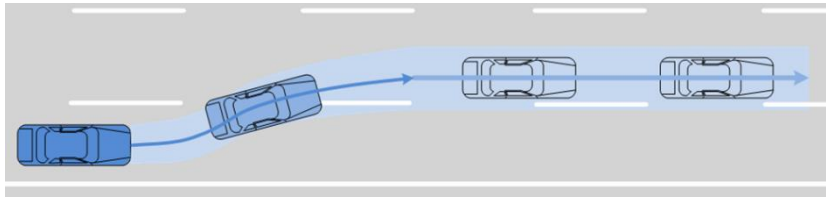
The proposed collision probability does not generate particles for both the ego vehicle and the surrounding vehicle. The future trajectory of the ego vehicle is accurate because it is controllable. As the beginning of the proposed collision probability estimation, a reachable set of ego vehicle is calculated passes through the future trajectory of the ego vehicle.

If only the range of prediction horizon ($t_p = 2\text{sec}$) is used, the reachable set is rather short for collision checking. Therefore, reachable set is calculated by dividing two horizons. The first horizon is the prediction horizon ($0 \sim t_p$). As described in Chapter 3.4.1, the ego vehicle is predicted through MPC and uncertainty is propagated. The second horizon is the collision check horizon ($t_p \sim t_{CP}$). It is assumed that from the last position of the first horizon, the road path is passed horizontally. The uncertainty of the second horizon is assumed to be the last uncertainty of the first horizon. If the uncertainty continues to

grow until too far into the future, uncertainty consideration will be excessive. And since the second horizon assumes that only the road geometry is followed, light calculation is possible. The reachable set of ego vehicle is shown in Figure 4.21.



(a) Lane keeping situation to represent two horizon: the prediction horizon and the collision check horizon.



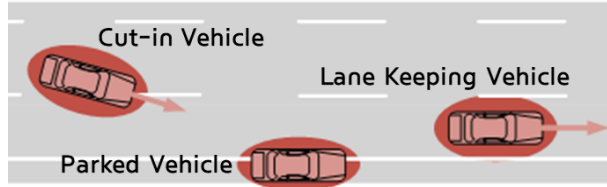
(b) Lane change situation to represent road geometry following in the collision check horizon.

Figure 4.21. Reachable set of ego vehicle.

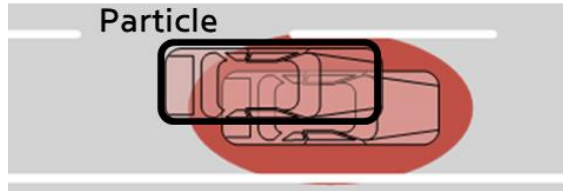
About surrounding vehicles, we randomly generate a given number N state vectors based on the given initial probability density function from the prediction algorithm. The reachable set of surrounding vehicle is shown in Figure 4.22. The one moment of reachable set is calculated. The state vectors are called particles and denoted as.

$$x_{n,p}^i = \hat{x}_{n,p} + \sqrt{\hat{P}_{n,p}} \cdot \tilde{r}^i \quad (i=1, \dots, N) \quad (4.11)$$

where the subscript p is the predictive time step; \hat{x}_n is the predicted position and orientation state vector of n -th surrounding vehicle; \hat{P} denotes the appropriate size of the covariance matrix of each predicted state; \tilde{r} is a white noise random vector of the proper size.



(a) Diverse surrounding vehicles



(b) Particles generation of surrounding vehicle.

Figure 4.22. Reachable set of surrounding vehicles.

Finally, the proposed collision probability is estimated as the ratio of overlapping particles among the whole particles. The conventional collision probability generates particles of ego vehicle and surrounding vehicle, causing heavy computation. On the other hand, since the proposed collision probability generates particle only for surrounding vehicle, the calculation time is small.

This gives the advantage of computational power considering that the collision probability is estimated in every prediction step. The estimation examples of the proposed collision probability is shown in Figure 4.23. Figure 4.24 represents the conceptual diagram for estimated collision probability at each step in prediction horizon. Algorithm 2 shows a pseudo code of the algorithm.

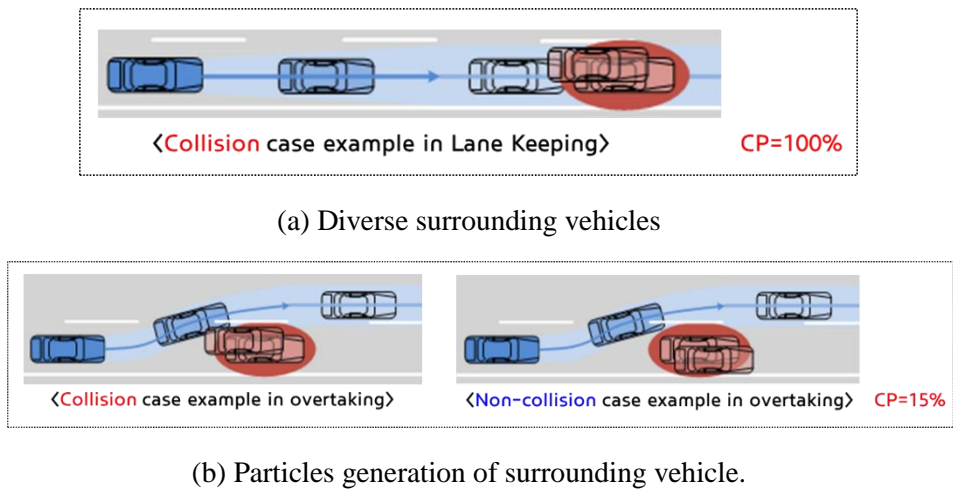


Figure 4.23. Estimation examples of the proposed collision probability.

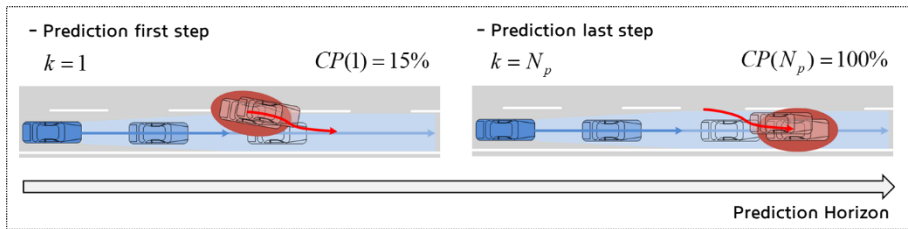


Figure 4.24. Conceptual diagram for estimated collision probability at each step in prediction horizon.

Algorithm 2 : Proposed Collision Probability Calculation

- 1: Inputs: Predicted states and its covariance within a pre-defined prediction horizon for the ego vehicle and all tracked surrounding vehicles
 - 2: Calculate reachable set of ego vehicle
 - 3: for all tracked surrounding vehicles, $n = 1, \dots, N_{target}$
 - 4: for every predictive time step, $p = 0, \dots, N_p$
 - 5: Initialize collision count with participant n at predictive time step p, $C.P.cnt_n^i = 0$
 - 6: From the given predicted state and covariance, randomly generate N particles, $\mathbf{x}_n^i[p]$
 - 7: for every particle, $i = 1, \dots, N$
 - 8: Generate one vehicle-body-shaped-polygons
 - 9: Check if the vehicle bodies can be possibly intersected with reachable set of ego vehicle
 - 10: if intersection is detected, $C.P.cnt_n^i = C.P.cnt_n^i + 1$
 - 11: else, $C.P.cnt_n^i = C.P.cnt_n^i$
 - 12: Approximate collision probability with participant n at predictive time step p
 - 13:
$$C.P._n^i = C.P.cnt_n^i / N$$
 - 14: end
 - 15: end
 - 16: end
-

Chapter 5 Decision-Making

When driving on the road, an appropriate lane change is necessary for various reasons. The reasons for the lane change are summarized as two cases: discretionary and mandatory [Toledo,'03, Toledo,'07a, Kesting,'07]. Firstly, the ego vehicle performs a Discretionary Lane Change (DLC) when it is difficult to maintain its original lane with a pre-set desired velocity. This may include most situations, such as an overtaking situation in which a preceding vehicle is too slow compared to an ego vehicle. Secondly, a Mandatory Lane Change (MLC) is required due to a lane drop or yielding to traffic near a ramp. The lane change is affected by road environments of a driving route. Reasons of lane change as shown in Figure 5.1.

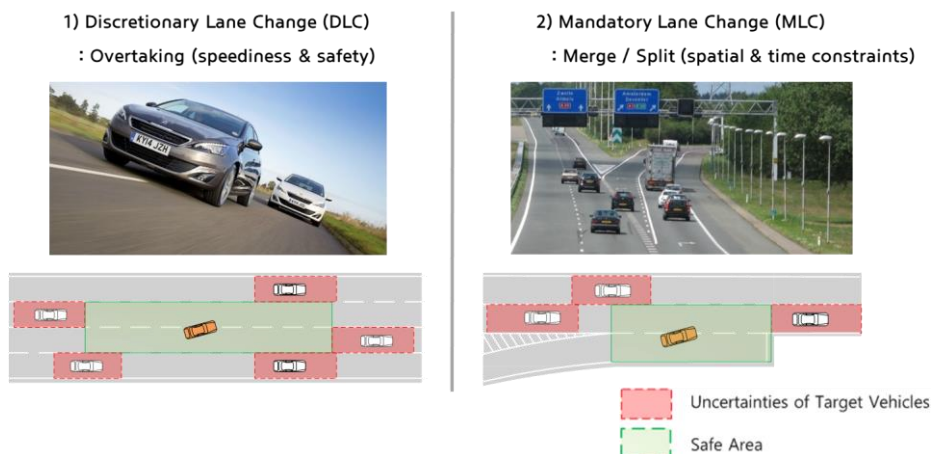


Figure 5.1. Reasons of lane change.

When the lane change is demanded by MLC and DLC, the suitable lane change behavior needs to be selected. A passive (wait) lane change model have limitations in handling diverse lane change situations. Therefore, an active (accelerate/decelerate) lane change model is required to cope with both lane changes reasons (DLC/MLC). For this, an appropriate decision-making is essential. Overall architecture of decision-making is shown in Figure 5.2.

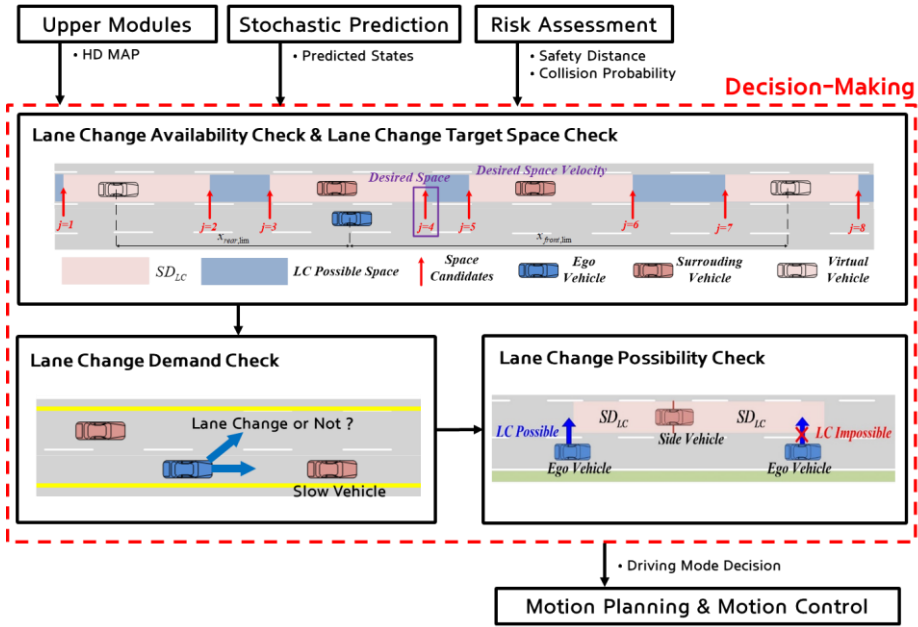


Figure 5.2. Overall architecture of decision-making.

Advanced overtaking requires active lane change, not passive lane change [Do,'17]. For active lane-change maneuver, three driving modes are devised: lane-keeping mode (LK); lane change mode (LC); and lane-keeping mode for

lane change (LKC). A flow chart of the driving mode decision is shown in Figure 5.3. During lane-keeping mode, the ego vehicle follows v_{set} or a preceding vehicle. A lane change is necessary as the reason of lane change exists like MLC or DLC. For lane change decisions, three concepts about lane change are developed: availability, demand, and possibility. After checking three concepts, the driving mode is determined. And lane change target space is decided in this dissertation. This plays a key role for demand checking and motion planning of active lane change. All the processes in the flow chart are based on relay concept. This is to prevent chattering of check activation and mode switch.

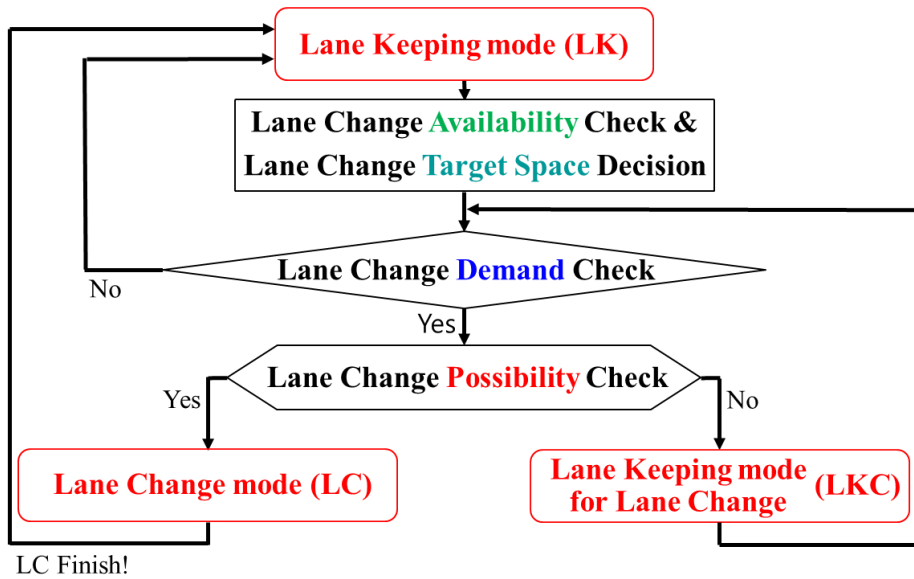


Figure 5.3. Flow chart of driving mode decision for lane change.

5.1. Lane Change Availability Check and Target Space Decision

The first step in determining the driving mode for lane change is to determine whether the lanes on both side can be essentially lane-changeable. This is affected by the road environment. It is important how many lanes on road and the lane where ego vehicle is located. To determine this, the proposed algorithm uses localization information of the upper module. Using the high-definition map information, the ego vehicle checks if both lanes are lane-changeable as shown in Figure 5.4. In Figure 5.4, left lane is only available for lane change. On only available lane, virtual vehicles are created as shown in Figure 5.5, which helps to reduce unnecessary calculation.

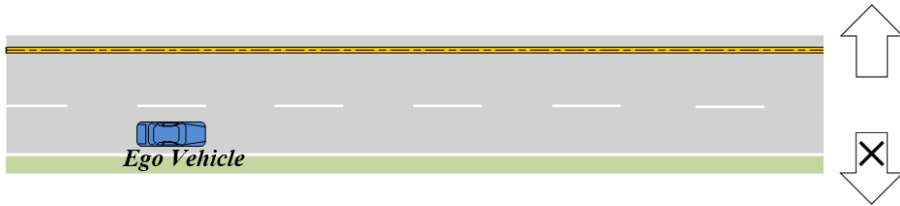


Figure 5.4. A Concept of lane change availability check.



Figure 5.5. Virtual vehicle creation on only available lane.

The second step in determining the driving mode for lane changes is to check the condition of side vehicles on the available lane. A concept of 'target space' has been developed in this dissertation. Target space means the space to enter for lane change between the vehicles on the target lane. Before deciding the target space, candidates of the target space are identified. As shown in Figure 5.6, space candidates for lane changes could be yielded by applying SD_{LC} to the virtual vehicles and detected vehicles in the target lane. One side vehicle makes two space candidates. Each space candidate has a ' j ' index. The states of each space, such as its position and velocity, depend on the states of the vehicle that created it.

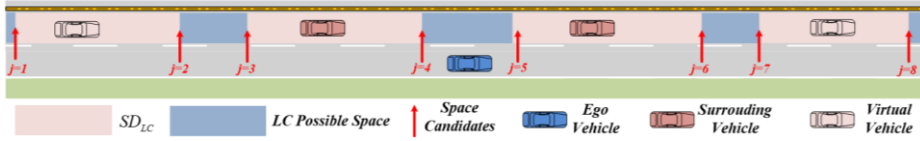


Figure 5.6. Space candidate for lane change based on safety distance.

Since the ego vehicle could accelerate and decelerate for the active lane change, the diverse behaviors of the ego vehicle need to be assumed to find the optimal space for a lane change. It is assumed that the ego vehicle has several acceleration candidates as shown in Figure 5.7. It is assumed that the acceleration of the ego vehicle reaches several candidates with a certain jerk ($1m/s^3$). The minimum value of the acceleration candidates ($a_{cand,min}$) is constant ($-2m/s^2$). The maximum value of the acceleration candidates is varied depending on a preceding vehicle or road limit. The limit values of the

acceleration candidates are expressed as follows:

$$a_{cand,max} = \begin{cases} \min(a_{cand,free}, a_{cand,prc}) & \text{if } p_{prc} < SD_{LK} \\ \min(a_{cand,free}, a_{cand,road}) & \text{elseif } p_{road} < SD_{LK} \\ a_{cand,free} & \text{otherwise} \end{cases} \quad (5.1)$$

$$\text{s.t. } a_{cand,prc} = k_{a_{cand}} \times (p_{x,prc} - SD_{LK})$$

$$a_{cand,road} = k_{a_{cand}} \times (p_{x,road} - SD_{LK})$$

where $a_{cand,free}$ is the maximum value ($2m/s^2$) when there is no need for safety control for a preceding vehicle or road limit. $k_{a_{cand}}$ is gain for safety control for a preceding vehicle (0.3). Subscript *prc* means the preceding vehicle. Subscript *road* means the road limit such as ramp. $N_{a_{cand}}$ is the number of acceleration candidates.

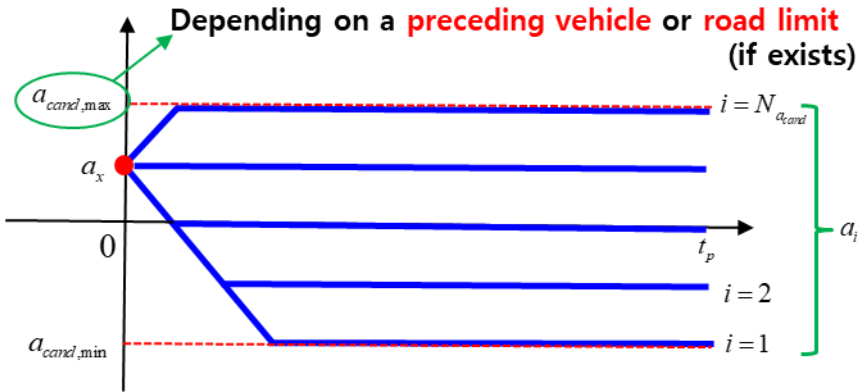


Figure 5.7. Acceleration candidates of ego vehicle prediction for searching the lane change space.

Several acceleration candidates are derived between the maximum and minimum acceleration as shown in Figure 5.7. The assumed behavior of the ego vehicle is predicted according to acceleration candidates. The assumed

behavior is expressed as follows:

$$\begin{aligned} v_i(n+1) &= v_i(n) + a_i(n) \times t_{sam} \\ p_i(n+1) &= p_i(n) + v_i(n) \times t_{sam} \end{aligned} \quad (5.2)$$

where subscript i is the i -th acceleration candidate.

A target space shall be decided among space candidates. Two conditions are used for determining the target space. These conditions are derived by the decision rule of human drivers in the lane-change maneuver. Drivers do not intend to enter a space that is too far or too narrow for a lane change. The first condition is the time that the ego vehicle arrives at space. The second condition is the clearance between consecutive space candidates. An optimization problem is formulated to decide the target space. The space candidate, which has the lowest cost, is selected as the target space. The selected space receives a cost advantage for a chattering prevention. The optimization problem is as follows:

$$\begin{aligned} \min_{i,j} J_{ij} &= T_{ij} / C_j \\ \text{s.t. } T_{ij} &= p_{ij} / v_{ij}, \\ p_{ij} &= \sum_{n=1}^{N_p} (p_j(n) - p_i(n) \pm SD_{LC,ij}(n)) / N_p \\ v_{ij} &= \sum_{n=1}^{N_p} (v_j(n) - v_i(n)) / N_p \\ C_j &= \sum_{n=1}^{N_p} (p_{j+1}(n) - p_j(n)) / N_p \end{aligned} \quad (5.3)$$

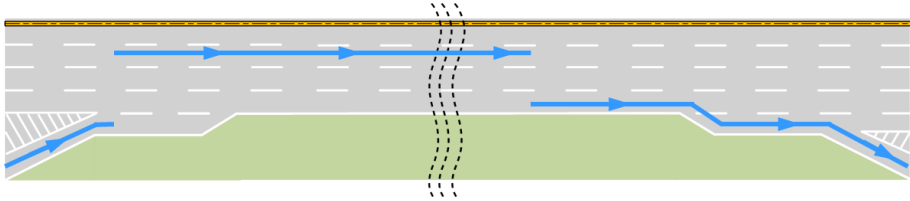
where J means the optimization cost; subscript j is the j -th space candidate; T denotes the time for arriving at the space candidates; N_p is maximum prediction step and C denotes the clearance between the consecutive space candidates.

5.2. Lane Change Demand Check

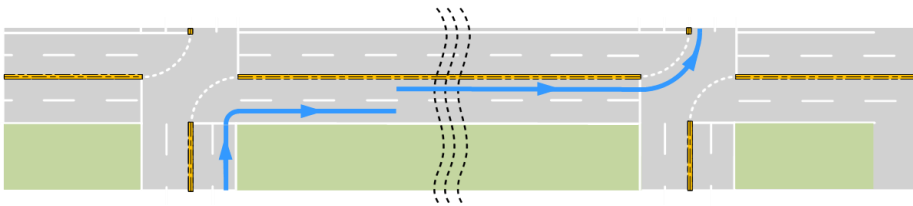
The level of autonomous driving in this research is Level 3 or higher, so the proposed algorithm must make lane change demand by itself. The lane change is demanded differently according to the MLC or the DLC. The MLC is related by road information. Using a map and localization information is needed to determine if the MLC is necessary. For example, off-ramp and on-ramp are MLC factors on the highway. In the on-ramp, the lane change needs to be completed within the limited distance. Therefore, the lane change is demanded as soon as the ego vehicle enters the on-ramp. Meanwhile, the ego vehicle must move to the exit lane before reaching the off-ramp. Therefore, the lane change is demanded until the ego vehicle reaches the exit lane.

Because it is too inefficient to do such route planning every time, this study created the concept “main path” as shown in Figure 5.8. The blue line in Figure 5.8 represents main path. The autonomous vehicle makes driving on main path the top priority. Then, when the ego vehicle deviates from main path, the vehicle needs to perform lane change in the direction of main path. In Figure 5.8 (a), it is possible to enter and exit the highway described above. In Figure 5.8 (b), the main path is defined to make a right turn and a left turn at the next intersection, which leads to lane change naturally. Therefore, the proposed algorithm can perform route planning for MLC simply by defining the main path on the high-definition map. To determine the demand for the MLC, only two factors are needed: 1) whether the ego vehicle is above main path or not,

and 2) if not above main path, which is the direction for main path.



(a) Main path on highway road.



(b) Main path on urban road.

Figure 5.8. Concept of main path.

In a DLC situation, the condition of surrounding vehicles is important. The DLC is a situation where the ego vehicle are driving on the main path and overtaking by a slow vehicle ahead. Figure 5.9 represents an overtaking situation where the ego vehicle employs the available left lane for overtaking.

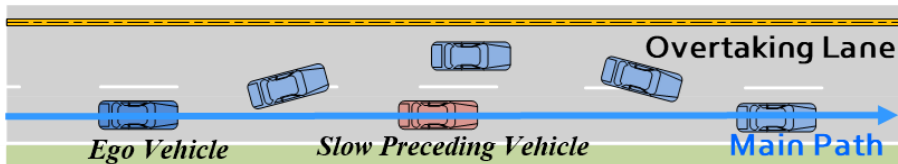


Figure 5.9. Overtaking situation.

To determine whether overtaking proceeds, it is important to decide what

information in the adjacent lane will be used. Previous studies have utilized traffic flow for the overtaking decision. In previous research, traffic flow is characterized by microscopic and macroscopic points of view [Li,'04]. Since local sensors of the ego vehicle could only measure a limited area, the microscopic point of view has been utilized in overtaking decisions [Suh,'18]. In an ideal situation, it is reasonable to use the traffic flow for overtaking decisions. However, side vehicles drive with various velocity on a real road. When drivers decide to overtake, they judge based on the velocity of the space they are going to go, rather than the average velocity of the target lane. Therefore, in this study, the target space defined above is used for overtaking decisions. The decision algorithm utilizes the velocity of the vehicles in front of the target space. The velocity of the vehicle in front of the target space is named as a target space velocity (v_{space}). The minimum velocity of all perceived vehicles in front of the target space is named as a minimum target space velocity ($v_{space,min}$). The perceived vehicles mentioned herein refer to vehicles on the target lane. Lane change is demanded by comparing $v_{space,min}$ with the velocity of the preceding vehicle (v_{pre}).

When actual drivers overtake, the velocity difference between the target lane and the current lane must go above a certain level. And this velocity difference is related to the velocity of the ego vehicle. The lower the velocity of the ego vehicle, the greater the velocity difference between the two lanes to attempt to overtake. In this study, ' ε ' has been developed to reflect this velocity difference characteristic. This prevents frequent lane change demand in congested traffic. ε is determined by the velocity of ego vehicle and the set

velocity as follows:

$$\varepsilon = \begin{cases} (-17 / 30) \times v_e + v_{set} / 3 & \text{if } v_e < v_{set} / 2 \\ v_{set} / 20 & \text{otherwise} \end{cases} \quad (5.4)$$

When overtaking, it is necessary to change lane twice. Once when the ego vehicle meets a slow preceding vehicle. In this case, lane change is demanded to overtaking lanes. Another is when the ego vehicle returns from the overtaking lane to the driving lane. In this case, lane change is demanded of driving lanes. Therefore, different conditions are needed for two reasons. The enter (to the overtaking lane) condition, which is defined as:

$$(v_{prc} < v_{set}) \wedge (v_{prc} + \varepsilon < v_{space, \min}) \wedge (p_{prc} < 2SD_{LK}) \quad (5.5)$$

The return (to the lane of main path) condition is defined as follows:

$$(v_{set} \leq v_{space, \min}) \vee (v_{prc} + \varepsilon < v_{space}) \quad (5.6)$$

To prevent chattering of demand check activation, the demand check process is based on relay concept. For this, a demand probability (\Pr_{demand}) is defined in this study. The demand probability varies with each condition. And it has a value between 0 and 1. This probability is calculated as shown in Algorithm 3. This calculation is applied for both lanes respectively. When this probability has a value greater than 0.5, a lane change to the corresponding lane is finally demanded.

If the lane change is demanded, the turn signal is activated to the target lane. The turn signal is a basic method that is always performed when a lane change demand is activated. The turn signal is a basic role for transmitting the intention for lane change to side vehicles on target lane.

Algorithm 3 : Lane Change Demand Check

```
1:  Inputs: demand conditions (availability of lane, overtaking condition,
    return condition), demand probability
2:  if the ego vehicle is on main path
3:      if adjacent lane is available
4:          if overtaking condition
5:               $\Pr_{demand} = \min(1, \max(0, \Pr_{demand} + \lambda_{LC1})$ 
6:          else
7:               $\Pr_{demand} = \min(1, \max(0, \Pr_{demand} - \lambda_{LK})$ 
8:          else
9:               $\Pr_{demand} = \min(1, \max(0, \Pr_{demand} - \lambda_{LK})$ 
10: else
11:     if adjacent lane is available
12:         if return condition
13:              $\Pr_{demand} = \min(1, \max(0, \Pr_{demand} + \lambda_{LC2})$ 
14:         else
15:              $\Pr_{demand} = \min(1, \max(0, \Pr_{demand} - \lambda_{LK})$ 
16:         else
17:              $\Pr_{demand} = \min(1, \max(0, \Pr_{demand} - \lambda_{LK})$ 
19: end if
```

Table 7. Parameters for Lane Change Demand Check

Parameters	Values	Parameters	Values
λ_{LC1}	0.1	λ_{LC2}	0.2
λ_{LK}	0.025		

5.3. Lane Change Possibility Check and Traffic Pressure Mode for Interactive Lane Change

When a lane change is demanded, the driving mode changes from LK mode to LKC mode or LC mode. To decide which mode to proceed between LKC mode and LC mode, the ego vehicle needs to judge a possibility of the lane change based on SD_{LC} of side vehicles. If any side vehicle is situated closer than SD_{LC} , the lane change is impossible. Figure 5.10 shows a concept of the lane change possibility. When relative positions of side vehicles are smaller than the SD_{LC} of each vehicle in the all prediction horizon, a lane change is risky. The condition of the lane change risk is given by:

$$|p_{ms}| < |SD_{LC,ms}| \quad (5.7)$$

where subscript ms means the ms -th side vehicles on target lane ($m = 1, \dots, N_{ms}$); and N_{ms} means the number of side vehicles.

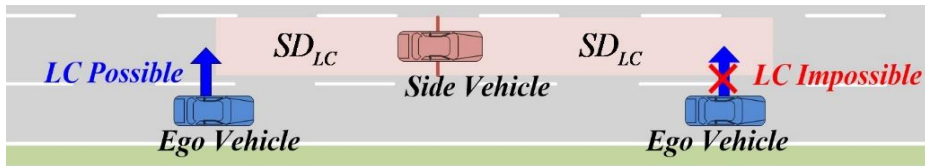


Figure 5.10. A concept of lane change possibility based on safety distance.

To prevent chattering of possibility check activation, the possibility check process is based on relay concept. For this, a possibility probability ($\text{Pr}_{\text{possibility}}$)

is defined in this study. The possibility probability varies with each condition. And it has a value between 0 and 1. This probability is calculated as shown in Algorithm 4. This calculation is applied for both lanes respectively. When this probability has a value greater than 0.9, a lane change to the corresponding lane is finally possible.

Algorithm 4 : Lane Change Possibility Check	
1:	Inputs: lane change risk condition, possibility probability
2:	if lane change risk condition
3:	$Pr_{possibility} = \min(1, \max(0, Pr_{possibility} + \lambda_{risk}))$
4:	else
5:	$Pr_{possibility} = \min(1, \max(0, Pr_{possibility} + \lambda_{non-risk}))$
6:	end if

Table 8. Parameters for Lane Change Possibility Check

Parameters	Values	Parameters	Values
λ_{risk}	-1	$\lambda_{non-risk}$	0.3

The LC mode is started when a lane change is possible. Even during the lane change mode, the lane change possibility is continuously checked. The possibility has been checked until the ego vehicle crosses the lane. If lane change is demanded but lane change is impossible, LKC mode is in progress. Figure 5.11 represents mode decision based on lane change possibility.

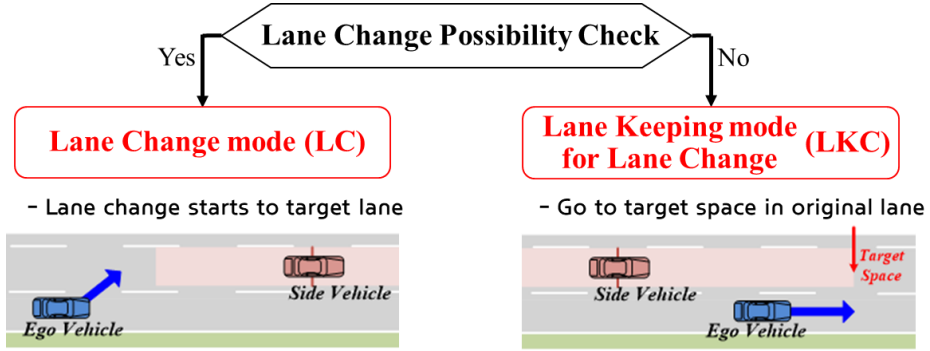


Figure 5.11. Driving mode decision based on lane change possibility.

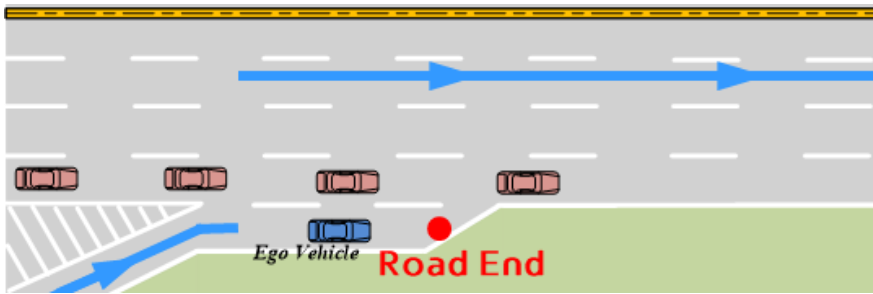
In LKC mode, a special case exists to need ‘traffic pressure’ described in Section 4.2. The safety distance-based lane change space may not exist because vehicles on the target lane are close together in congested traffic. In this research, in order to counteract this, we developed a lane change yield intention inference. And the safety distance reflecting the yield intention helps to judge the appropriate space for lane change. However, apart from yield intention inference, it is important to transmitting the intention to change with the appropriate lane through traffic pressure in congested traffic. When traffic pressure mode is activated, desired lateral motion is planned to drive to the target lane. This makes it possible to perform interactive lane change. The condition that traffic pressure is triggered is when the space for lane change is less than the length of the vehicle. This condition is given by:

$$C_{\text{target}} < L_{\text{vehicle}} \quad (5.8)$$

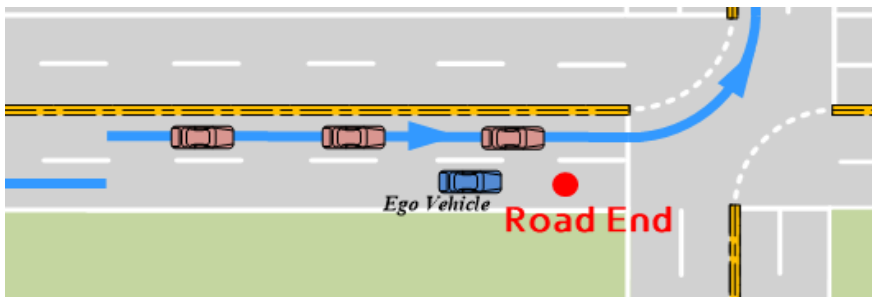
where C_{target} means the space between consecutive front and rear vehicles of target space; L_{vehicle} means the length of the ego vehicle.

5.4. Limit Mode Decision by Road End

One of the most difficult situations in lane change is to change lanes within the limit conditions in the MLC situation. In this study, the lane change is demanded by main path before the road end is reached. However, if there are many vehicles on the target lane and there is no space to change the lane, it may be impossible to succeed the lane change within the limit conditions. Figure 5.12 shows situations where the lane change is impossible in the MLC sections.



(a) Road end on highway road.



(b) Road end on urban road.

Figure 5.12. Situations where the lane change is impossible in the MLC sections.

In this case, it is necessary to determine a driving mode decision and an appropriate motion planning. In this research, the concept of ‘limit mode’ and ‘limit velocity’ have been developed. Limit mode is decided by the remained distance for ego vehicle to reach road end. The remained distance is determined from road end with a certain margin as follows:

$$d_{\text{lim}} = d_{\text{road-end}} - (v_e \times \sqrt{(2 \times W) / a_{y,\text{evasive}}} + d_{\text{margin}}) \quad (5.8)$$

where $d_{\text{road-end}}$ means the distance between ego vehicle and road end; W is road width; $a_{y,\text{evasive}}$ means the lateral acceleration for evasive lane change ($1.5m/s^2$); and d_{margin} means the marginal distance ($10m$).

Normally limit mode is 0 and changes to 2 levels as ego vehicle approaches the road end. First, limit mode changes to 1 as the ego vehicle approaches the road end. When limit mode is 1, the lane change is demanded for the lane toward main path. And before the ego vehicle reaches the road end, the limit velocity is planned by the velocity at which the ego vehicle can perform the lane change. Second, when the planned limit velocity changes below threshold velocity, the limit mode changes to 2. In this case, stop or go motion is required. The driving mode is unconditionally the LC mode. And, according to lane change risk, the limit velocity is set to the stop velocity or the minimum limit velocity. This process is expressed in Algorithm 5. A lane change time is described in detail in the following Chapter 6.

Algorithm 5 : Limit Mode and Limit Velocity Decision

```
1: Inputs: set velocity ( $v_{set}$ ), remained distance of road end ( $d_{lim}$ ), lane
   change time ( $t_{LC}$ ), minimum limit velocity ( $v_{lim.min} = 5kph$ ), lane change
   risk condition.
2:  $mode_{lim} = 0$ ,  $v_{lim} = v_{set}$ 
3: if ( $d_{lim} < v_{set} \times t_{LC}$ )
4:      $mode_{lim} = 1$ ,  $v_{lim} = d_{lim} / t_{LC}$ ,  $Pr_{demand} = 1$ 
5:     if ( $v_{lim} < v_{lim.min}$ )
6:          $mode_{lim} = 2$ ,  $v_{lim} = v_{lim.min}$ ,  $Pr_{possibility} = 1$ 
7:         if lane change risk condition
8:              $v_{lim} = -1 kph$ 
9:     end if
```

Chapter 6 Motion Planning and Control

Desired motion is planned according to the driving mode decided above. In motion planning, reference and bound of states are determined. For tracking planned motion, a SMPC is utilized [Suh,'18]. Solver FORCES is used to solve the problem of SMPC [Domahidi,'14]. The solver is operated in MATLAB. Since the distributed vehicle model is used, motion planning and control are also divided into longitudinal and lateral motions. Figure 6.1 shows the overall architecture of motion planning and control.

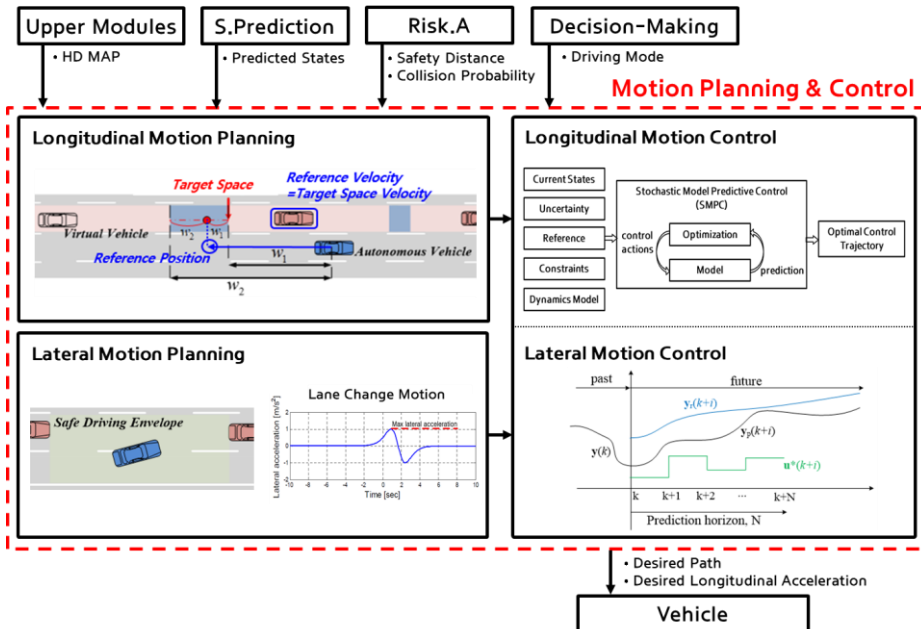


Figure 6.1. Overall architecture of motion planning and control.

6.1. Longitudinal Motion Planning and Control

In the longitudinal motion planning, references and bounds of the longitudinal states are determined as shown in Figure 6.2. The longitudinal states consist of position, velocity, and acceleration. For reference, velocity and position are used as reference states and are as follows:

$$\bar{x}_{lon,ref} = [p_{ref} \quad v_{ref} \quad 0]^T \quad (6.1)$$

where subscript *ref* denotes the reference of states.

For bounds, the position is only considered. A safe driving envelope is defined for collision avoidance. The envelope is shown as green box in Figure 6.2. To guarantee safe driving, the envelope is decided as an area in which the ego vehicle could drive without collision with surrounding vehicles. The bounds can be expressed as:

$$p_{bound} = [p_{min} \quad p_{max}]^T \quad (6.2)$$

where *min* and *max* mean the upper (resp. lower) bound of the safe driving envelope.

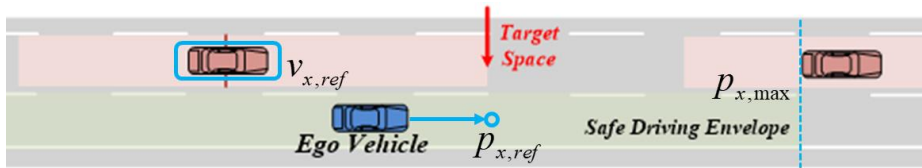


Figure 6.2. Reference and bound of longitudinal motion planning.

The first priority goal of autonomous vehicles is to prevent collisions with surrounding vehicles and maintain safety. Therefore, the planning and control of longitudinal motion for this is the first priority. In any driving mode, this always be taken into account. A vehicle subject to such safety control is designated as ‘risky vehicle’. In general, the risky vehicle is the preceding vehicle as shown in Figure 6.3. Primarily, the preceding vehicle refers to a vehicle located directly in front of the same lane as an autonomous vehicle.

In this research, it is determined whether the autonomous vehicle and surrounding vehicle collide through collision probability. Therefore, not only preceding vehicle in the general situation, but all vehicles in which collision probability exists are considered to be the risky vehicle. This concept is shown in Figure 6.4.

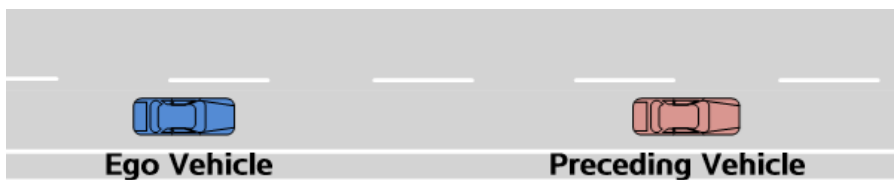
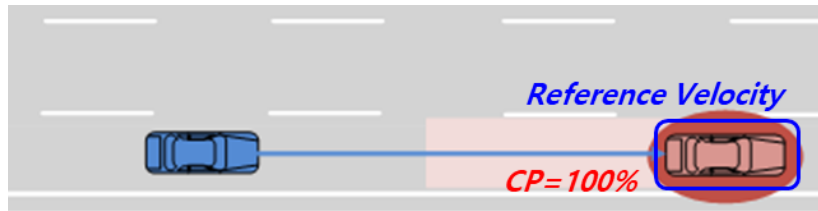
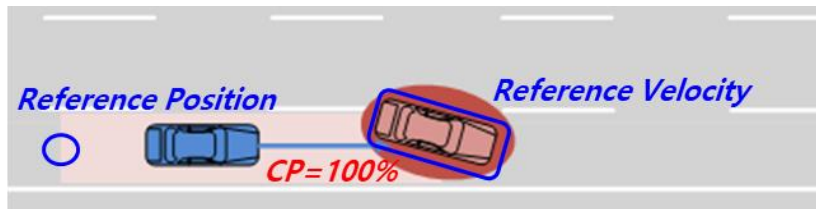


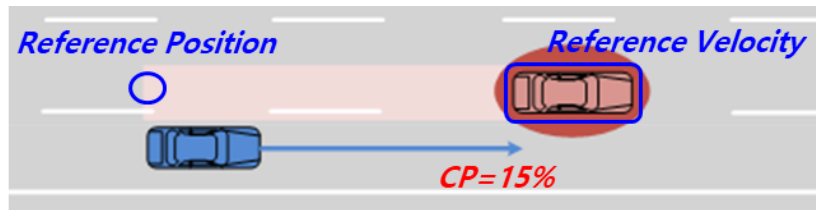
Figure 6.3. Preceding vehicle in lane keeping driving.



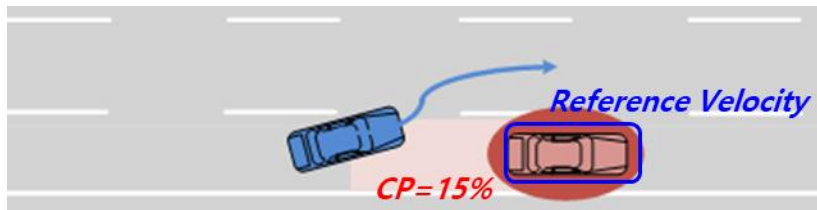
(a) Velocity matching for far preceding vehicle.



(b) Safety with cut-in vehicle.



(c) Passing with biased side vehicle.



(d) Overtaking with low collision risk vehicle.

Figure 6.4. Risky vehicles based on collision probability.

In any mode, the reference of states are determined by a risky vehicle which has probability of collision with ego vehicle. The states of risky vehicle are

expressed as *risk* by subscript. The reference velocity is decided as the set velocity or the velocity of a risky vehicle. It is inefficient to follow the velocity of the risky vehicle identically when the risky vehicle is too far away, as shown in Figure 6.4 (a). Therefore, the distance to the risky vehicle affects the reference velocity. The reference position is set to prevent a rear collision when a risky vehicle is closer than SD_{LK} . This could be the case when a side vehicle cuts-in, as shown in Figure 6.4 (b). For risk vehicles, the reference states are expressed as:

$$v_{ref, risk} = \begin{cases} CP_{risk} \times v_{risk} + (1 - CP_{risk}) \times v_{set} & \text{if } p_{risk} < SD_{LK} \\ CP_{risk} \times v_{safe} + (1 - CP_{risk}) \times v_{set} & \text{otherwise} \end{cases}$$

$$\text{s.t. } v_{safe} = \alpha \cdot v_{set} + (1 - \alpha) \cdot v_{risk} \quad (6.3)$$

$$\alpha = \frac{p_{risk} - SD_{LK}}{p_{risk}}$$

$$p_{ref, risk} = CP \times \min[0, p_{risk} - SD_{LK}] \quad (6.4)$$

where subscript *risk* means states of risky vehicles that have collision probability; subscript *ref, risk* means reference states for safety control of risky vehicles; α is variable for velocity matching with far risky vehicle.

In any mode, the bounds of risky vehicle can be expressed as:

$$p_{min, risk} = -p_{sp}$$

$$p_{max, risk} = \min[p_{sp}, p_{risk}] \quad (6.5)$$

where p_{sp} denotes the open distance when the vehicle blocking the safety envelope does not exits (100 m).

There is a special case for risky targets. It is a situation where the ego vehicle is overtaking a stationary vehicle. In the overtaking situation, if the ego vehicle considers the risky target as shown in Figure 6.5, the ego vehicle may not be

able to overtake preceding vehicle and stop forever. Therefore, the overtaking velocity has been developed in this dissertation.

$$\begin{aligned}
 v_{ref, risk} &= \begin{cases} v_{ref, ov} & , \text{ if LC mode} \\ v_{ref, risk} & , \text{ else} \end{cases} \\
 \text{s.t. } v_{ref, ov} &= \begin{cases} p_{stat} / t_{LC} & , \text{ if } TTC_{stat} < t_{LC} \\ v_{set} & , \text{ else} \end{cases} \\
 TTC_{stat} &= p_{stat} / v
 \end{aligned} \tag{6.6}$$

where subscript *stat* means stationary vehicle; TTC_{stat} denotes time to collision of stationary vehicle; t_{LC} is lane change time; $v_{ref, ov}$ denotes overtaking velocity.

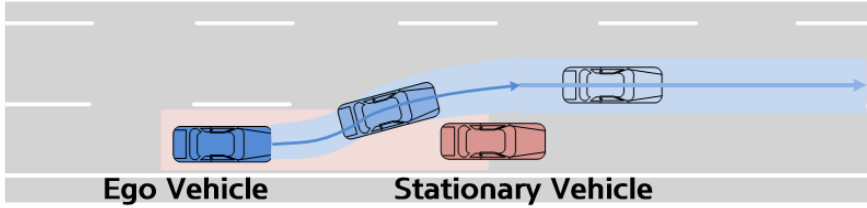


Figure 6.5. Overtaking is possible, but the ego vehicle is forever stopped.

For active lane change driving, longitudinal motion planning beyond collision avoidance is necessary. If the lane change is demanded by driving mode decision algorithm, the ego vehicle must perform the lane change objective. For this purpose of lane change, it is required to drive to the target space developed in this study. The behavior for this purpose is named ‘side’. The states of side vehicle are expressed as *side* by subscript. The motion plan for side vehicles is affected by the driving mode. Only in LKC mode or LC mode when the lane change is demanded, the motion plan of side vehicles is

proceeded. The side velocity is determined with v_{space} . The side position is also determined as an internecine point by the SD_{LC} of the consecutive vehicles in the target space. Figure 6.6 represents reference position planning for the side vehicles. For side vehicle of lane change objective, the reference states are expressed as:

$$v_{ref, side} = v_{space} \quad (6.7)$$

$$\begin{aligned} p_{ref, side} &= \min[p_{safe1}, p_{safe2}] \\ \text{s.t. } p_{safe1} &= p_{prc} - SD_{LK} \\ p_{safe2} &= \frac{w_2(p_{spf} - SD_{LC, spf}) + w_1(p_{spr} + SD_{LC, spr})}{w_1 + w_2} \\ w_1 &= |p_{spf} - SD_{LC, spf}| \\ w_2 &= |p_{spr} + SD_{LC, spr}| \end{aligned} \quad (6.8)$$

where subscript *spf* means the vehicle in front of target space; subscript *spr* means the vehicle behind target space; and subscript *ref, side* means reference states for going target space of side vehicles

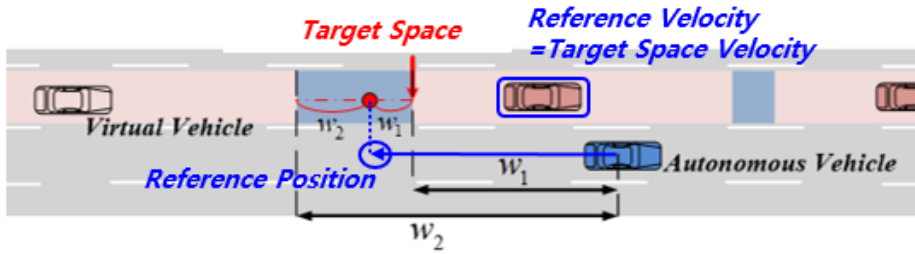


Figure 6.6. Desired motion planning for side vehicles.

For side vehicles, the upper and lower bound can be expressed as:

$$\begin{aligned} p_{\min, side} &= \begin{cases} -p_{sp}, & \text{if } p_{spr} > 0 \\ p_{spr}, & \text{else} \end{cases} \\ p_{\max, side} &= \begin{cases} p_{spf}, & \text{if } p_{spf} > 0 \\ p_{sp}, & \text{else} \end{cases} \end{aligned} \quad (6.9)$$

Autonomous vehicles must comply with the regulated speed according to the road environment. Therefore, v_{ref} is determined as v_{set} , when the calculated v_{ref} is greater than v_{set} . Also, whether or not the ego vehicle have crossed the lane determines the longitudinal motion plan. When performing lane change in LC mode and crossing the lane, there is no need to plan the motion for side vehicles anymore. Therefore, at this time, even in LC mode, the motion plan is proceeded only for risky vehicle as shown in Figure 6.7. Therefore, the final motion plan considering this is as follows.

$$v_{ref} = \begin{cases} \min[v_{set}, v_{ref, risk}, v_{ref, side}], & \text{before crossing lane} \\ \min[v_{set}, v_{ref, risk}] & , \quad \text{after crossing lane} \end{cases} \quad (6.10)$$

$$p_{ref} = \begin{cases} \min[p_{ref, risk}, p_{ref, side}], & \text{before crossing lane} \\ p_{ref, risk} & , \quad \text{after crossing lane} \end{cases} \quad (6.11)$$

$$p_{\min} = \begin{cases} \min[p_{\min, risk}, p_{\min, side}], & \text{before crossing lane} \\ p_{\min, risk} & , \quad \text{after crossing lane} \end{cases} \quad (6.12)$$

$$p_{\max} = \begin{cases} \min[p_{\max, risk}, p_{\max, side}], & \text{before crossing lane} \\ p_{\max, risk} & , \quad \text{after crossing lane} \end{cases} \quad (6.13)$$

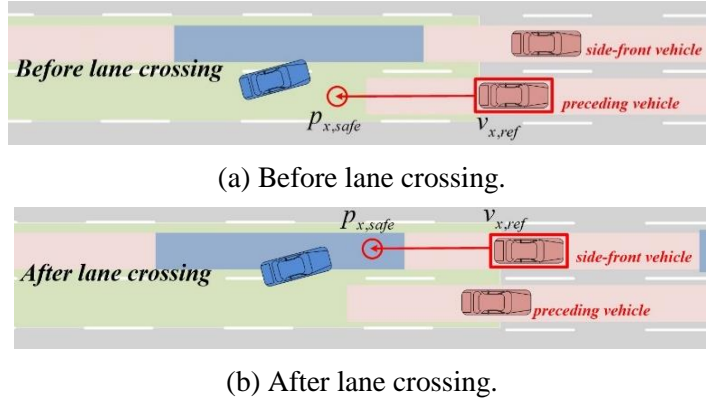


Figure 6.7. Final motion planning based on driving mode and lane crossing.

In order to proceed with autonomous driving in all driving sections, a time occurs when considering road end as specifically described in section 5.4. Depending on limit, limit velocity needs to be reflected in the motion plan. In the MLC situation, it is necessary to complete the lane change without going beyond the road end. Therefore, as the ego vehicle gets closer to the road limit, the ego vehicle must drive at a speed of limit velocity or lower. When limit mode does not turn on, limit velocity is set velocity. The velocity plan reflecting limit mode is as follows.

$$v_{ref} = \min[v_{ref}, v_{lim}] \quad (6.14)$$

In prediction horizon, all references and constrains are calculated. Reference velocity in prediction horizon is shown in Figure 6.8. All states are decided based on prediction information. For the planned behavior, the control inputs are calculated using model predictive control. Therefore, the control inputs are determined taking into account future motions of ego vehicle and surrounding vehicles.

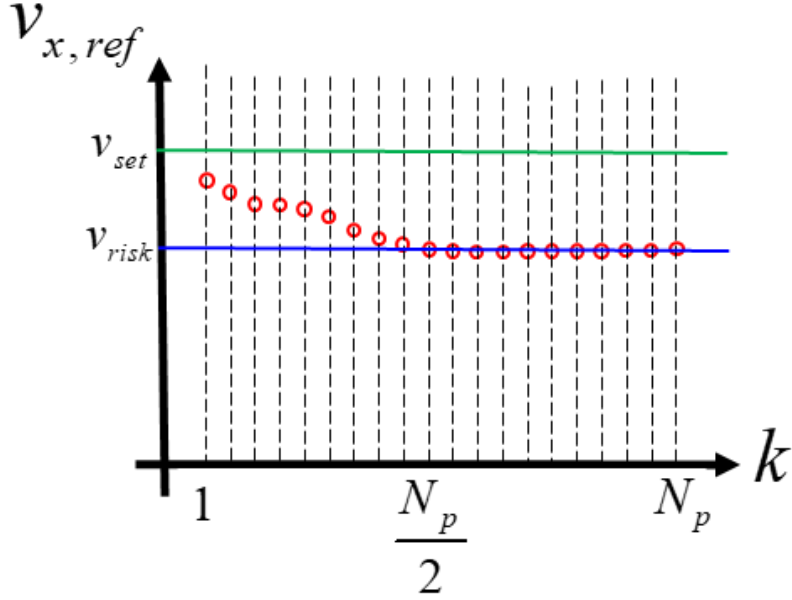


Figure 6.8. Reference velocity in prediction horizon.

The SMPC problem is presented to calculate the desired longitudinal acceleration. The SMPC problem is formulated with the vehicle dynamics model, reference, bound, and input constraint. Repeating at each time step, the solving process of the optimization problem is formulated as follows:

$$\begin{aligned}
 & \min \sum_{n=0}^{N_p-1} \mathbb{E} \left(\left\| \bar{x}_{lon}(n+1) - \bar{x}_{lon,ref}(n+1) \right\|_{\mathbf{Q}_{long}}^2 + \left\| u_{lon}(n) \right\|_{\mathbf{R}_{long}}^2 \right) \\
 & \text{s.t. } \bar{x}_{lon}(n+1) = A_{lon}(n)\bar{x}_{lon}(n) + B_{lon}(n)u_{lon}(n) \\
 & \quad \Pr \left(g_{lon}^T(n+1)x_{lon}(n+1) \leq \bar{x}_{lon,bound}(n+1) \right) \geq 1 - \varepsilon_{lon}(n) \\
 & \quad g_{lon} = \begin{bmatrix} 1 & 0 & 0 \\ -1 & 0 & 0 \end{bmatrix}^T \\
 & \quad u_{lon,min} \leq u_{lon}(n) \leq u_{lon,max} \\
 & \quad (n = 0, \dots, N_p - 1)
 \end{aligned} \tag{6.15}$$

where Q_{lon} and R_{lon} are the state and input weighting matrix of longitudinal states. $\bar{x}_{lon}(n)$ is the predicted longitudinal states of ego vehicle at time $t+n$ derived by applying the control sequence u_{lon} to the longitudinal model Equation (3.6) with initial condition $\bar{x}_{lon}(0) = \bar{x}_{lon}(t)$. g_{lon} and $x_{lon, bound}$ are related to a longitudinal safe driving envelope, which is defined to guarantee collision avoidance. ε_{lon} is the longitudinal risk parameter, which is related to a chance constraint to be satisfied with a specified probability. By this parameter, it becomes SMPC, not MPC. The details of SMPC is described in [Suh,'18]. $u_{lon, min}$ and $u_{lon, max}$ denote longitudinal control input constraints. Table 9 presents the parameters of the longitudinal SMPC problem.

Table 9. Parameters of the longitudinal SMPC problem

Parameter	Value
Q_{long}	$diag(10, 40, 0)$
R_{long}	80
$u_{lon, max}$	$-3 [m / s^2]$
$u_{lon, min}$	$1.5 [m / s^2]$

6.2. Lateral Motion Planning and Control

In the lateral motion planning, references and bounds of the longitudinal states are determined. The lateral states consist of sideslip angle, yaw rate, lateral position, and yaw angle. Reference state of sideslip angle is always zero, which improves stability. Yaw rate could be represented as a lateral position [Rajamani,'11]. Desired state of yaw angle is determined by road curvature, which improves road following. Therefore, the only lateral position is the target of motion planning. Reference states of lateral motion are followed:

$$\begin{aligned}\bar{x}_{lat,ref} &= \begin{bmatrix} \beta_{ref} & \gamma_{ref} & e_{\psi,ref} & e_{y,ref} \end{bmatrix}^T \\ &= \begin{bmatrix} 0 & \frac{\ddot{e}_{y,ref}}{v_x} & p \cdot \rho & e_{y,ref} \end{bmatrix}^T\end{aligned}\quad (6.16)$$

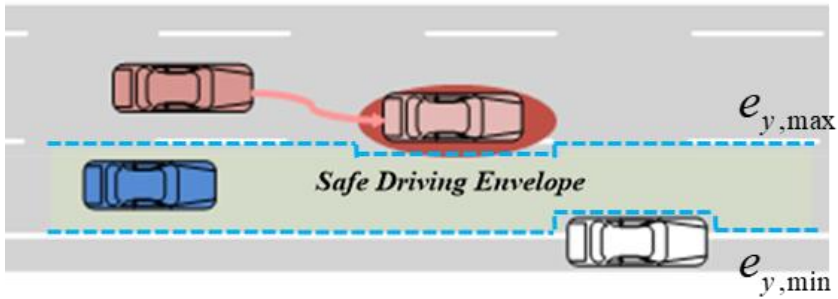
For bounds, the position is only considered. Like longitudinal motion planning, a safe driving envelope is defined for collision avoidance. The envelope is shown as green box in Figure 6.8. To guarantee safe driving, the envelope is decided as an area in which the ego vehicle could drive without collision with surrounding vehicles. The bounds can be expressed as:

$$\bar{x}_{lat,bound} = \begin{bmatrix} e_{y,min} & e_{y,max} \end{bmatrix}^T \quad (6.17)$$

where \min and \max mean the lower (resp. upper) boundary of the safe driving envelope.

Lateral motion planning is conducted based on driving mode shown in Figure 6.9. Basically, a desired motion is planned to keep within the designated lane

according to the driving mode. The location of surrounding vehicles can act as a more powerful upper or lower bound than the lane depending on the collision probability of side vehicles. Figure 6.9 (a) shows this concepts of lateral motion planning affected by side vehicles.



(a) Lateral motion planning in LK or LKC mode.



(b) Lateral motion planning in LC mode.

Figure 6.9. Lateral motion planning based on driving mode.

In LK mode or LKC mode, the desired lateral position is defined as zero, which means that the vehicle tracks the centerline. In the LC mode, the desired lateral position is defined as the hyperbolic tangent path. This desired position reflects the lane change and has a low acceleration jerk [Suh,'18]. As shown in

Figure 6.10, only lateral acceleration limit is the tuning parameter that determines the lane change time. In LC mode, the desired lateral position could be given by:

$$e_{y,ref} = \begin{cases} C_1 \cdot \tanh(C_2 \cdot k + C_4) + C_3 + e_{y,0}, & \text{if LC mode} \\ 0, & \text{otherwise} \end{cases}$$

$$\text{s.t. } C_1 = \frac{\pm W_{road} - e_{y,0}}{2} \quad C_2 = \sqrt{\frac{\pm a_{y,lim}}{a_{y,0} \cdot C_1}} \quad (6.18)$$

$$C_4 = \frac{\pm W_{road} - e_{y,0}}{2} \quad C_3 = -\frac{t_{LC}}{2} C_2$$

$$t_{LC} = \frac{2}{C_2} \tanh^{-1} \left\{ \frac{W_{road} - C_4 - e_{y,0}}{C_1} \right\}$$

where subscript $a_{y,lim}$ is the lateral acceleration limit; W_{road} is the road width; and t_{LC} is the lane change time.

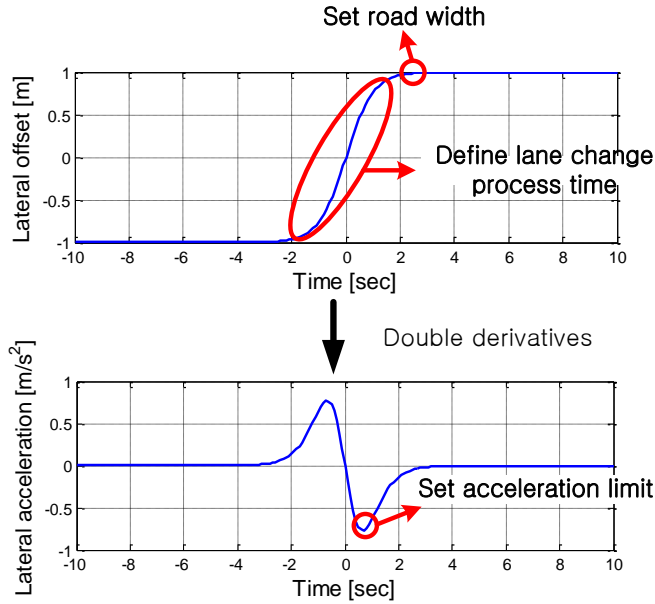


Figure 6.10. Lane change motion planning of lane change maneuver.

Special case of lane keeping is transmitting lane change intention to vehicles on target lane. When traffic pressure mode turns on, the ego vehicle does not follow the center of the path even though driving mode is LC mode. To transmit lane change intention actively, reference of lateral position is slightly movement from the current lane center to the direction of the lane that is target of pressure. In traffic pressure mode, equations of lateral states reference can be given by:

$$e_{y,ref} = \pm \frac{W_{road}}{2} \mp \frac{W_{vehicle}}{2} \mp \varepsilon_y \quad (6.19)$$

where ε_y is the degree to which traffic pressure is applied strongly.

The ego vehicle basically have to drive within a defined lane. The bounds of lateral position are determined depending on what direction to perform the lane change. The bound can be expressed as:

$$\begin{bmatrix} e_{y,min} & e_{y,max} \end{bmatrix}^T = \begin{cases} \begin{bmatrix} \frac{3}{2}W_{road} & -\frac{1}{2}W_{road} \end{bmatrix}^T & \text{if left lane change} \\ \begin{bmatrix} \frac{1}{2}W_{road} & -\frac{3}{2}W_{road} \end{bmatrix}^T & \text{elseif right lane change} \\ \begin{bmatrix} \frac{1}{2}W_{road} & -\frac{1}{2}W_{road} \end{bmatrix}^T & \text{otherwise} \end{cases} \quad (6.20)$$

In addition to the lane, the surrounding vehicles must be additionally considered to prevent collision. The vehicle with collision probability among the vehicles on the right lane influences the determination of lower bound of lateral state, which can be expressed as:

$$e_{y,min} = \max[e_{y,min}, p_{y,risk} + \sigma_{y,risk}] \quad (6.21)$$

The vehicle with collision probability among the vehicles on the left lane influences the determination of upper bound of lateral state, which can be expressed as:

$$e_{y,\max} = \min[e_{y,\max} \cdot p_{y,risk} + \sigma_{y,risk}] \quad (6.22)$$

The SMPC problem is presented to calculate the desired steering angle. The SMPC problem is formulated considering the vehicle dynamics model, reference, constraints, and input limit. Repeating at each time step, the solving process of the optimization problem is formulated as follows:

$$\begin{aligned} \min \quad & \sum_{n=0}^{N_p-1} \mathbb{E} \left(\left\| \bar{x}_{lat}(n+1) - \bar{x}_{lat,ref}(n+1) \right\|_{Q_{lat}}^2 + \left\| u_{lon}(n) \right\|_{R_{lat}}^2 \right) \\ \text{s.t.} \quad & \bar{x}_{lat}(n+1) = A_{lat}(n) \bar{x}_{lat}(n) + B_{lat}(n) u_{lat}(n) + F_{lat}(n) \rho \\ & \Pr \left(g_{lat}^T(n+1) x_{lat}(n+1) \leq \bar{x}_{lat,bound}(n+1) \right) \geq 1 - \varepsilon_{lat}(n) \\ & g_{lat} = \begin{bmatrix} 0 & 0 & 0 & 1 \\ 0 & 0 & 0 & -1 \end{bmatrix}^T \\ & |u_{lat}(n)| \leq u_{lat,\lim} \\ & |u_{lat}(n+1) - u_{lat}(n)| \leq \dot{u}_{lat,\lim} \\ & (n = 0, \dots, N_p - 1) \end{aligned} \quad (6.23)$$

where Q_{lat} and R_{lat} are the state and input weighting matrix of lateral states. $\bar{x}_{lat}(n)$ is the predicted lateral states of ego vehicle at time $t+n$ derived by applying the control sequence u_{lat} to the longitudinal model Equation (3.7) with initial condition $\bar{x}_{lat}(0) = \bar{x}_{lat}(t)$. g_{lat} and $x_{lat,bound}$ are related to a longitudinal safe driving envelope, which is defined to guarantee collision avoidance. ε_{lat} is the longitudinal risk parameter, which is related to a chance constraint to be satisfied with a specified probability. By this parameter, it becomes SMPC, not MPC. The details of SMPC is described in [Suh,'18].

$u_{lat,lim}$ denotes the maximum magnitude of the lateral control input. $\dot{u}_{lat,lim}$ denotes the maximum magnitude of the rate of change of the lateral control input. Table 10 presents the parameters of the lateral SMPC problem.

Table 10. Parameters of the lateral SMPC problem

Parameter	Value
Q_{lat}	$\begin{cases} diag(200,160,10,10), & \text{if LC mode} \\ diag(100,200,60,10), & \text{else} \end{cases}$
R_{lat}	60
$u_{lat,lim}$	180 [deg]
$\dot{u}_{lat,lim}$	80 [deg/ s]

Chapter 7 Performance Evaluation

7.1. Simulation Test

We evaluated the proposed algorithm through simulation test. Simulation test is essential before performing vehicle test. In this research, the performance of the proposed algorithm was evaluated through various simulations before vehicle test. Simulation can reproduce various situations repeatedly before the actual vehicle test. Therefore, it is possible to validate the performance of the algorithm in various situations. In addition, simulation test plays an important role when comparing the performance of different algorithms. By evaluating several algorithms for the same situation, it is possible to confirm the improvement of the proposed algorithm.

7.1.1. Simulation Environment

Simulation is a step of evaluating the algorithm before vehicle test, so it is important to simulate the actual vehicle situation similarly. We constructed our own simulation environment based on MATLAB. It is easy to change and compatible with the proposed algorithm. The structure of the developed simulation environment is shown in Figure 7.1.

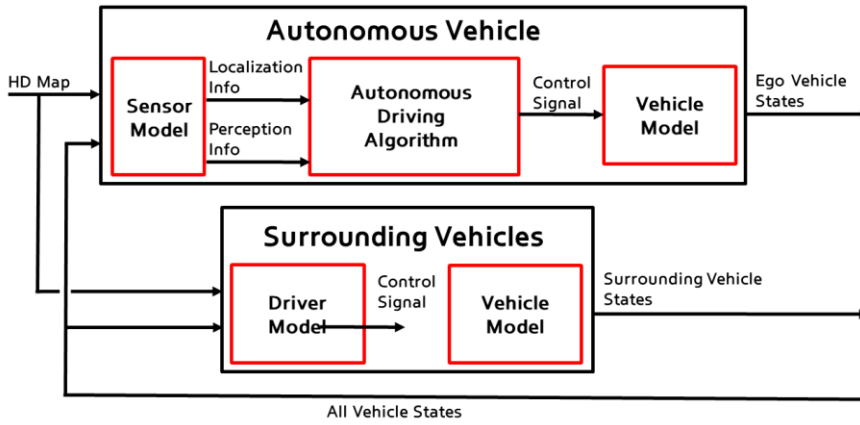


Figure 7.1. Configuration of multi-vehicle simulation tool.

The following models are important for the simulation of autonomous vehicles: road model, vehicle model, sensor model, control module model and driver model. The high definition map built on the actual road was used as a road model. The vehicle model was a kinematic model which is the simplest vehicle model. Since autonomous driving does not drive to the extreme performance of the vehicle, a kinematic model is adopted for simplicity of tuning and efficiency of simulation [Lee,'16]. The vehicle model is applied to all vehicles of the autonomous vehicle and surrounding vehicles. To describe vehicle motions, the state vector and input vector are defined as follows:

$$\mathbf{x}_n = [x \quad y \quad \theta \quad v_x \quad a_x]^T \quad (7.1)$$

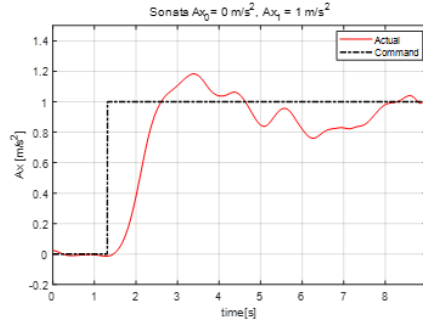
$$\mathbf{u} = [a_x \quad \delta_f]^T \quad (7.2)$$

The vehicle dynamics is shown as follows:

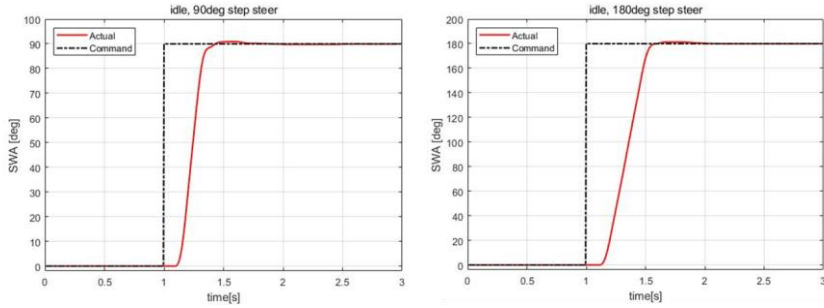
$$\begin{aligned} \dot{x} &= v_x \cos(\psi) \\ \dot{y} &= v_x \sin(\psi) \\ \dot{\theta} &= v_x \tan(\delta_f) / L_{vehicle} \\ \dot{v}_x &= a_x \end{aligned} \quad (7.3)$$

The sensor model only applies to the autonomous vehicle. In the sensor model, the recognition range and the accuracy of state estimation of surrounding vehicles are important. These are affected by the perception module of the autonomous vehicle. In this study, a total of three perception modules were used [Lee,'19, Lee,'20]. We analyzed the performance of each perception module and reflected it in the sensor model of the simulation.

The control module model is applied only to the autonomous vehicle. This is a model that embodies how it is reflected in the vehicle when the final control input of the autonomous vehicle is transmitted. In fact, if the control inputs are transmitted to the vehicle, the vehicle cannot track control inputs perfectly because of diverse delay and uncertainty. In this study, a total of three vehicles are used. We analyzed the performance of each control module and reflected it in the control module model of the simulation. Figure 7.2 represents the result of the analysis of the response to the control input of a vehicle.



(a) Longitudinal acceleration.



(b) Steering angle.

Figure 7.2. Control response analysis.

Autonomous vehicle is driven by the proposed algorithm, but surrounding vehicles must drive like real drivers. Therefore, the driver model is necessary to simulate the actual driving environment. Since the proposed algorithm proposed is for lane change maneuver, surrounding vehicles only perform lane keeping maneuver. Therefore, the driver model of the surrounding vehicles only needs to consider the clearance characteristics with preceding vehicle. To develop the adaptive cruise control algorithm, the driving characteristics were studied [Moon,'08]. These driving characteristics have been used for driver model in simulation test.

7.1.2. Overtaking simulation for decision-making evaluation

Overtaking is important situation in decision-making for lane change behavior. In the overtaking, speediness is important as well as maintaining safety with surrounding vehicles by changing the lane in the DLC situation. In order to evaluate the performance of the proposed algorithm, it was compared with the algorithms of other methods.

The first algorithm to be compared is to use the traffic flow [Suh,'16]. In DLC, when the velocity of the preceding vehicle is much slower than the set velocity of the ego vehicle, a lane change is demanded. However, the ego vehicle does not need to change the lane in this situation if it involves taking a risk. Therefore, the traffic flow speed of adjacent lanes should be considered. In previous research, traffic flow is characterized by microscopic and macroscopic points of view [Li,'04]. This dissertation focuses on the microscopic point of view because local sensors of the ego vehicle can only measure a limited area. A problem occurs if traffic flow is simply defined as the average speed of the side lane vehicles in the recognition range. The traffic flow is set to the average speed, considering the weight according to the distance, since the speed of the vehicles is more meaningful as the distance of the recognized vehicle is closer. Traffic flows on left and right lanes are defined using the recursive least square method with forgetting factors. The cost function of recursive least square with forgetting factors is as follows:

$$J(\hat{v}_{flow}) = \frac{1}{2} \sum_{k=1}^N \lambda^{t-k} \|\bar{v}(k|t) - \hat{v}_{flow}\|_2^2 \quad (7.4)$$

where λ denotes the forgetting factor; t denotes the current time; \bar{v}

denotes the average speed weighted by the distance of the object vehicles during a near future, which can be estimated from the object vehicle prediction; and \hat{v}_{flow} denotes traffic flow. \bar{v} is as follows:

$$\bar{v}(k|t) = \frac{\sum_{l=1}^m \left[\sum_{k=0}^N (v_{x,l}(k|t) / (N+1)) / \Delta p_{x,l}(t) \right]}{\sum_{l=1}^m [1 / \Delta p_{x,l}(t)]} \quad (7.5)$$

where m denotes the number of target vehicles in the target lane; $v_{x,l}$ denotes the velocity of the l -th target vehicle; and $\Delta p_{x,l}$ denotes the relative position of the l -th target vehicle.

A derivative of equation (7.4) equals zero, which means a minimum cost. From this method, the traffic flow is derived as:

$$\hat{v}_{flow}(t) = \left(\sum_{k=1}^t \lambda^{t-k} \right)^{-1} \left(\sum_{k=1}^t \lambda^{t-k} \times \bar{v}(k|t) \right) \quad (7.6)$$

Substitute $P(t)$ and simple mathematical techniques, traffic flow can be rewritten as:

$$\begin{aligned} \hat{v}_{flow}(t) &= \hat{v}_{flow}(t-1) + P(t) (\bar{v}(k|t) - \hat{v}_{flow}(t-1)) \\ \text{where } P(t) &= \frac{1}{\lambda} \left[P(t-1) - P(t-1) (\lambda I + P(t-1))^{-1} P(t-1) \right] \end{aligned} \quad (7.7)$$

Based on the set velocity of the ego vehicle, the preceding vehicle velocity and traffic flow of adjacent lanes, lane change is demanded. The condition is as follows in a discretional lane change. If three conditions are satisfied, a lane change is demanded.

$$[v_{preceding} \leq (v_{des} - \varepsilon)] \wedge [v_{preceding} \leq \hat{v}_{flow}] \wedge [p_{x,preceding} < 2 \times SD_{LK,preceding}] \quad (7.8)$$

The second algorithm to be compared is to use the supervised learning

method [Chae,'19]. In DLC, when the velocity of the preceding vehicle is much slower than the set velocity of the ego vehicle, a lane change is demanded. In situation of Figure 7.3, it is good to make a lane change between side-front vehicle and side-rear vehicle, but if conducting a lane change behind side-rear vehicle, the autonomous vehicle might face a slower driving situation. It is difficult to judge whether it is possible to enter in front of the side-rear. This is because the autonomous vehicle should consider algorithm operation methods, perception range, control characteristic and diverse uncertainty. The rule-based method could not this complex problem. Also, the rule-based method also has a disadvantage that the performance varies greatly depending on the tuning parameter. To overcome the limitations of the rule-based method, supervised learning method is adopted for overtaking decision.

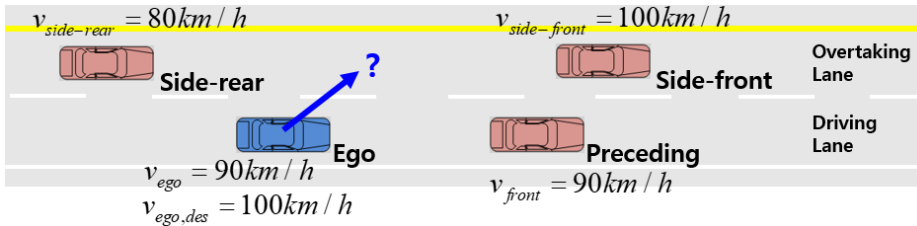


Figure 7.3. Difficult situation to decide lane change demand.

Learning method is adopted to judge whether it would be good or bad to conduct overtaking in various situations. Since it is not possible to implement all situations as actual vehicle conditions, simulation is used for data generation. Figure 7.4 shows the concept of supervised learning. Based on simulation-based data, the training is carried out and overtaking decision machine is

derived. Overtaking is determined based on the learned machine.

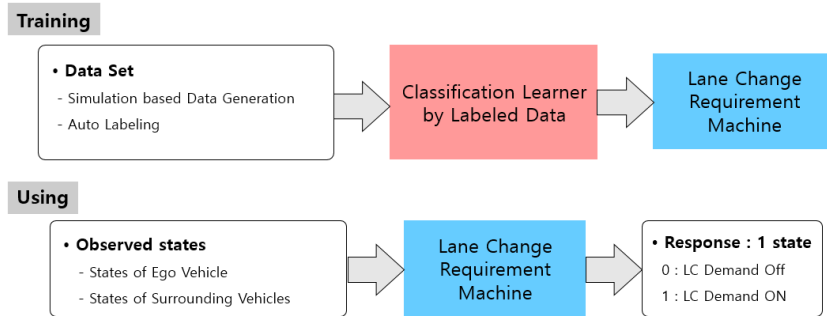
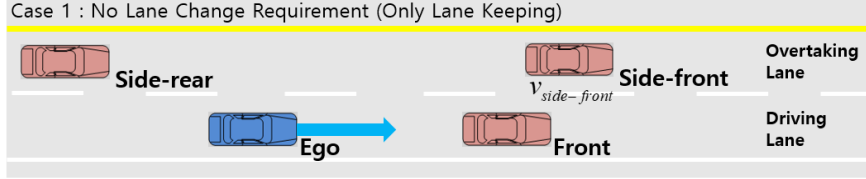


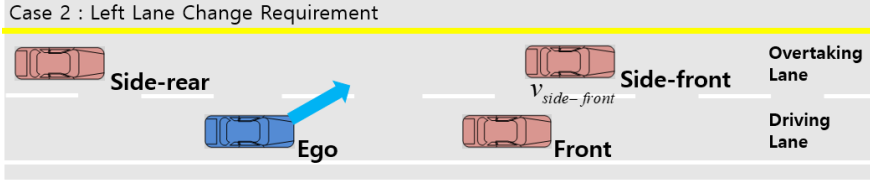
Figure 7.4. Concept of supervised learning for overtaking decision.

Various data sets are needed to develop the learning based the overtaking decision algorithm. A data generation was carried out through simulation studies. In simulation, the ego vehicle is equipped with the autonomous driving algorithm. Lane change demand module is excluded from the autonomous driving algorithm. Surrounding vehicles are tracking a pre-determined velocity and maintaining safety with a preceding vehicle. In the simulation, various situations are implemented by changing the initial condition of all the vehicles, and one simulation means one episode. A number of simulations are conducted for episode generation with changing to initial conditions as equation (7.9). Overall episode number is 18,750. Since there is the two case that overtaking is required or not, two simulations are carried out for each episode as shown in Figure 7.5. Simulation time is 60 sec and sampling time is 0.1 sec.

$$\begin{aligned}
v_{ego} &= 80:10:110 [kph], \quad v_{ego,des} = 110 [kph], \\
v_{front} &= 80:10:110 [kph], \quad \Delta p_{front} = 40:20:80 [m] \\
v_{side-rear} &= 80:10:120 [kph], \quad \Delta p_{side-rear} = -40:20:0 [m] \\
v_{side-front} &= 80:10:120 [kph], \quad \Delta p_{side-front} = 0:20:80 [m]
\end{aligned} \tag{7.9}$$



(a) Case 1: No lane change demand.



(b) Case 2: Left lane change demand.

Figure 7.5. Two case about one episode.

For a supervised learning, it is necessary to determine whether lane keeping is good or overtaking is good for each episode and to label it. In order to consider speediness, the case that the travelled distance is greater is labeled. If the travelled distance of the lane change is slightly bigger than that of the lane keeping, then the lane keeping is better. Also, minimum clearance is considered to reflect safety with surrounding vehicles. In the case of the lane change where minimum clearance is smaller than safe clearance, it is labeled as lane keeping.

Input variables is shown in equation (7.10). Response variable is labeled as 0 or 1 which means the lane keeping is better or the lane change is better. About

entire labelled data sets, the supervised learning is conducted using an ensemble method. The type of the ensemble method is bootstrap aggregating. Learning accuracy is 98.6%. Around 61% of the entire data sets predict that the lane keeping is better, while 39% predicts that the overtaking need to be required.

$$x = [v_{front} - v_{ego}, v_{front} - v_{ego,des}, \Delta p_{front}, v_{side-rear} - v_{ego}, v_{side-rear} - v_{ego,des}, \Delta p_{side-rear}, v_{side-front} - v_{ego}, v_{side-front} - v_{ego,des}, \Delta p_{side-front}] \quad (7.10)$$

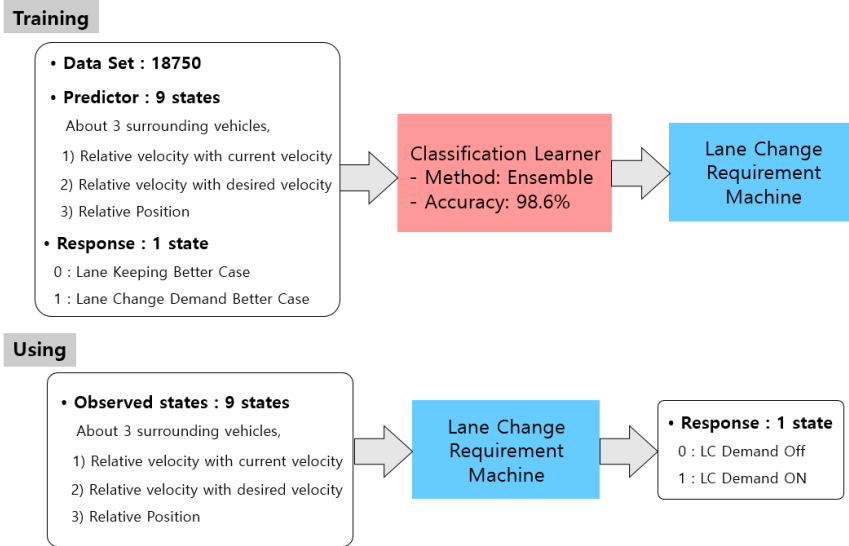


Figure 7.6. Schematic of supervised learning for overtaking decision.

A total of three algorithms have been validated in simulation study: 1) traffic flow based overtaking decision, 2) supervised learning based overtaking decision, 3) desired space velocity based overtaking decision (the proposed algorithm). Figure 7.7 shows simulation environment where there are nine

target vehicles. Initial velocity and desired velocity of target vehicles are less than 110km/h which is the desired velocity of the ego vehicle. This environment could make overtaking situations. Initial condition of all vehicles is shown in Table 11.

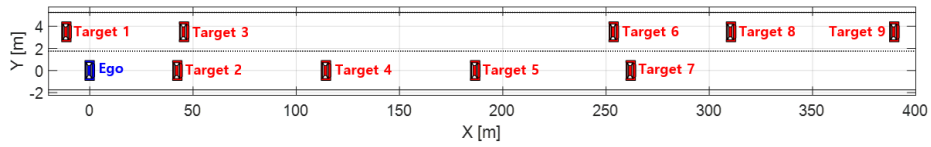


Figure 7.7. Validation simulation initial vehicle disposition.

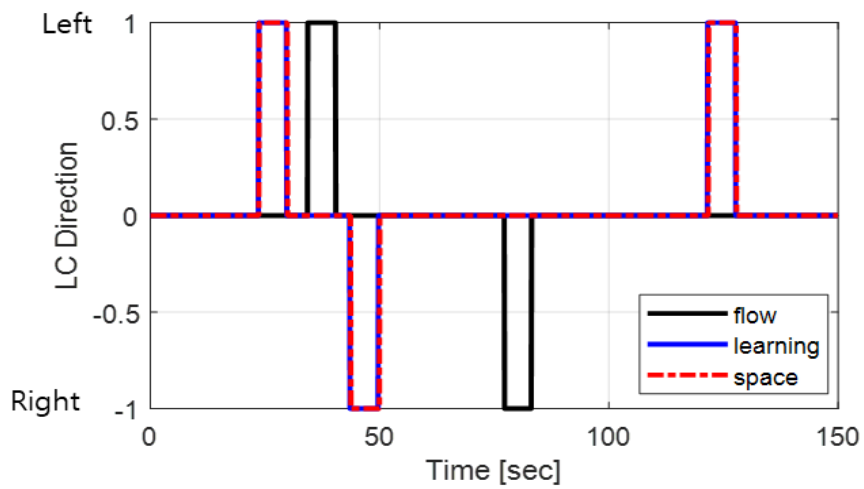
Table 11. Validation Simulation Initial Condition of Vehicles

	<i>Ini X Position</i>	<i>Ini Y Position</i>	<i>Ini Velocity</i>	<i>Set Velocity</i>	<i>Set Time Gap</i>
	<i>[m]</i>	<i>[m] (Lane)</i>	<i>[km/h]</i>	<i>[km/h]</i>	<i>[sec]</i>
<i>Ego</i>	<i>0</i>	<i>0</i>	<i>110</i>	<i>110</i>	<i>-</i>
<i>Target 1</i>	<i>-11</i>	<i>3.5 (1)</i>	<i>80</i>	<i>100</i>	<i>1.3</i>
<i>Target 2</i>	<i>42</i>	<i>0 (2)</i>	<i>90</i>	<i>90</i>	<i>1.3</i>
<i>Target 3</i>	<i>46</i>	<i>3.5 (1)</i>	<i>80</i>	<i>80</i>	<i>1.6</i>
<i>Target 4</i>	<i>114</i>	<i>0 (2)</i>	<i>90</i>	<i>100</i>	<i>0.8</i>
<i>Target 5</i>	<i>187</i>	<i>0 (2)</i>	<i>90</i>	<i>90</i>	<i>1.6</i>
<i>Target 6</i>	<i>254</i>	<i>3.5 (1)</i>	<i>80</i>	<i>100</i>	<i>1.6</i>
<i>Target 7</i>	<i>262</i>		<i>90</i>	<i>90</i>	<i>1.6</i>
<i>Target 8</i>	<i>310</i>	<i>3.5 (1)</i>	<i>80</i>	<i>100</i>	<i>1.3</i>
<i>Target 9</i>	<i>390</i>	<i>3.5 (1)</i>	<i>80</i>	<i>80</i>	<i>1.6</i>

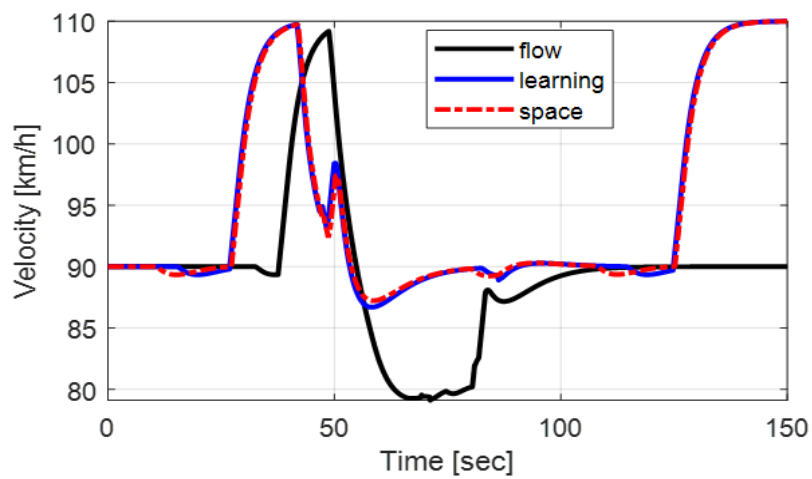
The base models uses the traffic flow based overtaking decision algorithm and the supervised learning based overtaking decision algorithm. The proposed model is the desired space velocity based overtaking decision algorithm. During 150 seconds, the traffic flow based model conducts two lane changes, while the supervised learning based model and proposed model conduct three lane changes. Therefore, the two models traveled more distances without significantly slowing down than the traffic flow based model. Also, the all models keep a minimum clearance of in-lane vehicle above 20m. Average calculation time of overtaking decision algorithms is shown in Table 12. The supervised learning method has a large calculation time. Since traffic flow and desired space methods are rule-based method, calculation time is small. As a results, the proposed decision algorithm has the same excellent performance as learning method and has much less computation time, even though the proposed decision algorithm is rule-based method,

Table 12. Average calculation time of overtaking decision algorithms

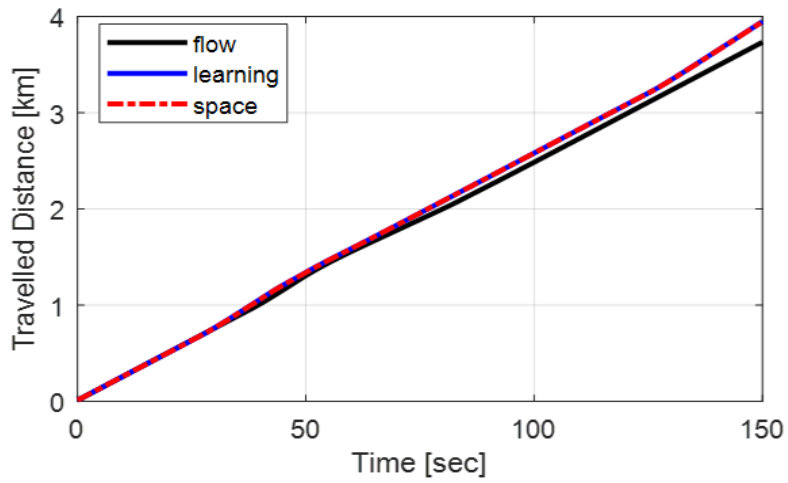
Decision Algorithm	Calculation Time [ms]
Traffic Flow	0.0016
Supervised Learning	1.78
Desired Space Velocity	0.0035



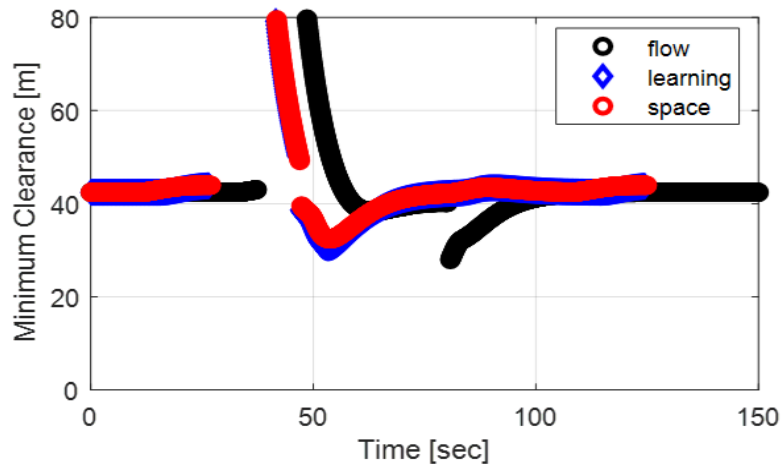
(a) Driving mode.



(b) Velocity.



(c) Travelled distance.



(d) Minimum clearance.

Figure 7.8. Simulation results.

7.1.3. Overtaking simulation to evaluate the effectiveness of virtual vehicle

To evaluate the effectiveness of virtual vehicle, the proposed overtaking algorithm has been evaluated through simulation. The simulation environment is a two-lane straight road. Figure 7.9 and Table 13 represent the initial condition of ego vehicle and surrounding vehicles. Seven surrounding vehicles were placed in arbitrary positions. Surrounding vehicles use the initial velocity as the set velocity and proceeds to safety control if a preceding vehicle exists. The time gap used for safety control is 1.36 s [Moon,'08]. The surrounding vehicles do not change lanes. Vehicle model used in the simulation has input constraints described in SMPC problems. To show the effectiveness of virtual targets, an algorithm without a virtual target has been compared with the proposed algorithm (with the virtual target).

Table 13. Validation Simulation Initial Condition of Vehicles

	<i>X Position [m]</i>	<i>Y Position [m]</i>	<i>Velocity [km/h]</i>
<i>Ego</i>	<i>0</i>	<i>0</i>	<i>100</i>
<i>Target 1</i>	<i>-70</i>	<i>3.5</i>	<i>110</i>
<i>Target 2</i>	<i>-30</i>	<i>3.5</i>	<i>100</i>
<i>Target 3</i>	<i>10</i>	<i>3.5</i>	<i>100</i>
<i>Target 4</i>	<i>68</i>	<i>3.5</i>	<i>90</i>
<i>Target 5</i>	<i>70</i>	<i>0</i>	<i>80</i>
<i>Target 6</i>	<i>110</i>	<i>0</i>	<i>80</i>
<i>Target 7</i>	<i>120</i>	<i>3.5</i>	<i>100</i>

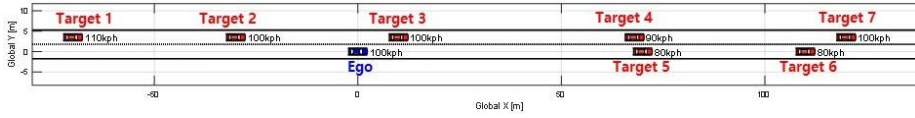
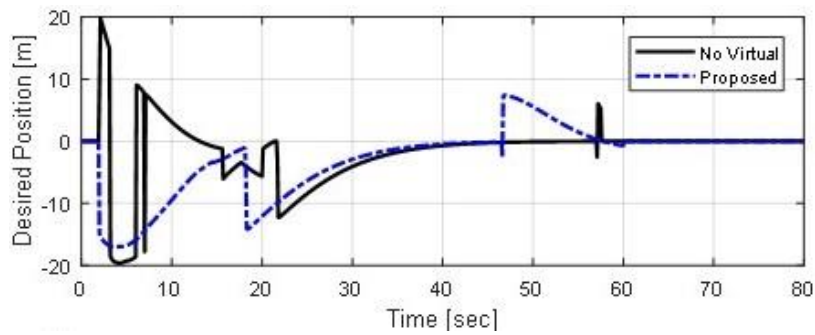
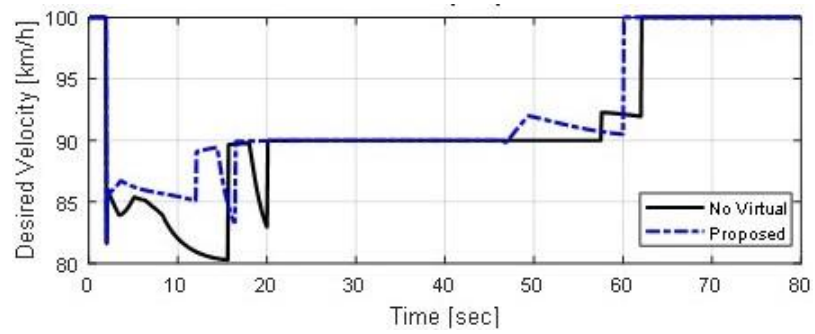


Figure 7.9. The initial condition of the simulation.

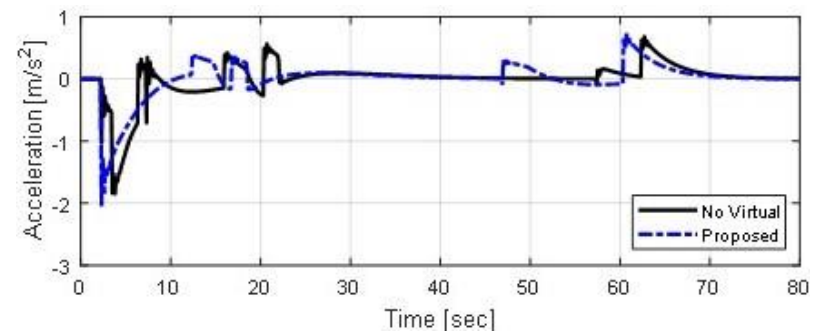
Figure 7.10 shows the simulation results. At two seconds, both algorithms demand the lane change to the overtaking lane because of the slower preceding vehicle. Then no virtual algorithm tries to enter in front of target 3. However, as target 4 is recognized in the perception range, it changes to enter the space between targets 2 and 3. This could be seen through the fluctuating desired position, desired velocity, and acceleration. On the other hand, the proposed algorithm attempts to enter the space between targets 2 and 3 as soon as a lane change is required. This is because the proposed algorithm always thinks virtual targets are placed on the perception range limit. The proposed algorithm could prepare for vehicles coming in outside the perception range. As a result, the proposed algorithm enters the overtaking lane more quickly. Then, it overtakes targets 5 and 6 and returns to the driving lane again. The proposed algorithm travels a greater distance with a smoother acceleration than no virtual algorithm.



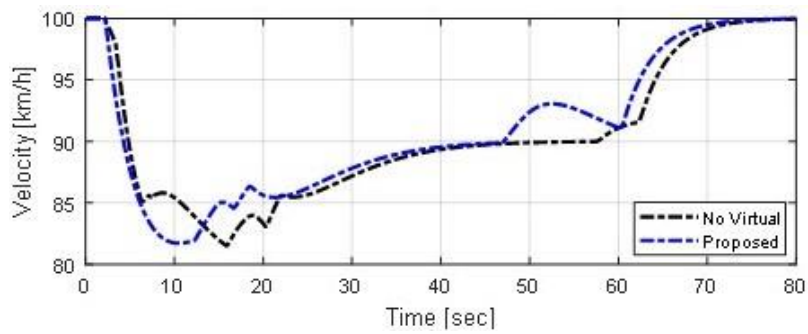
(a) Desired longitudinal position.



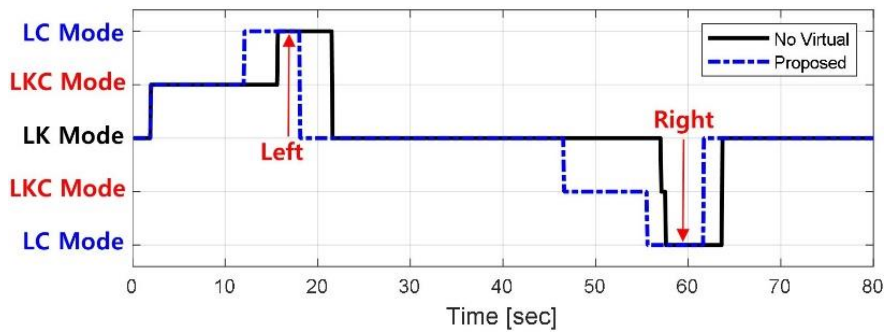
(b) Desired longitudinal velocity.



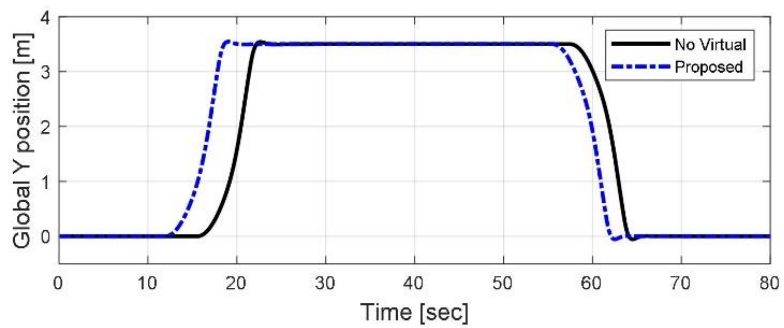
(c) Longitudinal acceleration.



(d) Longitudinal velocity.



(e) Driving mode.



(f) Global Y position.

Figure 7.10. Simulation results.

7.1.4. Simulation about cut-in vehicle safety to evaluate the stochastic risk assessment and the predictive control

The proposed autonomous driving algorithm employs appropriate stochastic predictions. The algorithm guarantees safety and human-like driving based on the stochastic risk assessment and the predictive control reflecting prediction. To evaluate the effectiveness of the stochastic risk assessment and the predictive control, the proposed algorithm has been evaluated through simulation. The situation, in which the front vehicle cuts-in, occurs very frequently on the road. At this time, if the cut-in vehicle is slower than ego vehicle, there is a risk of collision, so proper safety control is required. If the proactive control is reflected, a much safer and more human-like driving is possible.

The simulation environment is a two-lane straight road. Figure 7.11 represents the initial condition of ego vehicle and cut-in vehicle. Simulations are repeated in this environment that can be slightly modified for parameters. Simulation parameters are modified randomly and all parameters are selected to consider occurring in the actual road as shown in equation (7.11). The monte-carlo simulation has been run 145 times.

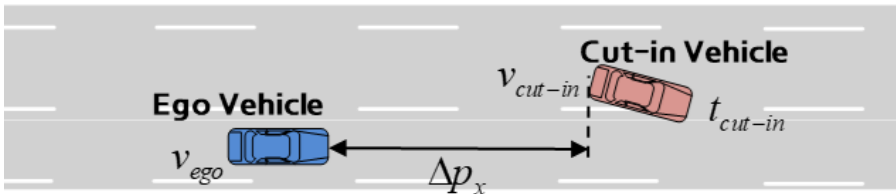
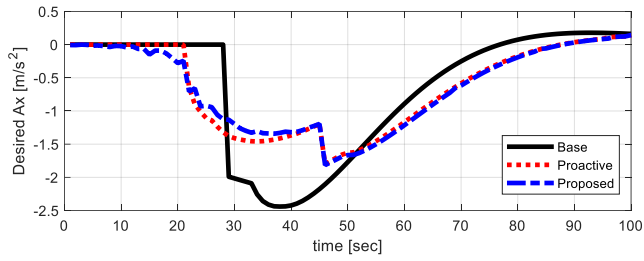


Figure 7.11. The initial condition of the simulation.

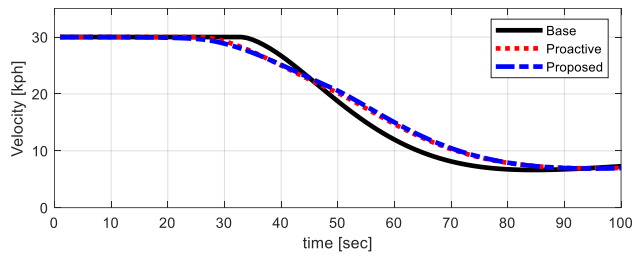
$$\begin{aligned}
v_{ego} &= 30 \text{ } kph \\
v_{cut-in, initial} &= [10 \quad 15 \quad 20 \quad 25] kph \\
v_{cut-in, set} &= [10 \quad 15 \quad 20] kph \\
t_{cut-in} &= [5 \quad 5.5 \quad 6] \text{ sec} \\
\Delta p_x &= 30 \text{ m}
\end{aligned} \tag{7.11}$$

A total of three algorithms were compared to check the performance of the algorithm. The base algorithm is an algorithm that does not use collision probability and proactive control. Without considering collision probability, safety control is performed when surrounding vehicle overlaps with the future behavior of the ego vehicle. In MPC for safety control, the current information is used instead of using predicted information. The second algorithm to be compared is an algorithm that uses prediction information in MPC. If the future behavior is assumed to collide, the planning for collision avoidance is reflected in the MPC. Finally, the proposed algorithm not only employs prediction information into the MPC, but also uses collision probability when assessing risk of future collision.

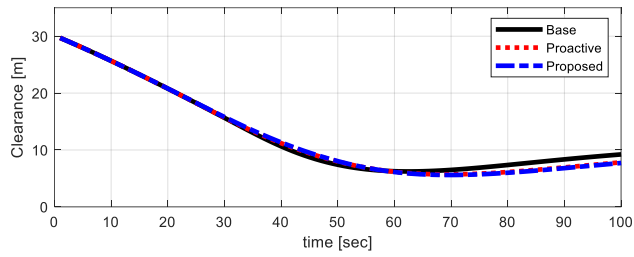
As shown in Figure 7.12 (c) and (d), it can be seen that all algorithms satisfy sufficient safety. However, it can be seen that the second and proposed algorithms reflecting future behavior in MPC use much less deceleration. This is because they predict the collision of the cut-in vehicle and decelerate in advance. The amount of deceleration of the proposed algorithm is the least because the deceleration is performed earlier.



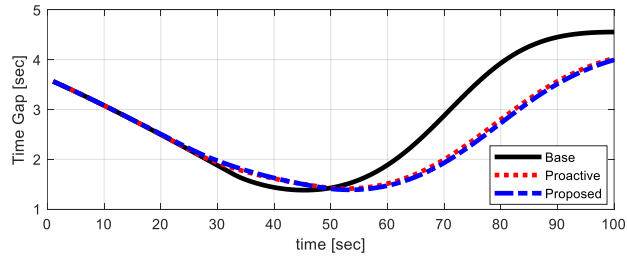
(a) Desired longitudinal acceleration.



(b) Velocity.



(c) Clearance

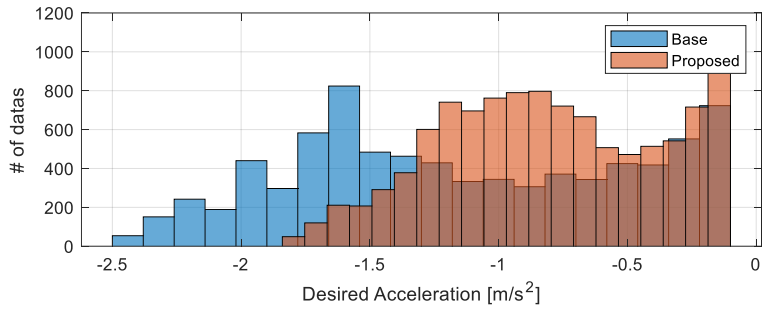


(d) Time gap.

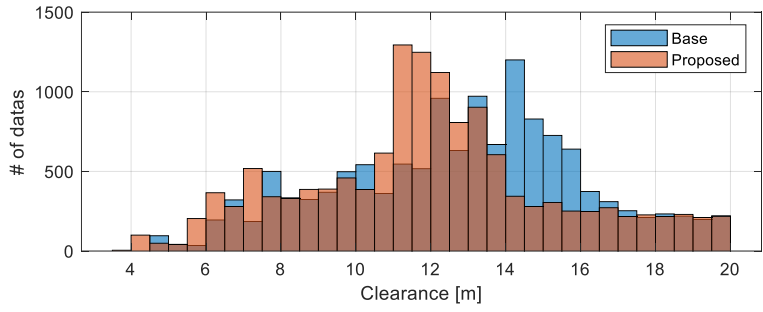
Figure 7.12. One case in monte-carlo simulation.

Results of repeated simulations have been expressed through histogram. Insignificant data was excluded to draw histogram. Desired acceleration below -0.1m/s^2 , clearance below 20m, and time gap below 4sec were considered for histogram. Figure 7.13 shows comparison of base and proposed algorithm. Both algorithms maintain the safety well, but the proposed algorithm shows better performance. The base algorithm uses too much deceleration. This can lead to poor ride quality, as well as a danger to the rear vehicle.

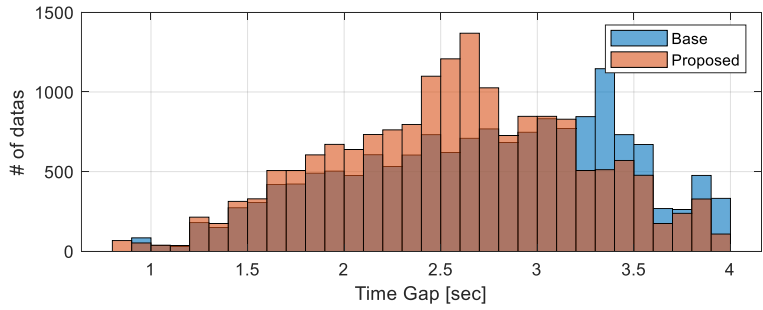
Figure 7.14 shows comparison of proactive and proposed algorithm. Both algorithms implement the proactive motion well, but the proposed algorithm shows better performance. The proposed algorithm shows better safety performance while using less deceleration.



(a) Desired longitudinal acceleration

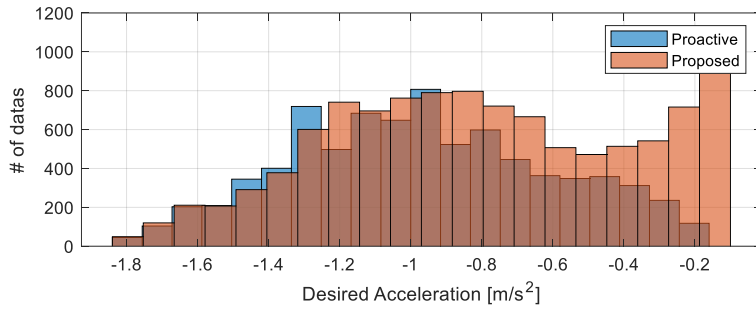


(b) Clearance

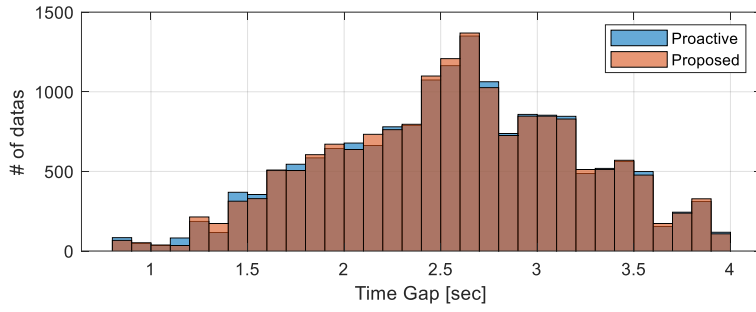


(c) Time gap.

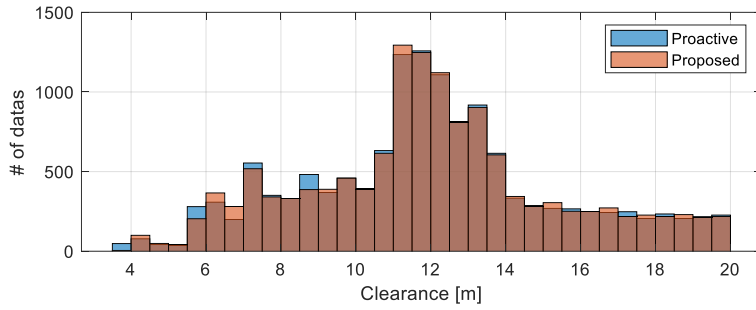
Figure 7.13. Comparison of base and proposed algorithms in monte-carlo simulation.



(a) Desired longitudinal acceleration



(b) Clearance



(c) Time gap.

Figure 7.14. Comparison of proactive and proposed algorithms in monte-carlo simulation.

7.1.5. Merging simulation in on-ramp to evaluate MLC

Simulation environment is shown in Figure 7.15. In the target lane, nine surround vehicles exist. These vehicles are platooning like real human driver's behavior. These vehicles' velocity is based on general highway situation. In the merge lane, the automated vehicle exist. This vehicle's initial velocity is based on general intersection situation. To show the effectiveness of the automated driving algorithm, monte-calro simulations are repeated in this environment that can be slightly modified for parameters. Simulation parameters are modified randomly and all parameters are selected to consider occurring in the actual road as shown in equation (7.12).

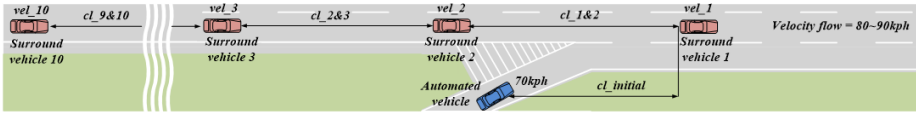
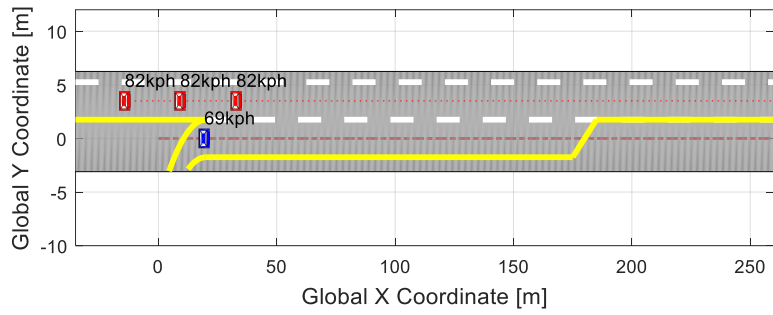


Figure 7.15. Simulation environment.

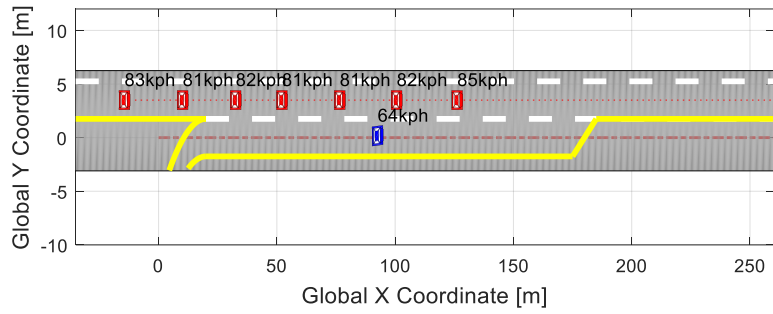
$$\begin{aligned}
 TG_{set} &= [0.8 \quad 1 \quad 1.2] \\
 velocity_{set} &= [80 \ 81 \ 82 \ 83 \ 84 \ 85 \ 86 \ 87 \ 88 \ 89 \ 90] [km/h] \\
 Initial\ clearance_{set} &= [0 \ 10 \ 20 \ 30 \ 40] [m] \\
 cl_{i,j} &= rand(TG_{set}) \times rand(velocity_{set}) / 3.6 + 4 \ [m] \\
 (i &= 1, 2, 3, \dots, 8 \ / \ j = i + 1) \\
 cl_{des,i} &= rand(TG_{set}) \times rand(velocity_{set}) / 3.6 + 4 \ [m] \\
 vel_i &= rand(velocity_{set}) \ [km/h] \\
 vel_{des,i} &= rand(velocity_{set}) \ [km/h] \\
 (i &= 1, 2, 3, \dots, 9) \\
 cl_{initial} &= rand(Initial\ clearance_{set}) \ [m]
 \end{aligned} \tag{7.12}$$

The simulation results via computer simulation are presented. Not only one simulation data but also repeated simulations data are analyzed. Analysis of one simulation data is as follows. In Figure 7.16, the driving situation at each time is presented. When time is 1second, all vehicles are placed depending on simulation initial condition. When time is 5second, the subject vehicle has decelerated to retain space in order to merge. When time is 9second, the subject vehicle has accomplished lane change on proper space between surround vehicles.

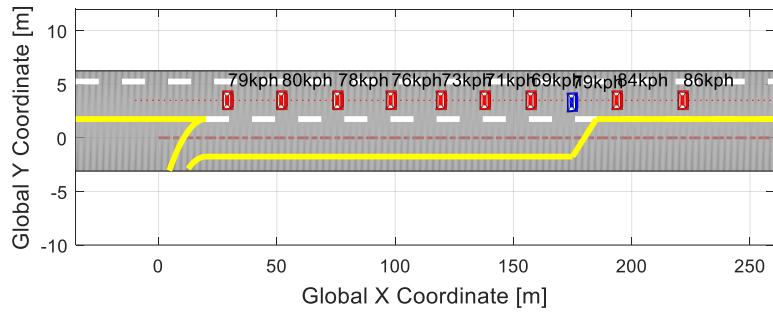
In Figure 7.17 (a), the ego vehicle has decelerated to place desired merge position which is selected as the safe space. Figure 7.17 (b) demonstrates the velocities of three vehicles that are the ego vehicle, a front vehicle and a rear vehicle. The front and rear vehicles mean the vehicles that are located adjacently to the merge space when the ego vehicle merges to the target lane. This means that this merge does not significantly interfere with the flow of traffic. In Figure 7.17 (c), the driving mode decision algorithm determines lane change appropriately. Based determination of the driving mode, lateral control input for autonomous driving vehicle is calculated. Figure 7.17 (d) demonstrates that the performance of controller is satisfied to change lane.



(a) $T=1\text{ sec.}$

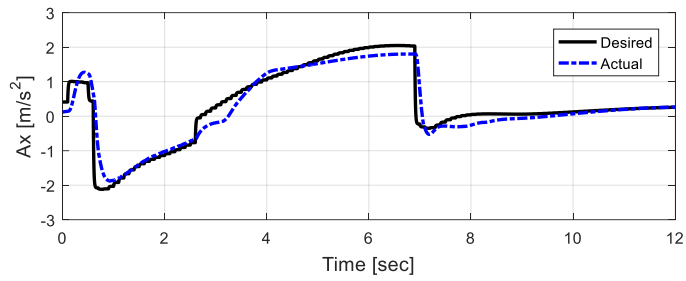


(b) $T=5\text{ sec.}$

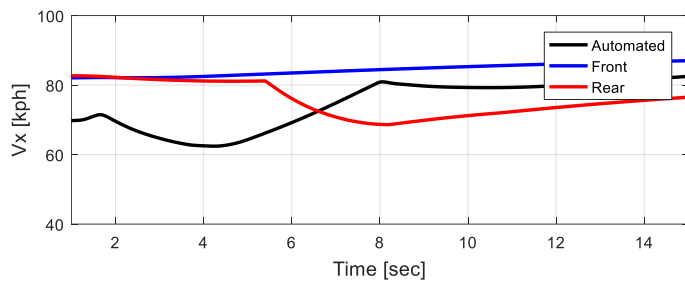


(c) $T=9\text{ sec.}$

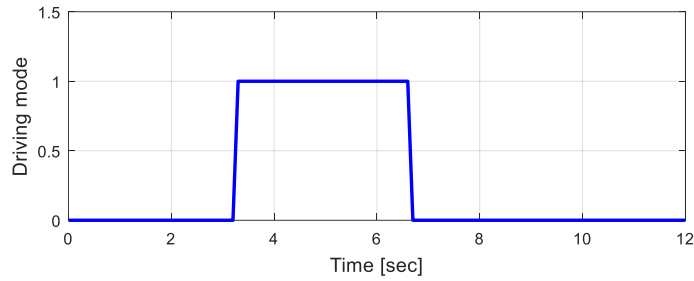
Figure 7.16. Driving situation of one case among monte-calro simulation.



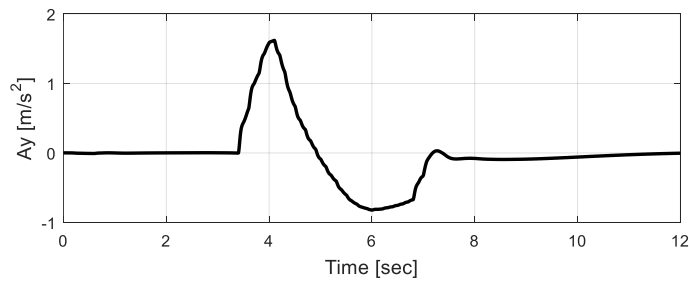
(a) Longitudinal acceleration.



(b) Velocity of three vehicles.



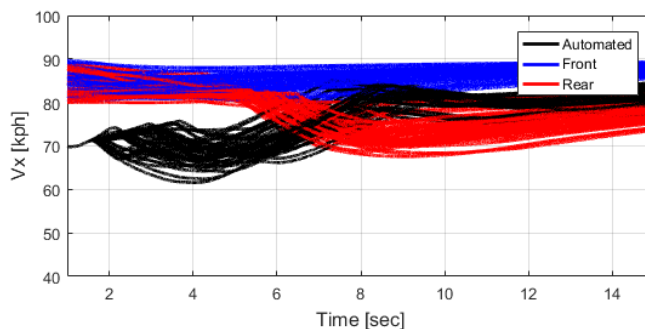
(c) Driving mode.



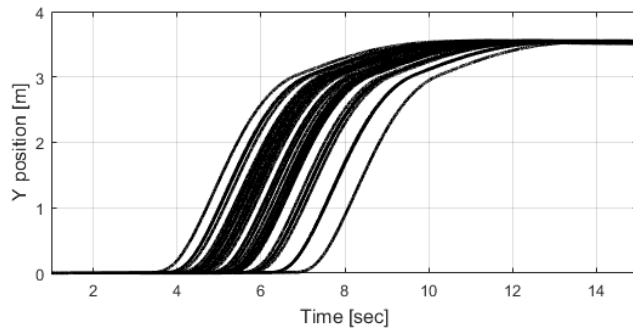
(d) Lateral acceleration.

Figure 7.17. Results of one case among monte-calro simulation.

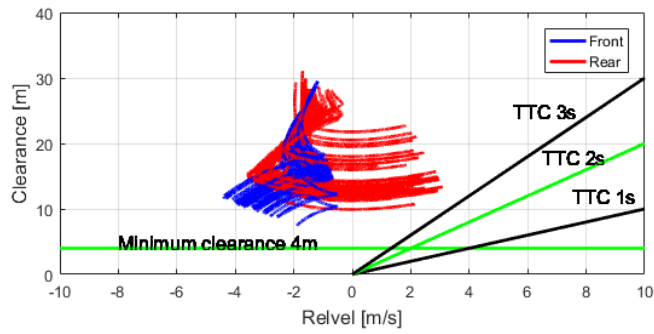
In this time, repeated simulations data is analyzed. Simulations are repeated in 45 times varying parameters. Through repeated simulations, it can be checked to ensure that whether the ego vehicle perform successful merging. Figure 7.18 (a) demonstrates stacked velocities of three vehicles that are the subject vehicle, a front vehicle and a rear vehicle. Adaptation of velocity flow in the target lane appears in all simulation cases. In Figure 7.18 (b), the lateral position of the subject vehicle is presented. The automated vehicle has varied a lane change point depending on varied simulation. Figure 7.18 (c) demonstrates domain of clearance and relative velocity with the front and rear vehicles. In all simulation cases, the data of first safety factor have maintained in safe region. This means that the automated vehicle maintains the safety with surround vehicles when merging. In Figure 7.18 (d), longitudinal position of the subject vehicle is presented when the subject vehicle is on the merge lane. This position shows second safety factor. Because this position maintains a positive, the automated vehicle is successful in merging.



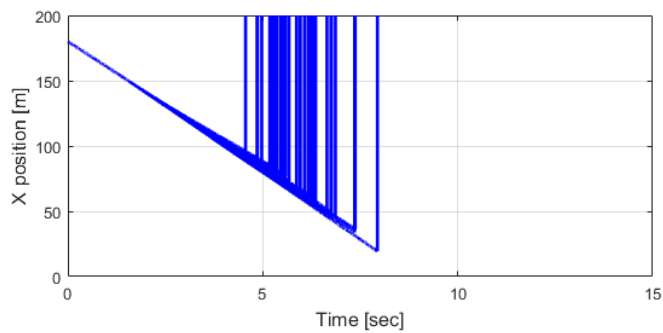
(a) Velocity of three vehicles.



(b) Lateral position.



(c) First safety factor: clearance and relative velocity domain.



(d) Second safety factor: escape distance (longitudinal position).

Figure 7.18. Accumulated results of monte-calro simulation.

7.1.6. Interactive lane change simulation in congested traffic to evaluate the yield intention inference

To evaluate the performance of lane change in congested traffic, the proposed interactive lane change algorithm has been evaluated through simulation. The simulation environment is a two-lane straight road. The simulation is a situation in which the ego vehicle has to move to the next lane because of the accident vehicle in front. The accident vehicle is 80 meters ahead. The next lane is congested and nine vehicles are driving at low speed. Out of nine side vehicles, the ego vehicle starts from the same longitudinal position as the fifth vehicle. Based on the fifth vehicle, the remaining eight vehicles are positioned according to their desired time gap. The velocity of the side vehicles and the desired time gap of each side vehicle are randomly determined for each monte-carlo simulation.

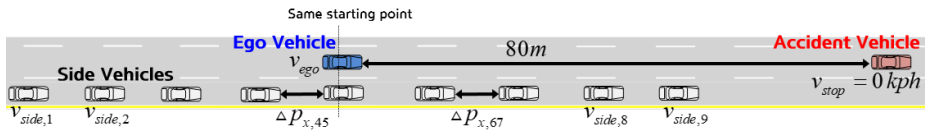


Figure 7.19. Initial conditions of lane change simulation in congested traffic.

An important feature of this simulation is the lane change yield intention. Real vehicles have different intentions to yield to lane changes depending on the driver's disposition. As shown in A, the yield propensity depends on the lateral position of the vehicle attempting to change lanes. To mimic this, three yield intentions were made and randomly distributed to nine side vehicles. The lateral position at which the yield starts was defined as p_{yield} . Therefore, some

vehicles give way to traffic pressure of autonomous vehicles, while others do not. It is important for autonomous vehicle to understand this well and to do interactive lane change.

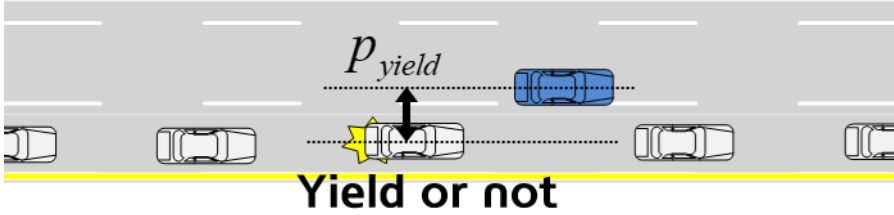


Figure 7.20. Lateral position related with yield intention of side vehicles.

Simulation parameters are selected to consider occurring in the actual road as shown in equation (7.13). The monte carlo simulation has been run 150 times.

$$\begin{aligned}
 v_{ego} &= 30 [km / h] \\
 v_{side,1} &= v_{side,2} = \dots = v_{side,9} = rand(5 \ 10 \ 15 \ 20) [km/h] \\
 TG_{des,i} &= rand(0.7 \ 1 \ 1.3 \ 1.6) [sec] \\
 p_{yield} &= rand(2.7 \ 2.2 \ 1.5) [m] \\
 (i &= 1,2,3,\dots,9) \\
 \Delta p_{x,(i)(i+1)} &= TG_{des,i} \times v_{side,i} + 2 \ m \\
 (i &= 1,2,3,\dots,8)
 \end{aligned} \tag{7.13}$$

A total of three algorithms were compared to check the performance of the algorithm. The compared algorithms use constant parameters for lane change safety distance. One is based on highway data and the other is based on urban data. The former is called the conservative safety distance (CSD) and the latter

is called the progressive safety distance (PSD). The proposed algorithm adopts the lane change safety distance with yield intention, which is called yield intention based safety distance (YISD).

Figure 7.21 shows the distribution of the time it takes to change lanes through monte-calro simulation. Figure 7.22 shows the distribution of clearance between the ego vehicle and the rear vehicle when changing lanes. This represents the performance of safety. The comparison result of the three algorithms is represented in Table 14. Here, the lane change completed time means the time until the simulation starts and the lane change is completed. The lane change success rate represents the ratio of the simulations that successfully change lanes among all simulations. The CSD shows the highest degree of safety. However, lane change completed time is too long and success rate is significantly low because the CSD is too conservative. The PSD has good lane change completed time and success rate, but its safety is low. The YISD shows the best lane change completed time and success rate, while ensuring sufficient safety performance.

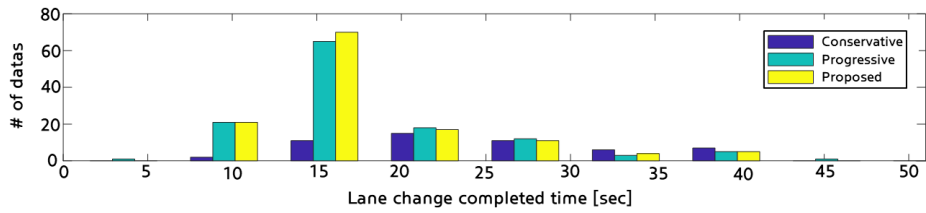


Figure 7.21. Lane change completed time in congested traffic.

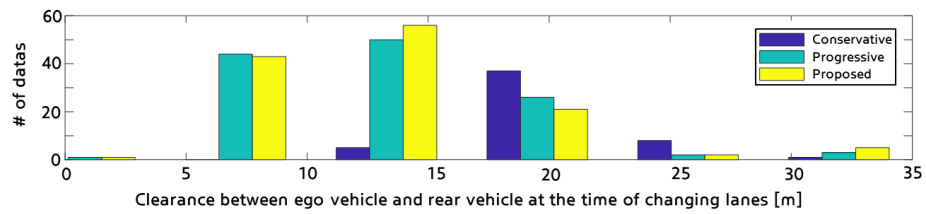


Figure 7.22. Clearance between ego vehicle and rear vehicle when finishing lane change in congested traffic.

Table 14. Interactive lane change performance in congested traffic

	<i>CSD</i>	<i>PSD</i>	<i>YISD</i>
<i>LC completed time [sec]</i>	<i>24.60</i>	<i>18.08</i>	<i>17.83</i>
<i>Clearance with rear vehicle [m]</i>	<i>19.97</i>	<i>13.05</i>	<i>13.36</i>
<i>LC success rate (between two vehicles)</i>	<i>0.36</i>	<i>0.84</i>	<i>0.86</i>
<i>Collision case</i>	<i>0</i>	<i>4</i>	<i>0</i>

7.2. Vehicle Test

We evaluated the proposed algorithm through vehicle test. The autonomous driving algorithms must be verified by vehicle test after verification is completed by simulation. The final goal of the proposed algorithm is to implement it on autonomous vehicles, so vehicle test is the final stage of verification. The proposed algorithm has been developed to cope with a changeable autonomous vehicle rather than a specific autonomous vehicle. The proposed algorithm is adaptive to the localization and perception modules, the upper modules of autonomous driving. Therefore, vehicle tests are conducted using various vehicles, not just one vehicle. Vehicle tests have been conducted using the three autonomous vehicles introduced in Section 2. Each of the three vehicles has different sensor sets, localization and perception modules. Therefore, it can be seen that the proposed algorithm shows stable performance for various uncertainties and changeability of vehicles. Lane change is an essential driving function regardless of the road environment. Therefore, vehicle tests have been conducted in both highway and urban environments. In Korea, a policy exists for the real road test of autonomous vehicles. This policy grants permission for autonomous driving through autonomous driving test, fail safe test, and driver override test. Three test vehicles used in this dissertation accepted this permission, so the vehicles are able to drive on actual roads.

7.2.1. Self-directed Test using First Vehicle Platform

Before testing the vehicle with various external vehicles on the actual road, the vehicle test has been carried out by itself [Chae,'18]. This can confirm the basic algorithm operation in the actual vehicle that could not be confirmed in the simulation. The proposed autonomous driving algorithm is validated through self-directed vehicle test. As shown in Figure 7.23, there are two normal vehicles on the first lane and an autonomous lane on the second lane. At this time, the autonomous driving vehicle is required to make a lane change to the left. The test scenarios are summarized in Table 15. There are four scenarios in total and the initial speed and initial position of the three vehicles are different. Especially, the scenario 4 assumes that virtual vehicles exits closely in front of and behind both side vehicles in order to simulate a congestion situation. The target speed of the autonomous vehicle is the same as the initial speed.

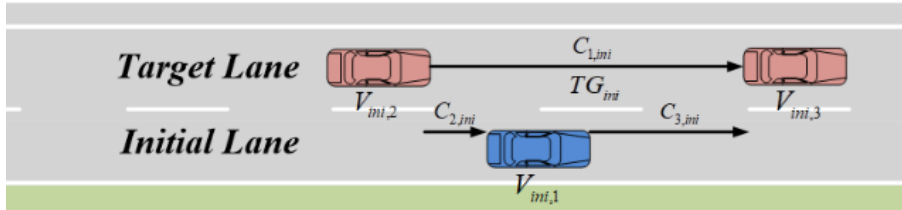


Figure 7.23. Three vehicles relation of test scenario.

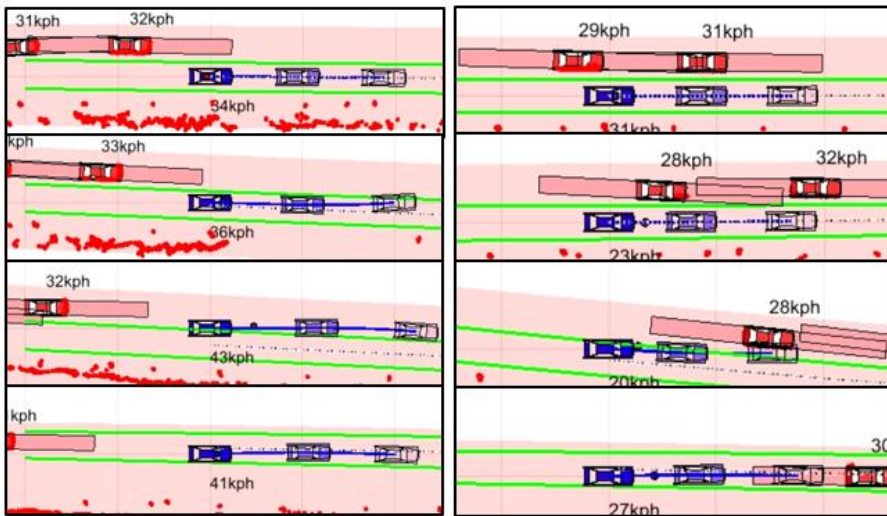
Table 15. Validation test initial condition of vehicles

No	$V_{ini,1}$	$V_{ini,2}$	$V_{ini,3}$	$C_{1,ini}$	$C_{2,ini}$	$C_{3,ini}$	TG_{ini}
1	30kph	30kph	30kph	10m	-10m	-20m	1.2
2	30kph	30kph	30kph	10m	-2m	12m	1.2
3	10kph	10kph	10kph	25m	-4m	21m	9.3
4	10kph	10kph	10kph	18m	-8m	10m	6.6

Figure 7.24 shows four snap shots of each test scenario. The blue vehicle is the autonomous vehicle and the red vehicles are the surrounding vehicles. The blue line is the target path of autonomous vehicle, and the blurred blue vehicles are the predicted information after one and two seconds, respectively. Red points are point cloud of LiDAR sensor. On the right side of the autonomous vehicle, guardrails and trees are recognized by LiDAR. On the left side, the corners of the surrounding vehicles are recognized by LiDAR and perceived as vehicles by the perception algorithm. The long rectangular box around the red vehicle indicates the safe distance used in the motion planning algorithm. The green line indicates the lanes recognized by the camera sensor, and the black dotted line is the centerline of the lanes processed by the lane filter.

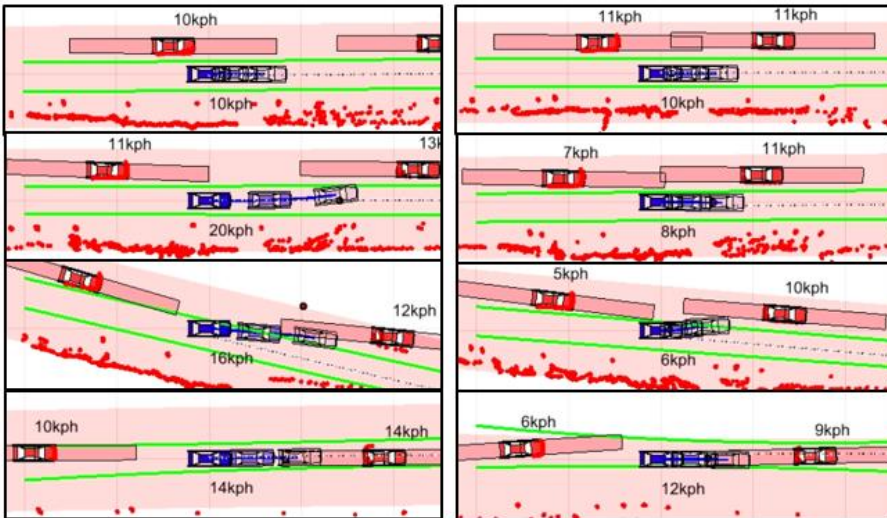
The first snapshot in each scenario shows the initial condition. In all scenarios, although a lane change is required, there is a lane change risk due to safety distance of the side vehicles on the target lane. The second snapshots shows the autonomous driving vehicle taking action to be able to change lanes. In scenario 1, the autonomous vehicle determines that it is best to move in front of the side-

front vehicle, and accelerate. In scenario 2, the autonomous vehicle determines that it is best to move behind the side-rear vehicle, and decelerates. In scenario 3, the autonomous vehicle judges that there is sufficient space between the side-rear vehicle and the side-front vehicle and accelerates to enter that space. As mentioned above, the scenario 4 assumes that virtual vehicles exits closely in front of and behind both side vehicles in order to simulate a congestion situation. Therefore, the autonomous vehicle does not judge that it is good to move at the most forward or the rearmost point like scenario 1, 2. The autonomous vehicle proceeds with traffic pressure to convey the lane change intention to the side-rear vehicle. In other words, the autonomous vehicle goes into space between two side vehicles and attaches slightly to the target lane. The third snapshots shows the autonomous driving vehicle performing the lane change. Especially, in scenario 4, the side-rear vehicle responded to traffic pressure, giving space for lane change. The fourth snapshots shows that the lane change has been successfully completed while keeping the safety with the surrounding vehicles.



(a) Scenario 1.

(b) Scenario 2.

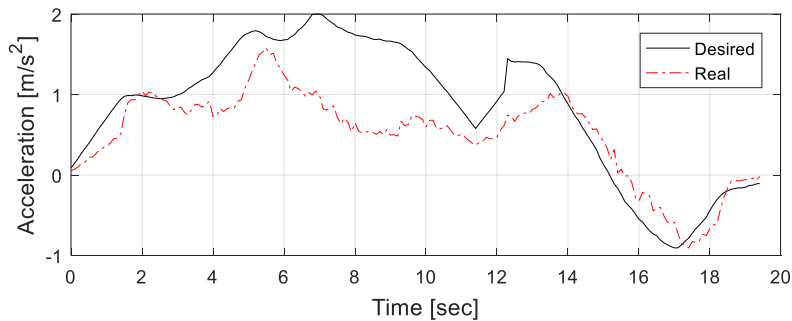


(c) Scenario 3.

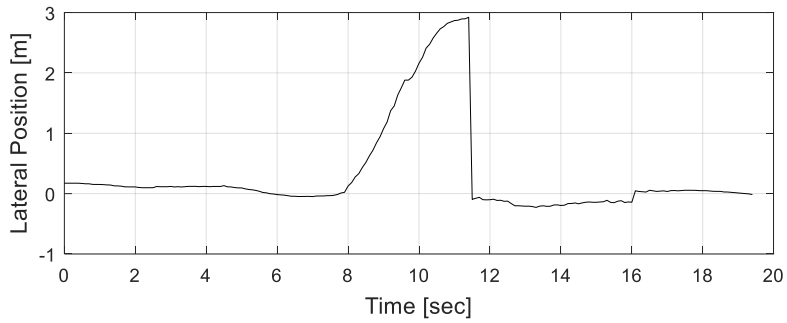
(d) Scenario 4.

Figure 7.24. Four snap shots of each test scenarios.

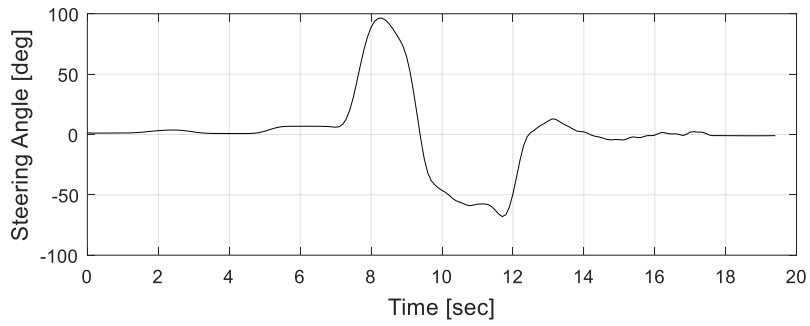
Figure 7.25 shows test results of scenario 3. Figure 7.25 (a) shows the longitudinal acceleration. From 0 to 8 seconds, the autonomous vehicle accelerates to a space where lane change is possible. The vehicle makes longitudinal control considering the safety with the side-front vehicle from 8 seconds, when the lane change starts. Figure 7.25 (b) demonstrates, through lateral position by measured camera sensor, that the lane change starts from 8 seconds and the autonomous vehicle arrives at the target lane about 11 seconds. Figure 7.25 (c) shows the steering angle used to performing lane change, demonstrating that the lane change is completely on the target lane at about 16 seconds. Figure 7.25 (d) demonstrates domain of clearance and relative velocity with the side-front and side-rear vehicles. Black dots are before lane change. Red circles are during and after lane change. Initially, the side-rear vehicle is so close that the lane change cannot be performed. After the distance from the side-rear vehicle is extended, the lane change begins. This shows that the autonomous vehicle maintains the safety with surround vehicles when lane changing.



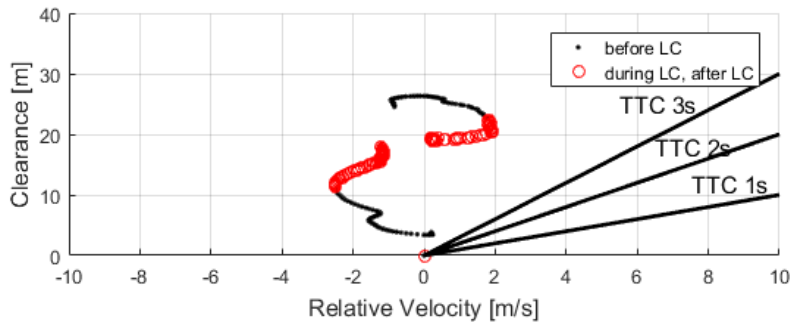
(a) Longitudinal acceleration.



(b) Lateral position.



(c) Steering angle.



(d) Safety with surrounding vehicles.

Figure 7.25. Test results of scenario 3.

7.2.2. Highway DLC and MLC Test using First Vehicle Platform

The proposed lane change algorithm has been evaluated through a real vehicle test. Figure 7.26 shows the test environment where the three highways connect by three ramps as a circulation course. This environment makes the DLC and the MLC consecutively. Information on each road section is given in Table 16.



Figure 7.26. Vehicle test environment.

Table 16. Information of each road section

	<i>Kind</i>	<i>Feature</i>	<i>Lane change reason</i>
①	<i>Ramp</i>	<i>Max curvature = 300 m</i>	-
①	<i>On- ramp</i>	<i>Limited distance = 200 m</i>	<i>Mandatory</i>
①→②	<i>Normal</i>	<i>The number of lanes: 3</i>	<i>Discretionary</i>
②	<i>Off-ramp</i>	<i>Go to exit lane from 1 km ahead</i>	<i>Mandatory</i>
②	<i>Ramp</i>	<i>Max curvature = 350 m</i>	-
②	<i>On- ramp</i>	<i>Limited distance = 200 m</i>	<i>Mandatory</i>
②→③	<i>Normal</i>	<i>The number of lanes: 4</i>	<i>Discretionary</i>
③	<i>Off-ramp</i>	<i>Go to exit lane from 1 km ahead</i>	<i>Mandatory</i>
③	<i>Ramp</i>	<i>Max curvature = 200 m</i>	-
③	<i>On- ramp</i>	<i>Limited distance = 150 m</i>	<i>Mandatory</i>
③→①	<i>Normal</i>	<i>The number of lanes: 4</i>	<i>Discretionary</i>
①	<i>Off-ramp</i>	<i>Go to exit lane from 1 km ahead</i>	<i>Mandatory</i>

The vehicle test proceeded on a total of five and a half laps around the circular course. The total travelled distance is 103 km, and the number of lane changes conducted is 92. Figure 7.27-Figure 7.32 show the selected three lane change situations among the 92 lane changes. The three lane change situations are the on-ramp, the off-ramp, and the general road. Snapshots of the three lane change situations are shown in Figure 7.27, Figure 7.29, and Figure 7.31. In the snapshots, the blue line is the target path of the ego vehicle, and the blue

diamonds are the predicted positions of the ego vehicle after 1 and 2 s, respectively. The small red circle is a current position reference of the ego vehicle. The red points represent measured data of the LiDARs and radar sensors. The red vehicles represent surrounding vehicles. The pink rectangular box around the red vehicle indicates the safety distance. The green line indicates the lanes recognized by the camera sensor, and the black dotted line is the centerline of the lanes. In this dissertation, the driving mode is so important. The concepts of the lane change demand and possibility are expressed by arrows. The arrow indicates the driving mode and the direction of the lane change. The colored arrows indicate the lane change demand. A red arrow indicates that the action of the lane change is risk. Therefore, the lane change is impossible. A blue arrow shows that the lane change mode proceeds because the safety distances have been sufficiently guaranteed.

Figure 7.28, Figure 7.30, and Figure 7.32 represent test results of the three lane change situations: driving mode, acceleration, safety domain with surrounding vehicles, distance with side vehicles on target lane, steering angle and lateral position. These figures show that the ego vehicle succeeds in changing the lane, while using appropriate acceleration and maintaining safety with the surrounding vehicles. Figure 7.28 (a), Figure 7.30 (a) and Figure 7.32 (a) indicate the driving mode which is related with the lane change demand and possibility concept for the active lane change. In Figure 7.28 (b), Figure 7.30 (b) and Figure 7.32 (b), the time-varying safety distances are shown. The driving mode is decided by the safety distance and clearance with vehicles on target lane. The acceleration in Figure 7.28 (c), Figure 7.30 (c) and Figure

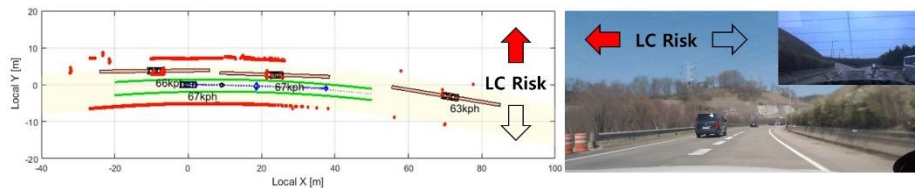
7.32 (c) is satisfactory for both smooth ride quality and clearance control. The acceleration tracking controller has been tuned for smooth ride quality in normal driving situations in which the desired acceleration is in the range of $\pm 1\text{m/s}^2$. The clearance control characteristics described in Figure 7.28 (d), Figure 7.30 (d) and Figure 7.32 (d) illustrate that the vehicle behaviors of the ego vehicle are in safe region with sufficient safety margin. It should be noted that, in emergency braking situations, the designed acceleration is of large values and the tracking performance should be much better and faster to avoid collisions. In emergency braking situations, a different set of gains is used for fast tracking performance. In Figure 7.28 (f), Figure 7.30 (f) and Figure 7.32 (f), it indicates the lane change moment that the lateral position has a sudden change in a very short time.

Figure 7.27 presents four snapshots of on-ramp driving. In the Figure 7.27 (a), the ego vehicle is demanded to conduct a left lane change by road environment. However, the side vehicles are located so close. Therefore, the lane change is impossible. These Figure 7.27 (b) and Figure 7.27 (c) show that the ego vehicle is performing a lane change in the desired space. In the Figure 7.27 (d), the ego vehicle completes the lane change and maintains safety with a preceding vehicle. The Figure 7.27 (e) indicates the biased steering input due to an on-ramp road with slight curvature. This shows that the lateral model with consideration for road curvature has good performance about the lane keeping and lane change.

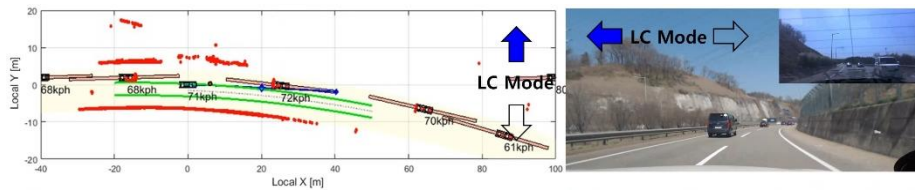
Figure 7.29 shows four snapshots of off-ramp. The ego vehicle could know that the vehicle is getting closer to off-ramp. A right lane change is demanded

in order to go to the exit lane. This is shown in Figure 7.29 (a). Since the side-rear vehicle is located so close, the ego vehicle decides to go forward in front of the side-rear vehicle. This is shown in Figure 7.29 (b). The Figure 7.29 (c) shows that the ego vehicle is changing the lanes. In addition, a signpost appear in the Figure 7.29 (c), the signpost means that current position of the ego vehicle is close to off-ramp. In the Figure 7.29 (d), the vehicle completes the lane change.

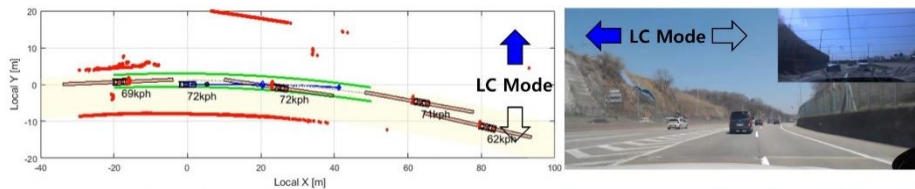
Figure 7.31 presents four snapshots of overtaking situation in the general road. The Figure 7.31 (a) shows that the preceding vehicle is too slow and traffic flow in the left lane is good. Therefore, the ego vehicle is needed to make a left lane change. It is impossible to perform the lane change immediately due to the vehicles in the side lane. However, the lane change is soon possible because a side vehicle moves to the other lane. The Figure 7.31 (b) and the Figure 7.31 (c) indicate that the ego vehicle performs the lane change and maintains safety with a preceding vehicle in the new lane. In the Figure 7.31 (d), the ego vehicle finishes overtaking a slow truck and matching the traffic flow in the new lane.



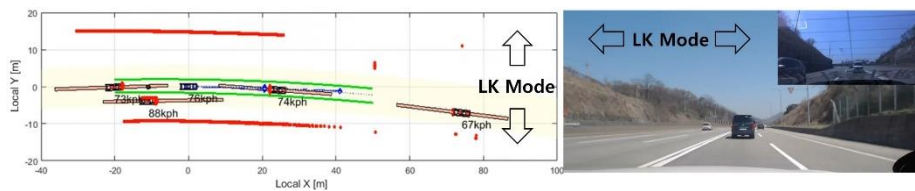
(a) First snapshot.



(b) Second snapshot.

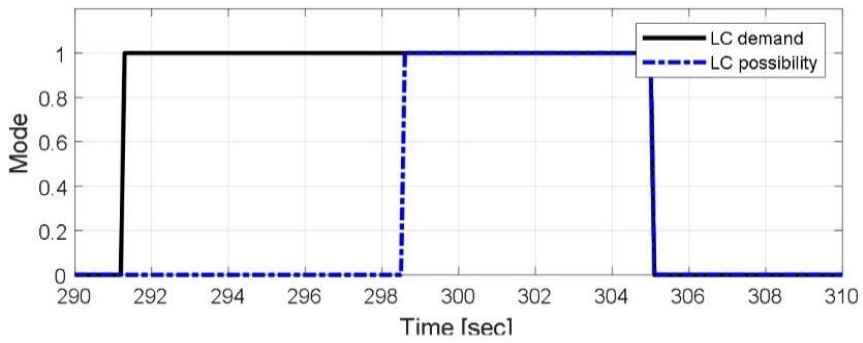


(c) Third snapshot.

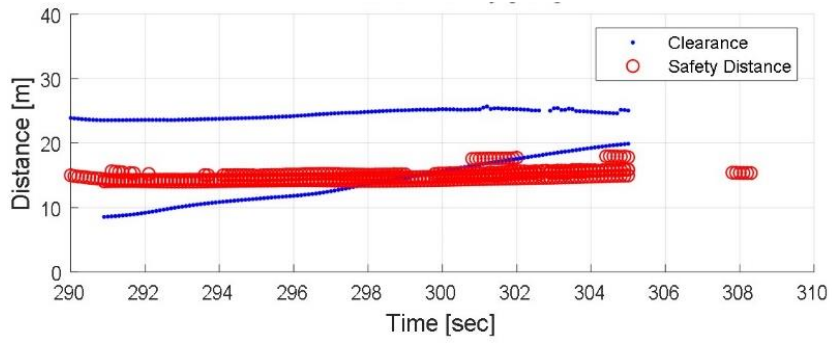


(d) Fourth snapshot.

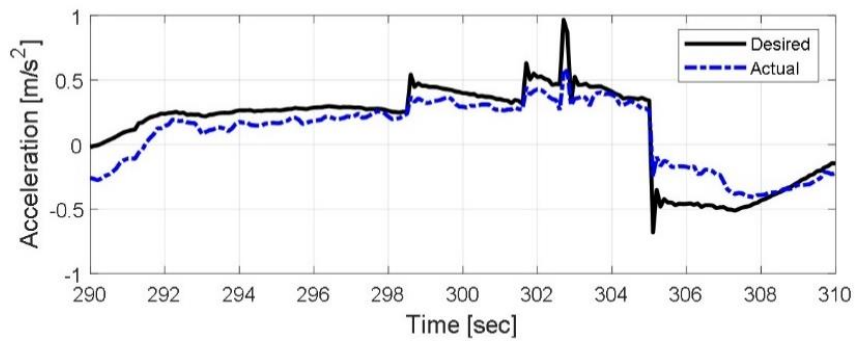
Figure 7.27. Snapshots in on-ramp (MLC).



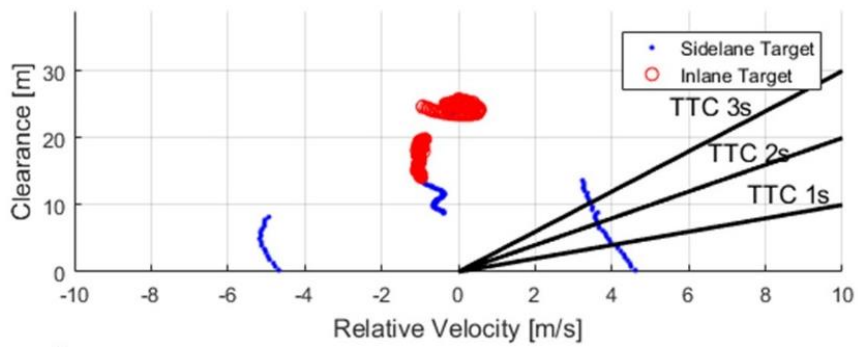
(a) Driving mode.



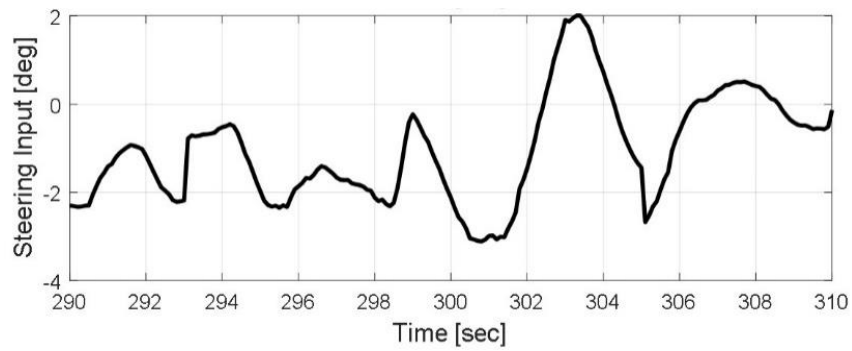
(b) Distance with vehicles on target lane.



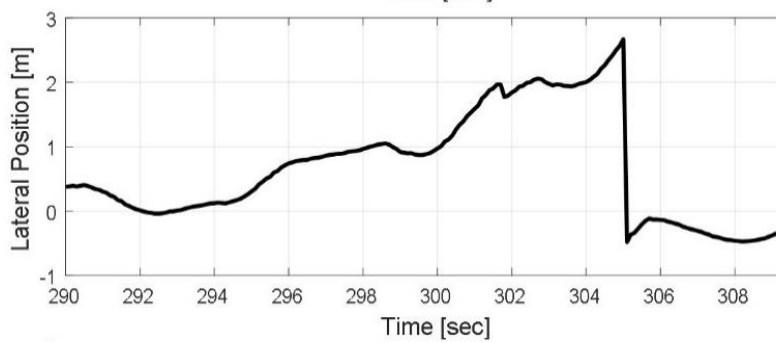
(c) Longitudinal acceleration.



(d) Safety domain with surrounding vehicles.

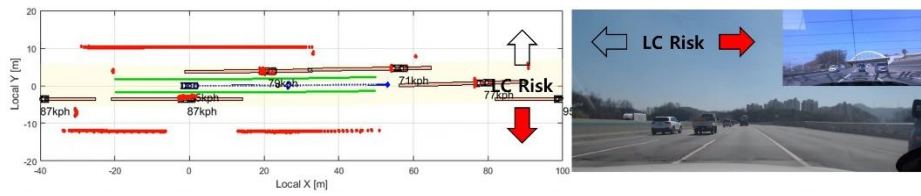


(e) Steering input.

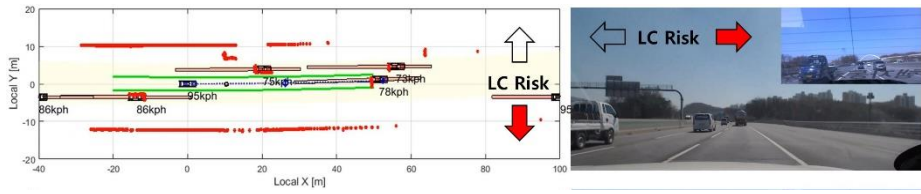


(f) Lateral position.

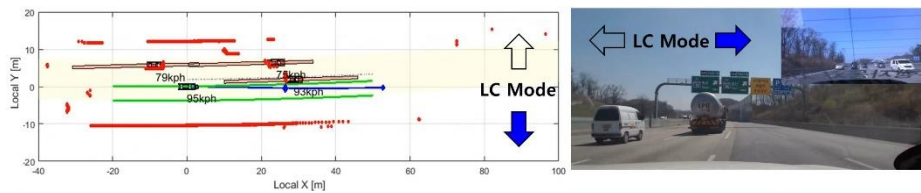
Figure 7.28. Test results in on-ramp (MLC).



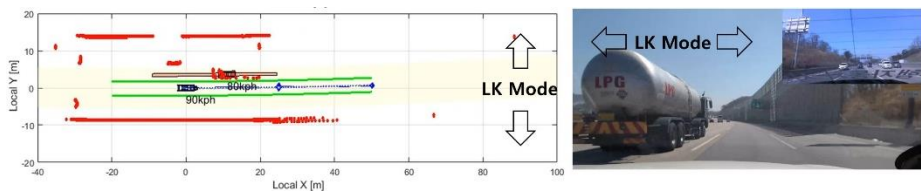
(a) First snapshot.



(b) Second snapshot.

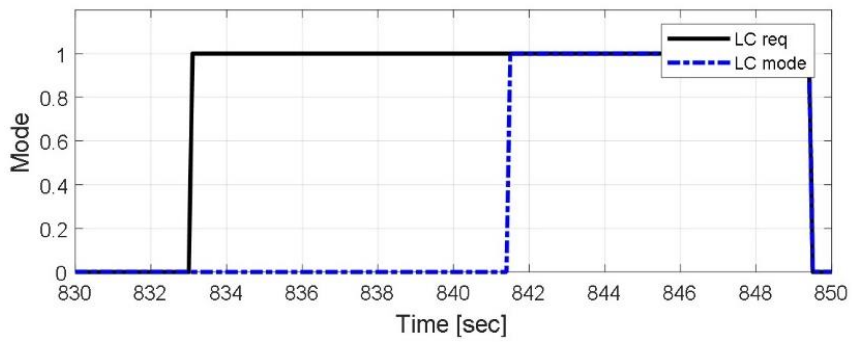


(c) Third snapshot.

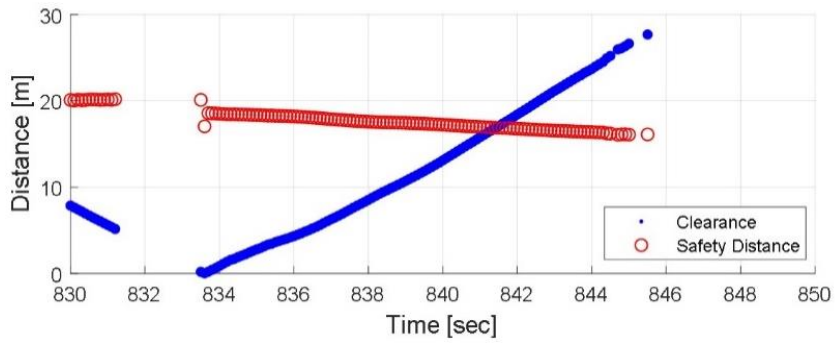


(d) Fourth snapshot.

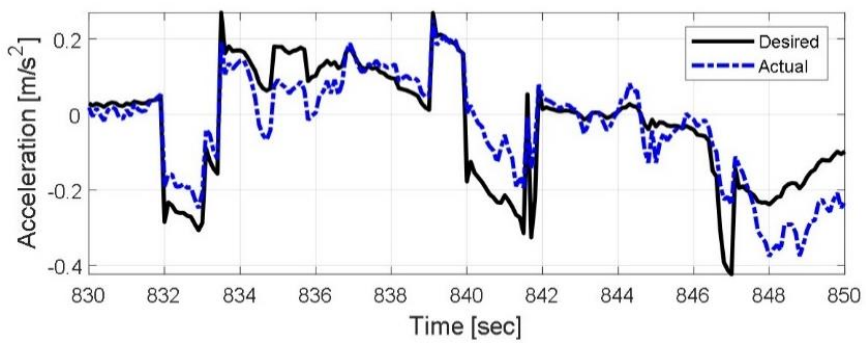
Figure 7.29. Snapshots in off-ramp (MLC).



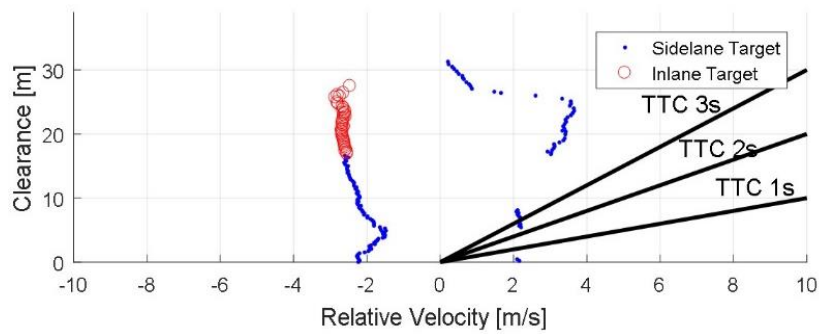
(a) Driving mode.



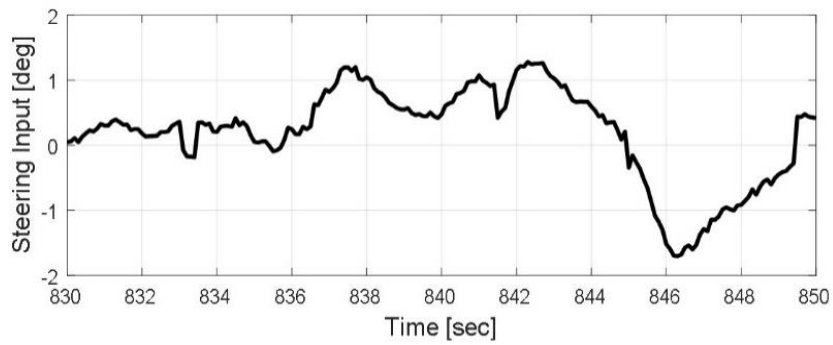
(b) Distance with vehicles on target lane.



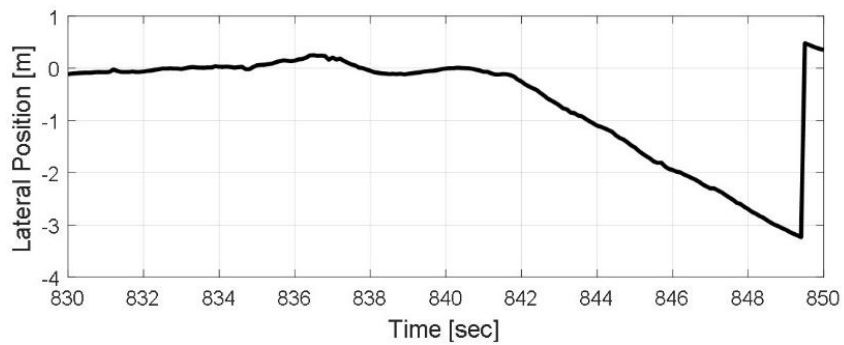
(c) Longitudinal acceleration.



(d) Safety domain with surrounding vehicles.

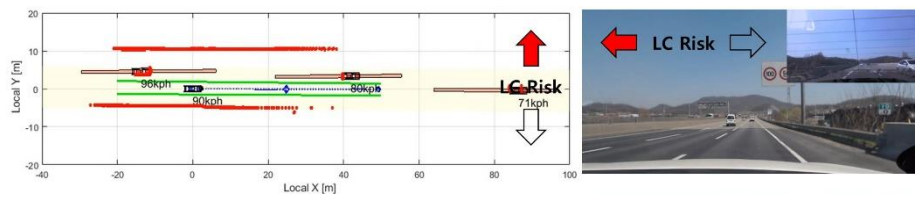


(e) Steering input.

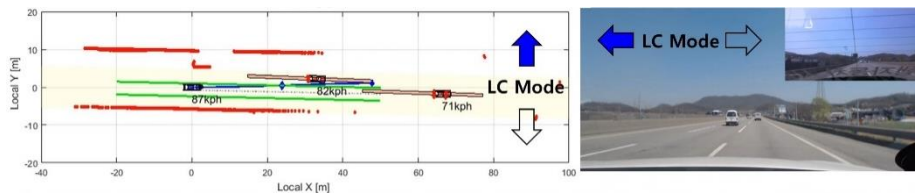


(f) Lateral position.

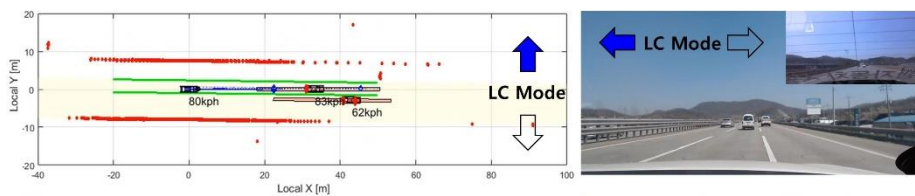
Figure 7.30. Test results in off-ramp (MLC).



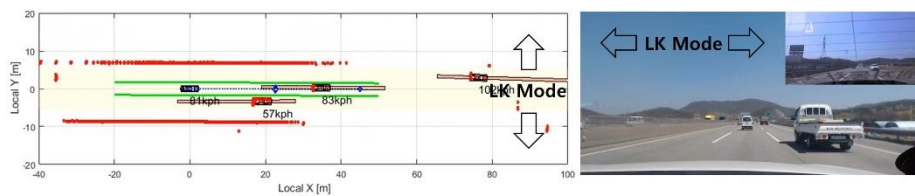
(a) First snapshot.



(b) Second snapshot.

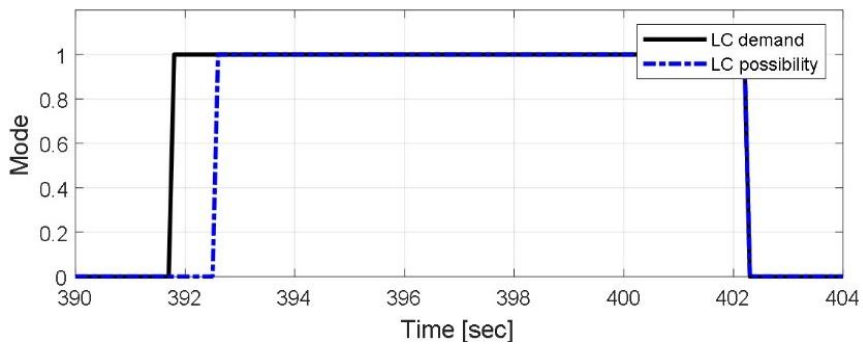


(c) Third snapshot.

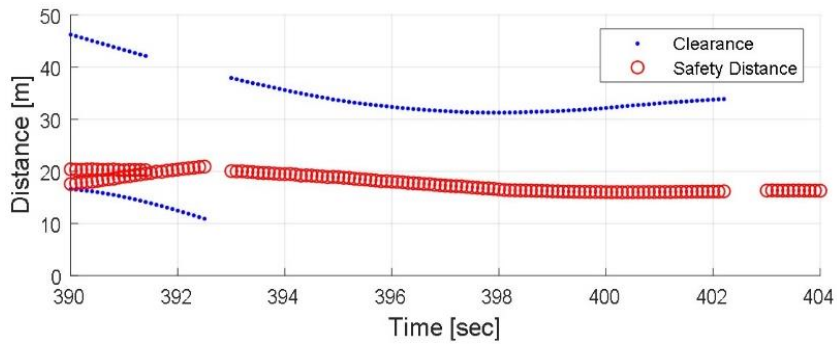


(d) Fourth snapshot.

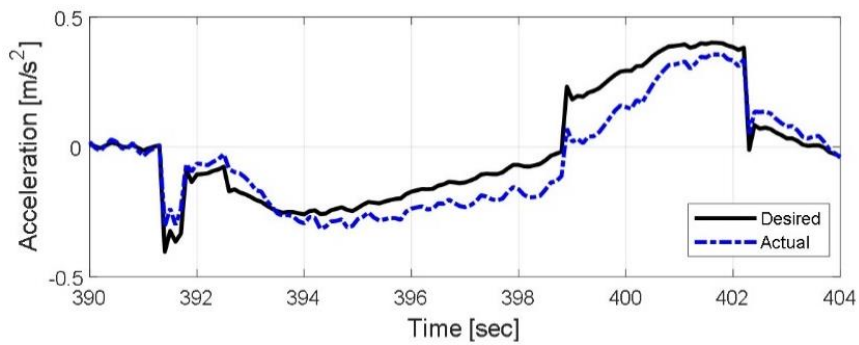
Figure 7.31. Snapshots in general road section (DLC: overtaking).



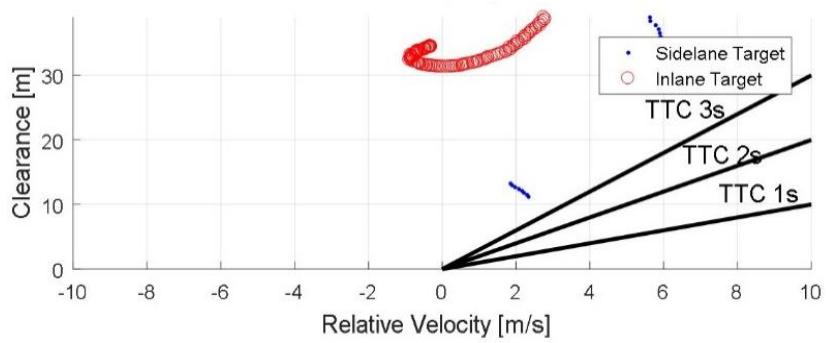
(a) Driving mode.



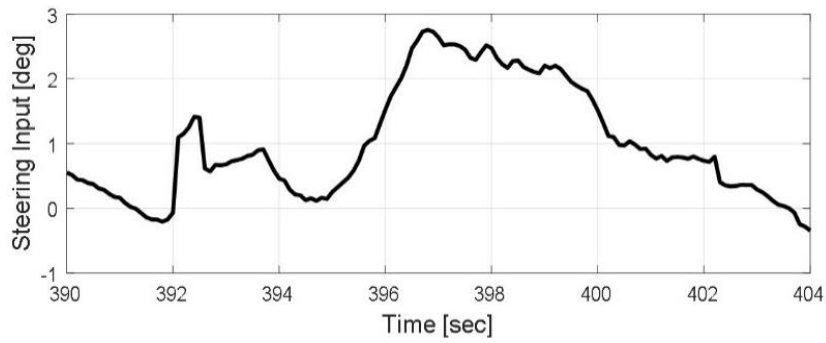
(b) Distance with vehicles on target lane.



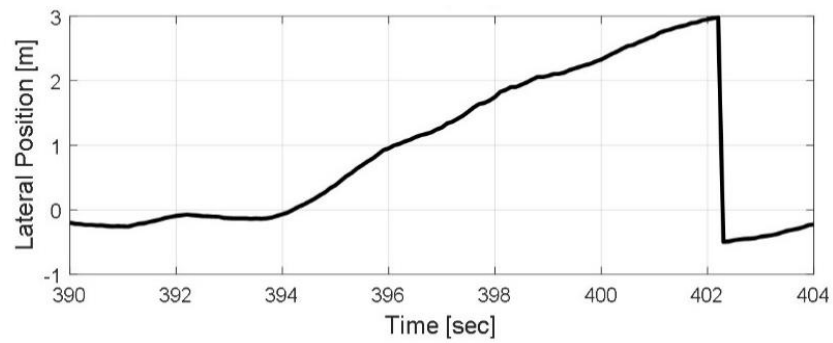
(c) Longitudinal acceleration.



(d) Safety domain with surrounding vehicles.



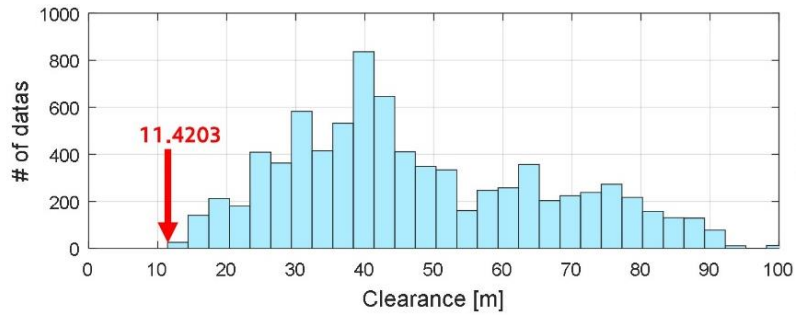
(e) Steering input.



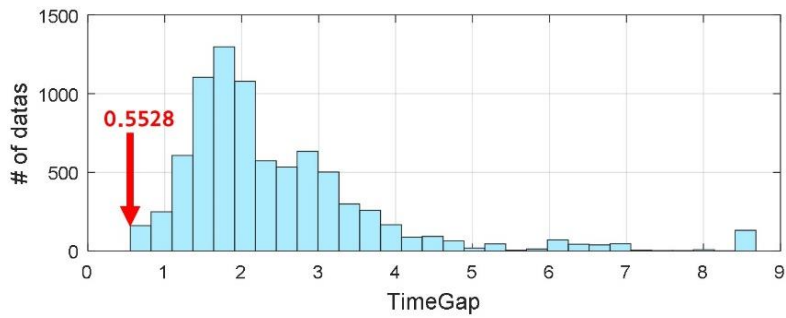
(f) Lateral position.

Figure 7.32. Test results in general road section (DLC: overtaking).

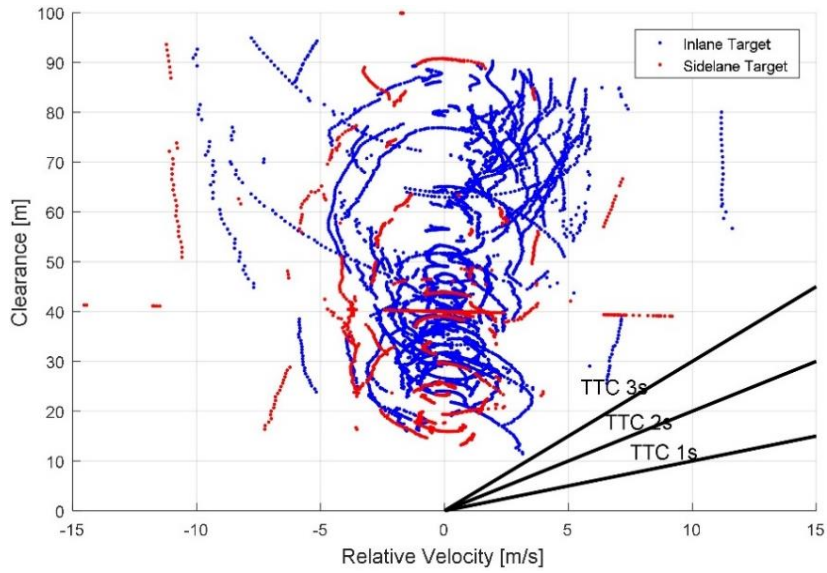
Figure 7.33 shows cumulative test data which has been collected in five and a half laps of the circular course. The total travelled distance is 103 km, and the ego vehicle performs the lane change 92 times. As shown in Figure 7.33 (a) and Figure 7.33 (b), the ego vehicle always maintains safety performance with a preceding vehicle. The minimum clearance is 11.4203 m, and the minimum time gap is 0.5528 s. This means that safety performance is maintained within the defined safety distances. In Figure 7.33 (c), a safety domain of relative velocity and clearance is shown. States with surrounding vehicles can be found all located within the safe area which appears in Section 2. This means that all lane changes have been carried out while keeping safety of the surrounding vehicles. Lastly, Figure 7.33 (d) represents the longitudinal and lateral acceleration of the ego vehicle during lane changes 92 times. Given that previous studies [Wan,'11, Toledo,'03, Ahmed,'99] about lane changes, the longitudinal and lateral acceleration are reasonable. This indicates that lane changes are performed without compromising the ride quality of passengers.



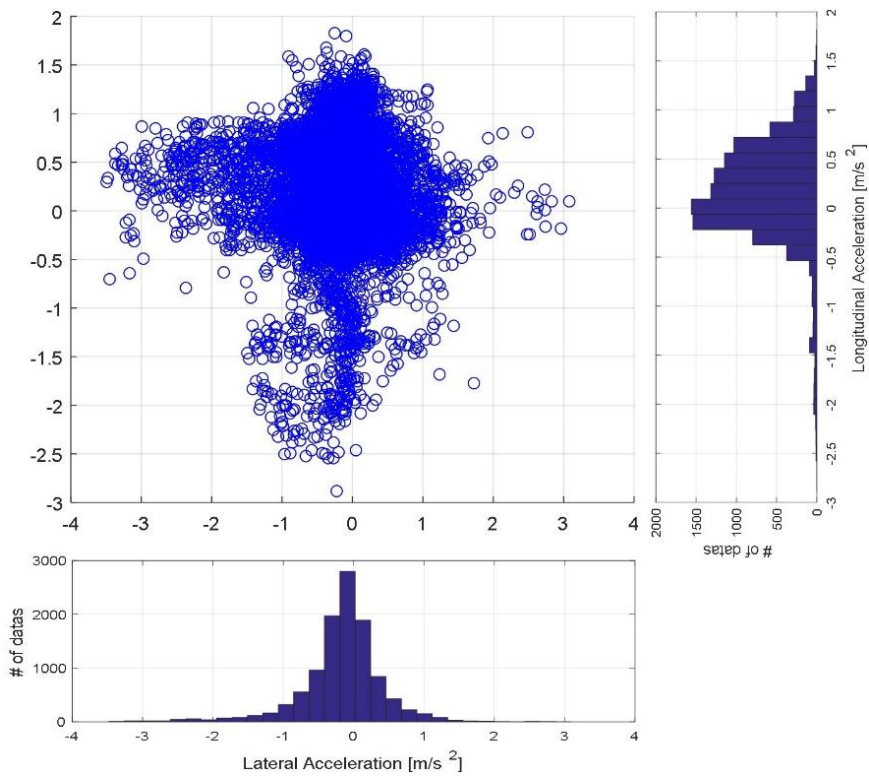
(a) Histogram of safety index: Clearance.



(b) Histogram of safety index: Time gap.



(c) Safety domain with surrounding vehicles.



(d) Longitudinal and lateral acceleration.

Figure 7.33. Vehicle test results: cumulative test data.

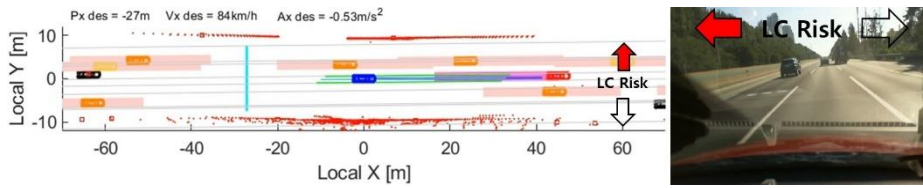
7.2.3. Highway Overtaking Test for DLC using Second Vehicle Platform

The proposed lane change algorithm has been evaluated through a real vehicle test [Chae,'20]. The test environment is the Gyeongbu Expressway in Korea. The highway is four lanes one way and has a speed limit of 110 km/h. The vehicle test has been conducted using the first and second lanes according to the road regulations. The total driving distance was 200 km and 106 lane changes were made for overtaking. Figure 7.34 represents the test environment.

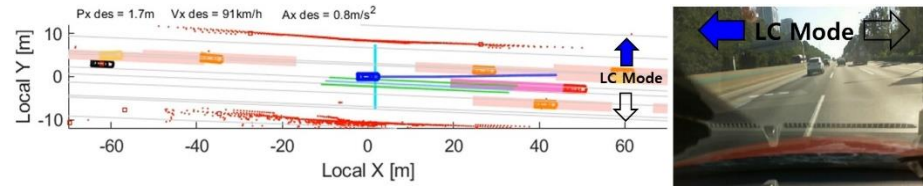


Figure 7.34. Vehicle test environment.

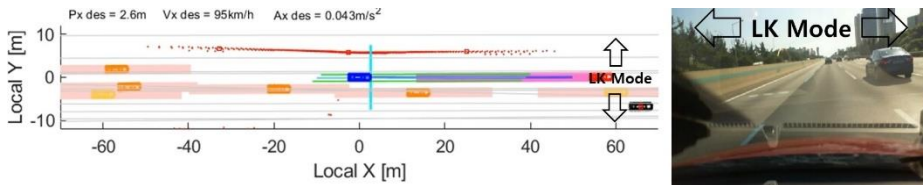
Figure 7.35 shows the snapshots of the selected one overtaking situation among the 106 lane-change maneuvers. The selected overtaking situation is a situation in which the ego vehicle enters to the overtaking lane after seeing a slow preceding vehicle. And because of slow vehicles in the driving lane, the ego vehicle continues to drive in the overtaking lane. Then, the ego vehicle returns to the proper space in the driving lane. As a result, the ego vehicle overtakes four vehicles. In the snapshots, the blue vehicle is the ego vehicle. The black vehicles are surrounding vehicles. Important vehicles among surrounding vehicles are colored vehicles. The red vehicle is the preceding vehicle. The orange vehicles are vehicles on side lanes. The boxes drawn around important vehicles indicate safe distances. The red points represent point clouds of the LiDAR sensors. The blue line means the desired path of the ego vehicle. The green lines represent the lanes recognized by the camera sensor. The azure line means the reference of a longitudinal position. It could be seen that the reference changes according to the decided target space. In this dissertation, the driving mode is very important. The concepts of lane change demand, and possibility are expressed by arrows. The arrow represents the driving mode and the direction of the lane change. The colored arrows indicate the lane change demand. A red arrow represents that the lane change is impossible. A blue arrow indicates that the lane change mode proceeds because the safe distances have been sufficiently guaranteed. The texts at the top of the snapshot represent the reference position, the reference velocity, and the desired acceleration, respectively.



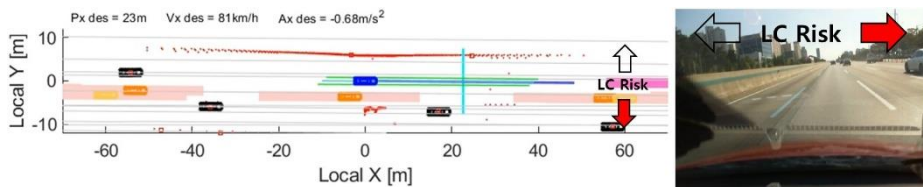
(a) First snapshot (Time: 11sec).



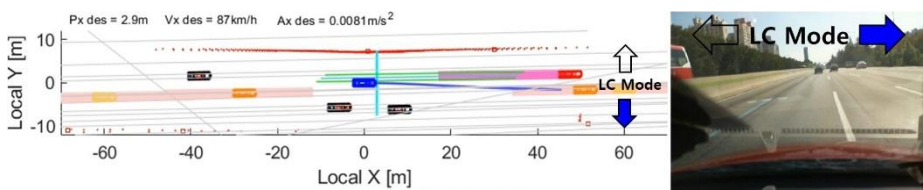
(b) Second snapshot (Time: 18sec).



(c) Third snapshot (Time: 69sec).



(d) Fourth snapshot (Time: 90sec).

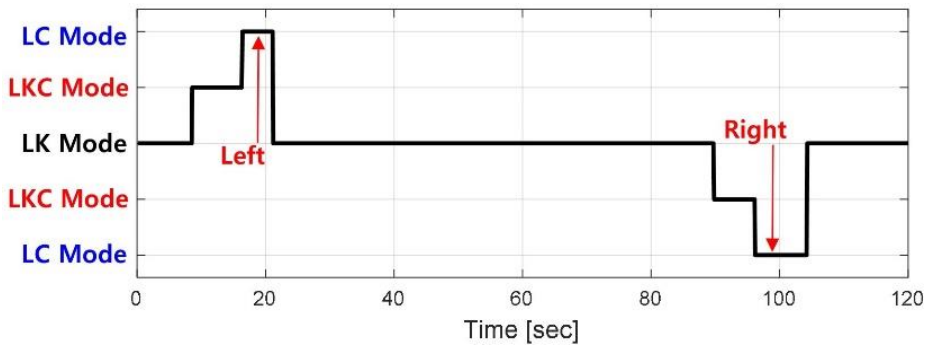


(e) Fifth snapshot (Time: 100sec).

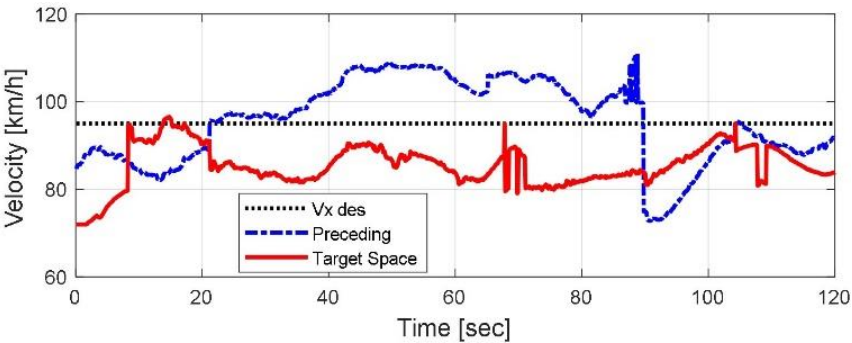
Figure 7.35. Vehicle test snapshots: the selected one overtaking situation.

Figure 7.36 represents the test results of the selected overtaking situation: driving mode, overtaking decision velocity, distance with surrounding vehicles, safety domain with surrounding vehicles, acceleration, and lateral position. These figures show that the ego vehicle proceeds to overtake, while using appropriate acceleration and maintaining safety with the surrounding vehicles. Figure 7.36 (a) indicates the driving mode that is related to the lane change demand and possibility concept for the overtaking. The left lane change is for entering to the overtaking lane, and the right lane change is for returning to the driving lane. In Figure 7.36 (b), the overtaking decision velocities are shown. The lane change demand is determined according to the decision velocities. In Figure 7.36 (c), the distances with the surrounding vehicle are indicated as clearance and safe distance. The gray area in Figure 7.36 (c) indicates the situation where the lane change is demanded. In the grayed out area of Figure 7.36 (c), the states of the nearest vehicle on the target lane are displayed. In other areas, the states of the preceding vehicle are displayed. When the clearance is greater than the safe distance in the gray area, lane change mode starts. This shows the concept of lane change possibility. In the case where lane change is not demanded, the lane-keeping situation shows the clearance and the safe distance from the preceding vehicle. It shows that the distance to the preceding vehicle is above the safe distance. The clearance control characteristics described in Figure 7.36 (d) show that the behaviors of the ego vehicle are in a safe region with a sufficient safety margin. The acceleration in Figure 7.36 (e) is satisfactory for both smooth ride quality and clearance control. Figure 7.36 (f) indicates the lane change moment and shows that the lateral

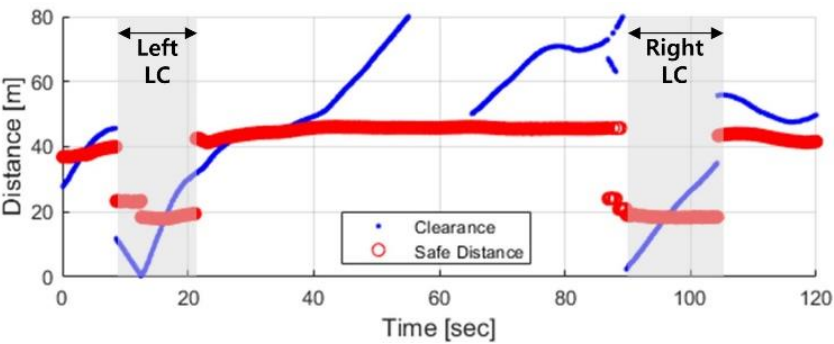
position has a sudden change within a very short time.



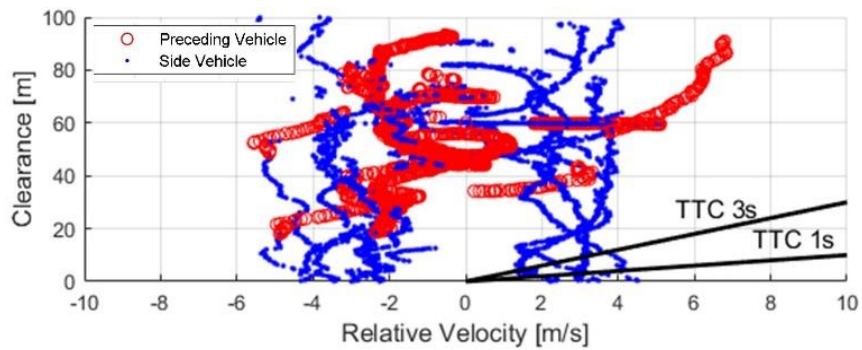
(a) Driving mode.



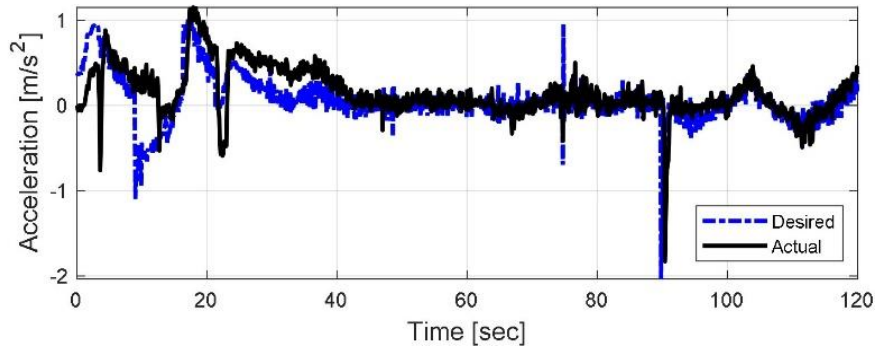
(b) Overtaking decision velocity.



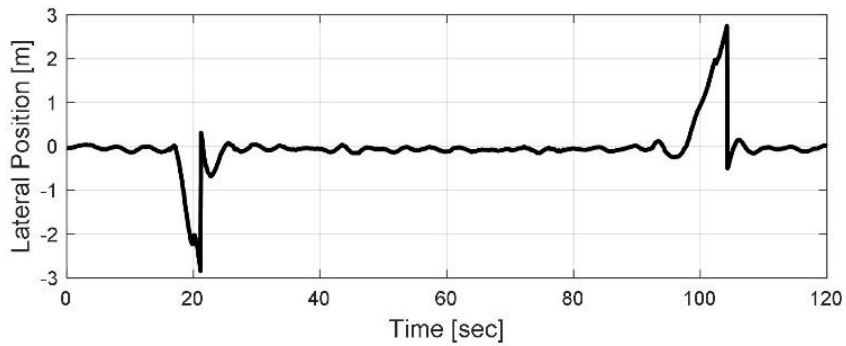
(c) Distance with surrounding vehicles.



(d) Safety domain with surrounding vehicles.



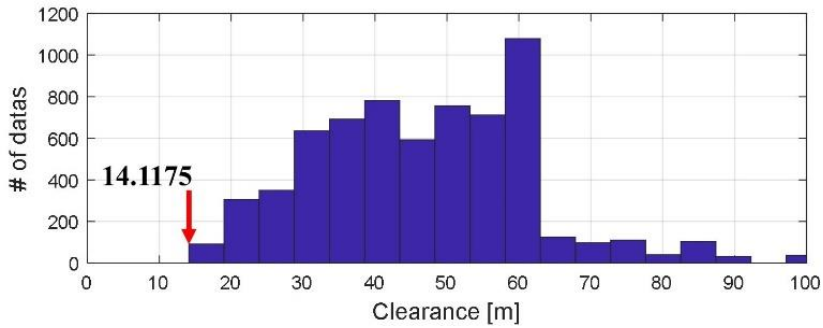
(e) Longitudinal acceleration.



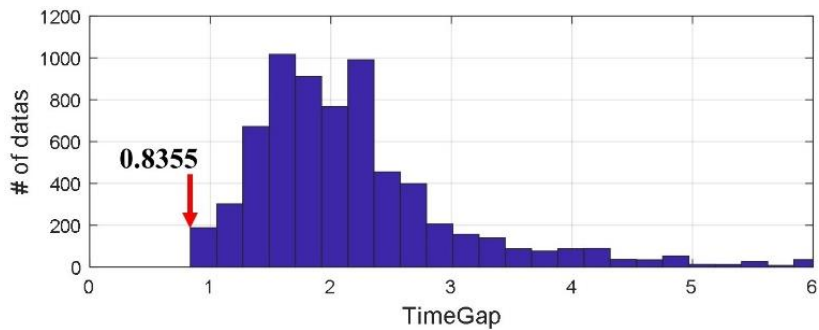
(f) Lateral position.

Figure 7.36. Vehicle test results: the selected one overtaking situation.

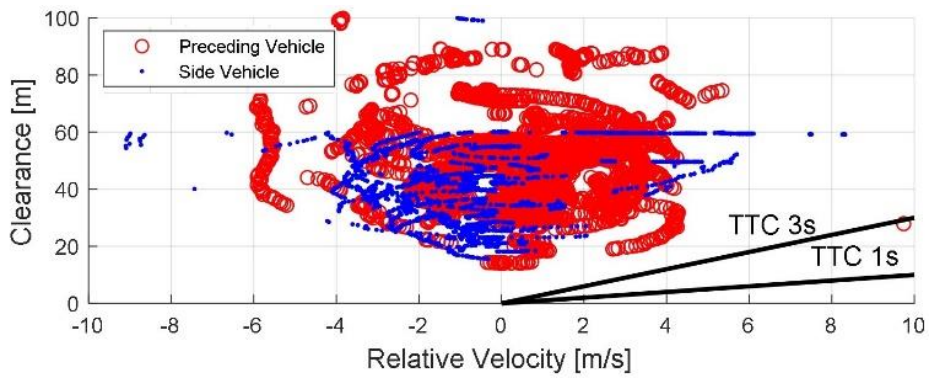
Figure 7.37 shows cumulative test data was about 106 lane changes. In Figure 7.37 (a), Figure 7.37 (b), and Figure 7.37 (c), the ego vehicle always maintains safety performance with a preceding vehicle. The minimum clearance is 14.1175 m, and the minimum time gap is 0.8355 s. This means that safety performance is maintained within the defined safe distances. All lane changes have been carried out while keeping the safety of the surrounding vehicles. Lastly, Figure 7.37 (d) represents the longitudinal and lateral acceleration of the ego vehicle during 106 lane changes. This indicates that overtaking maneuvers have been performed without compromising the ride quality of passengers.



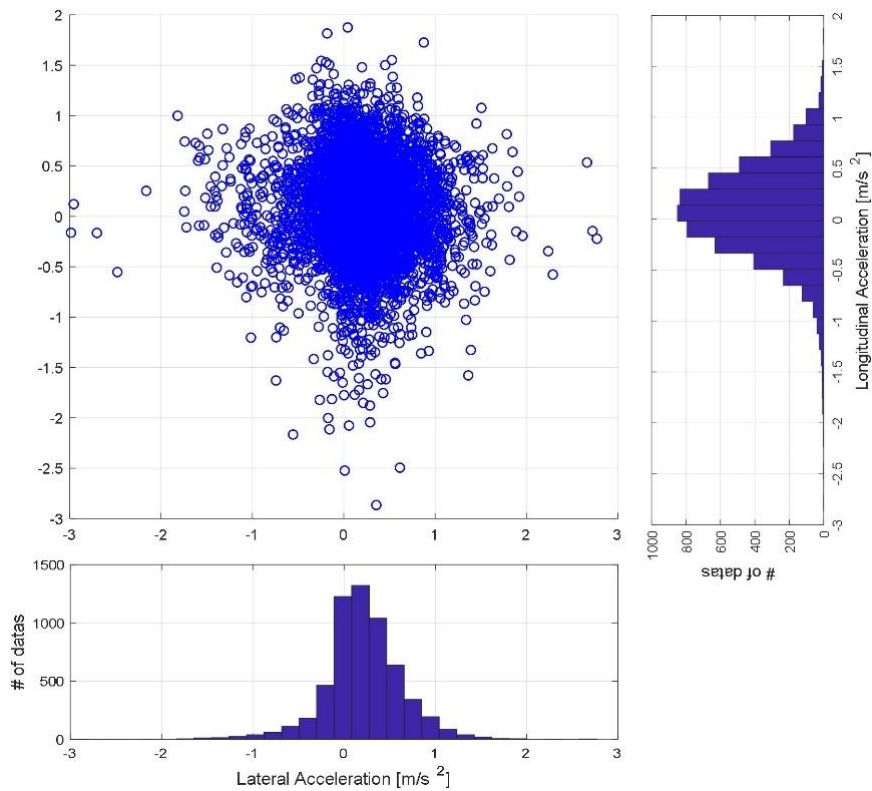
(a) Histogram of safety index: Clearance.



(b) Histogram of safety index: Time gap.



(c) Safety domain with surrounding vehicles.



(d) Longitudinal and lateral acceleration.

Figure 7.37. Vehicle test results: cumulative test data.

7.2.4. Urban DLC and MLC Test using Third Vehicle Platform

The proposed lane change algorithm has been evaluated through a real vehicle test. The test environment is the Sangam-dong, Seoul in Korea. The vehicle test has been conducted on circulation course that was designated as an autonomous driving test bed. This is a course for an autonomous circular shuttle bus. Figure 7.38 represents the test environment. Seoul City provides a high definition map in the autonomous driving test bed. Figure 7.39 shows the high definition map and the circulation course on the map.



Figure 7.38. Vehicle test environment.



Figure 7.39. High definition map of autonomous driving test bed in Seoul.

The environment is a complex urban road and has a speed limit of 50 km/h. The circulation course consists of a total of 4 straight roads. All roads vary from two lane to four lane roads as shown Figure 7.40. Figure 7.41 shows the all path and main path of the high definition map on the circular course. From main path, it can be seen that various lane changes are needed to proceed with the circulation course in a complex urban environment. The ego vehicle performs various lane change maneuvers while cycling in the environment. This study presents the two results of MLC and DLC in the most difficult situation.

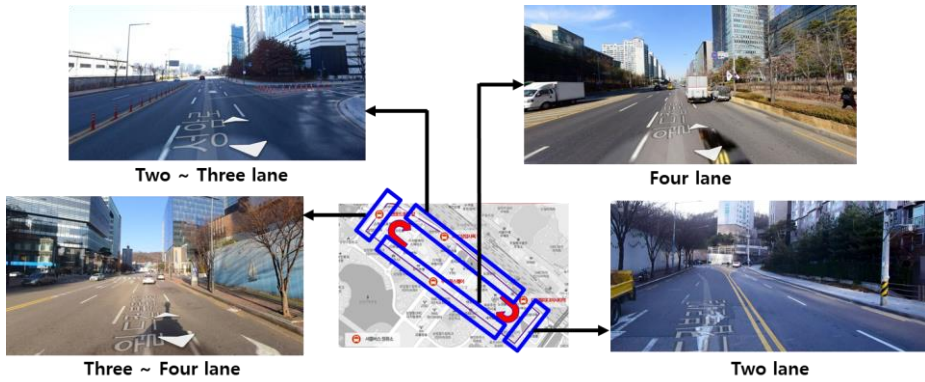


Figure 7.40. Complex urban road which is vehicle test environment.

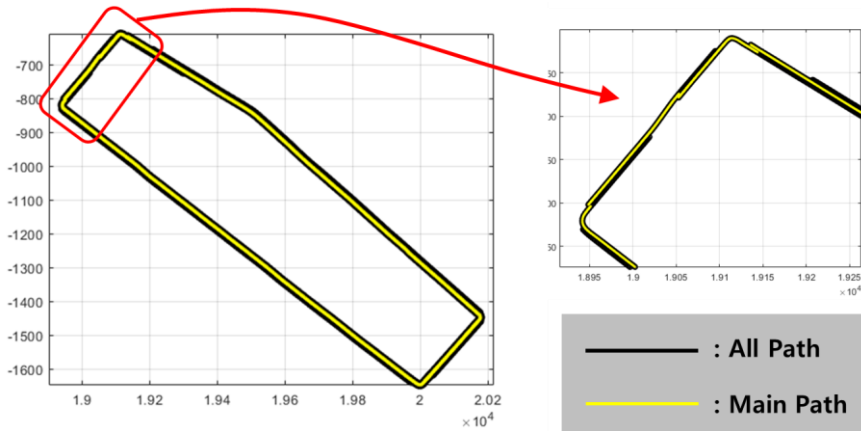


Figure 7.41. All path and main path on the high definition map.

Figure 7.42 shows the snapshots of the MLC situations. The selected situation is a situation in which the ego vehicle makes the MLC to follow main path after turning right. At this time, there are also a parked vehicle in front, so the ego vehicle needs to change lanes while maintaining safety with the parked vehicle. In the snapshots, the blue vehicle is the ego vehicle. The green points represent point clouds of the LiDAR sensors. The blue boxes are dynamic obstacles. The

red points represent static obstacles. The pink line means the future trajectory of the ego vehicle. In this dissertation, the driving mode is very important. The concepts of lane change demand, and possibility are expressed by arrows. The arrow represents the driving mode and the direction of the lane change. The colored arrows indicate the lane change demand. A red arrow represents that the lane change is impossible. A blue arrow indicates that the lane change mode proceeds because the safe distances have been sufficiently guaranteed.

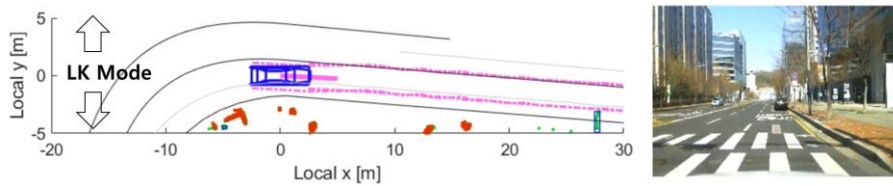
Figure 7.43 represents the test results of the selected MLC situation: driving mode, lateral position, acceleration, velocity, distance with surrounding vehicles, and trajectory. These figures show that the ego vehicle proceeds to MLC, while using appropriate acceleration and maintaining safety with the surrounding vehicles. Figure 7.43 (a) indicates the driving mode that is related to the lane change demand and possibility concept for the MLC. Figure 7.43 (b) indicates the lateral position which shows lane change motion based on driving mode. The acceleration is shown in Figure 7.43 (c). The velocity is shown in Figure 7.43 (d). The desired velocity is important in this scene. The set velocity on the road after a right turn is 22.5 km/h. In this situation, it can be seen that the lower desired velocity is set due to the front obstacle. And during lane change, the desired velocity is restored by overtaking velocity planning. In conclusion, the ego vehicle succeeds in changing lanes without stopping while maintaining safety with the vehicle in front. Figure 7.43 (e) shows that clearance with the parked vehicle remains above the safety distance. When the clearance is lower than the safety distance, it is already avoiding and passing sideways. Figure 7.43 (f) represents the path and trajectory of the ego vehicle.

To follow main path, the ego vehicle proceeds to MLC and shows the trajectory to complete it.

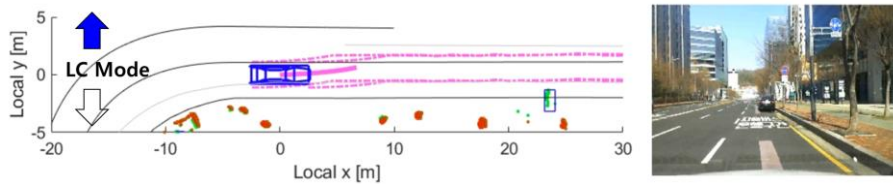
Figure 7.44 shows the snapshots of the DLC situations. The selected situation is a situation in which the ego vehicle makes the DLC to overtake the bus that has stopped in front. After the ego vehicle moves to the next lane to overtake the bus, the bus picks up all the passengers and departs quickly, crossing several lanes at once. Therefore, the bus proceeds to cut-in sharply in front of the ego vehicle, and it is possible to check the safety maintenance for cut-in vehicle.

Figure 7.45 represents the test results of the selected DLC situation: driving mode, lateral position, acceleration, velocity, distance with surrounding vehicles, and trajectory. These figures show that the ego vehicle proceeds to DLC, while using appropriate acceleration and maintaining safety with the surrounding vehicles. Figure 7.45 (a) indicates the driving mode that is related to the lane change demand and possibility concept for the DLC. Because the bus is stuck at a stop and stopped, it is difficult for the ego vehicle to determine the lane change mode from a distance. As the ego vehicle gets closer to the bus, it judges that it is impossible to pass by lane keeping and decides to perform lane change. Therefore, the ego vehicle inevitably stops behind the bus and then proceeds to change lane. Figure 7.45 (b) indicates the lateral position which shows lane change motion based on driving mode. The acceleration and velocity are shown in Figure 7.45 (c) and (d), respectively. Figure 7.45 (e) shows clearance and safety distance with the overtaken bus. When the ego vehicle changes lanes to overtake the bus, clearance with the bus remains above the safety distance. When the clearance is lower than the safety distance, it is

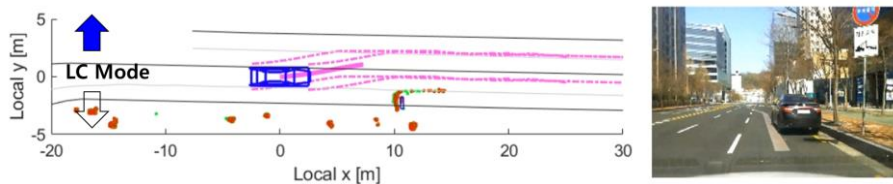
already avoiding and passing sideways. And after 150 seconds, the bus picks up all the passengers and accelerates, making a sharp cut-in in front of the ego vehicle. At this time, the clearance appears below the safety distance, but the clearance gets closer to the safety distance through proper safety control. Figure 7.45 (f) represents the path and trajectory of the ego vehicle. To overtake the temporary stopped bus, the ego vehicle proceeds to DLC despite deviating from main path.



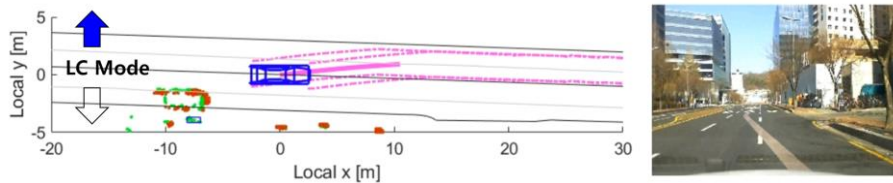
(a) First snapshot (Time: 15sec).



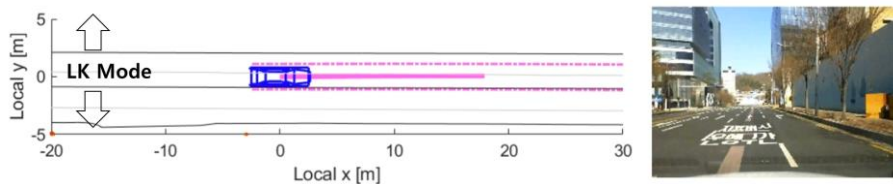
(b) Second snapshot (Time: 30sec).



(c) Third snapshot (Time: 65sec).

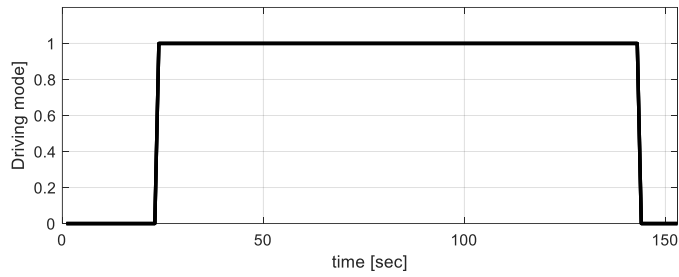


(d) Fourth snapshot (Time: 110sec).

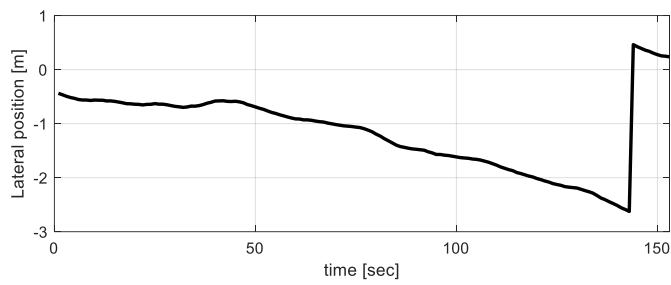


(e) Fifth snapshot (Time: 150sec).

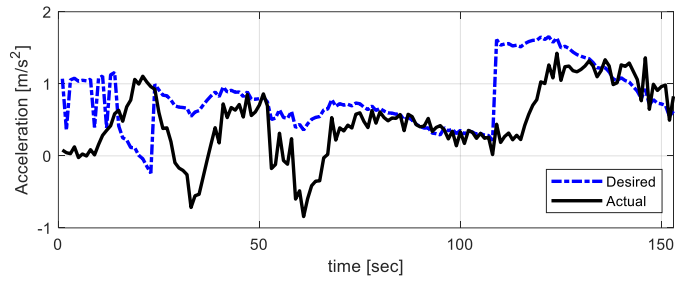
Figure 7.42. Vehicle test snapshots: the MLC situation.



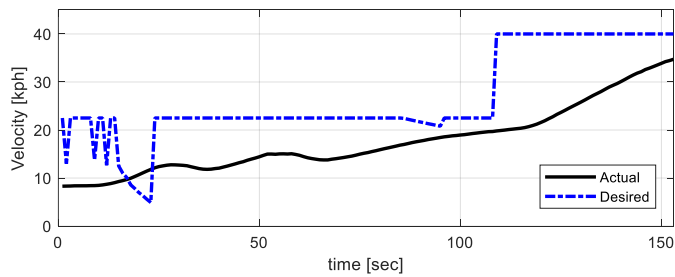
(a) Driving mode.



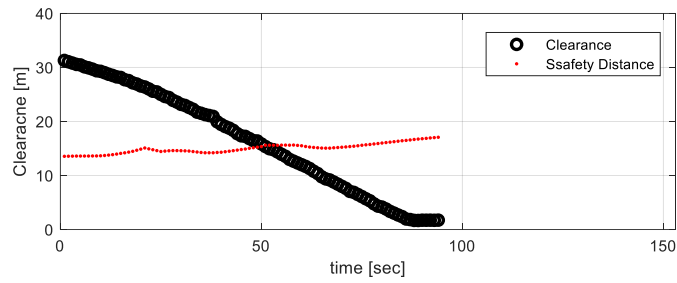
(b) Lateral position.



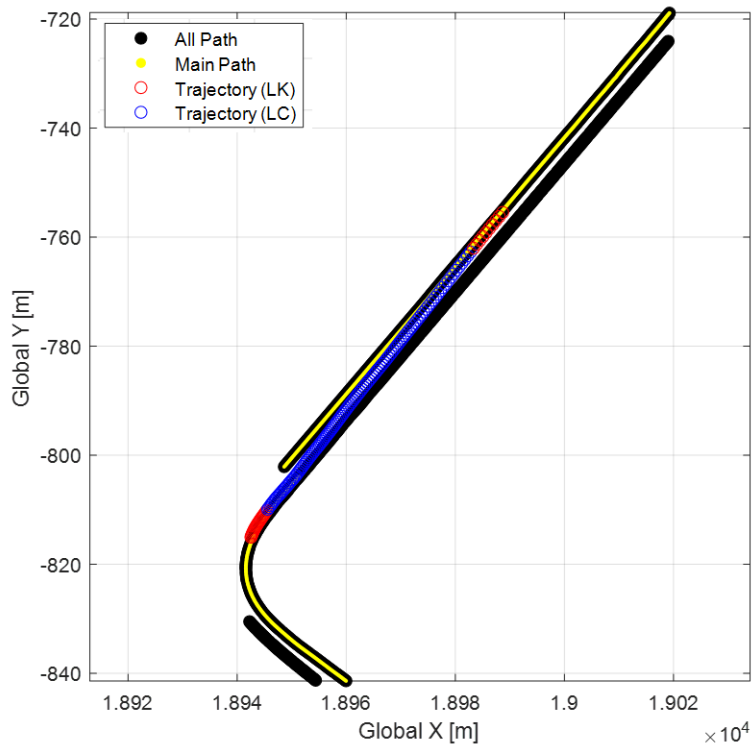
(c) Longitudinal acceleration.



(d) Longitudinal velocity.

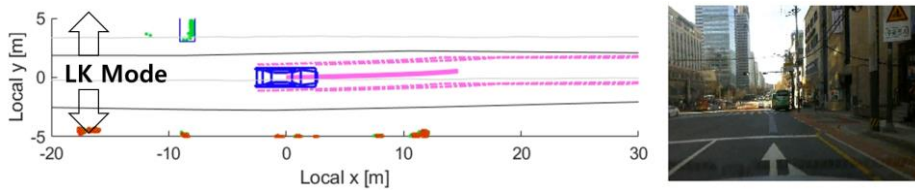


(e) Clearance with the parked vehicle in front.

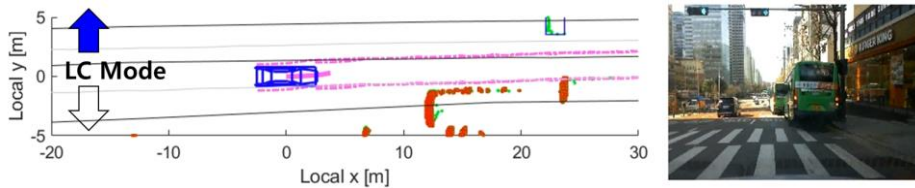


(f) Path and trajectory of the ego vehicle.

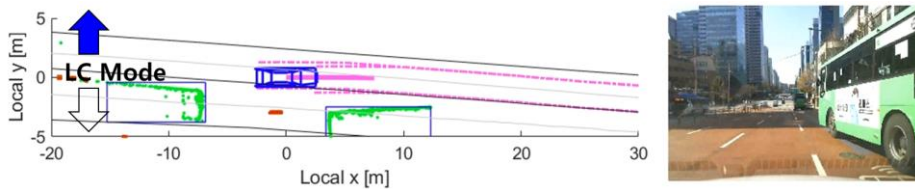
Figure 7.43. Vehicle test results: the MLC situation.



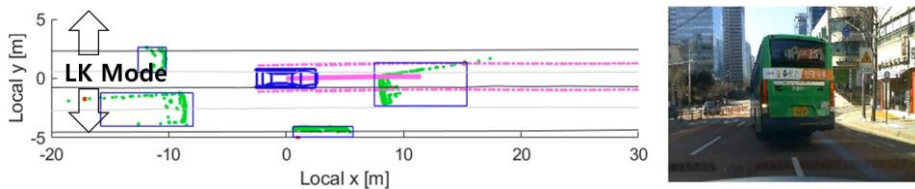
(a) First snapshot (Time: 5sec).



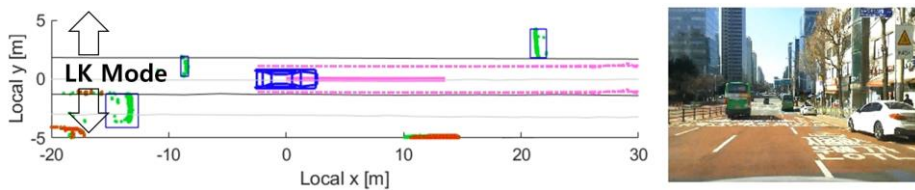
(b) Second snapshot (Time: 45sec).



(c) Third snapshot (Time: 150sec).

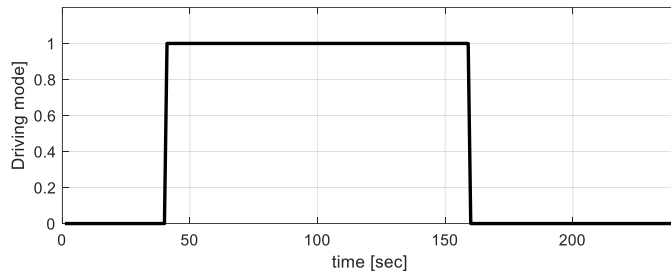


(d) Fourth snapshot (Time: 180sec).

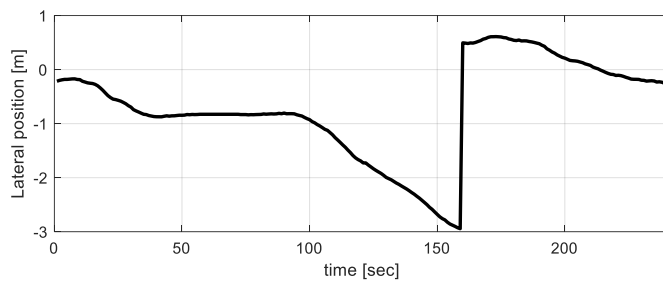


(e) Fifth snapshot (Time: 220sec).

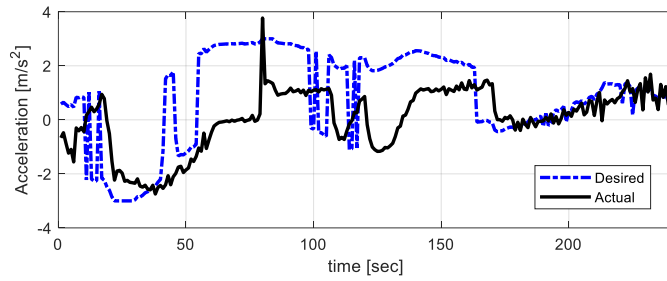
Figure 7.44. Vehicle test snapshots: the DLC situation.



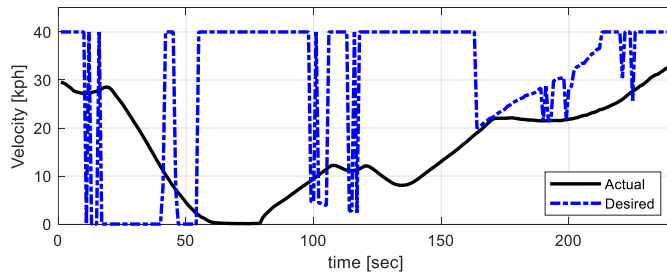
(a) Driving mode.



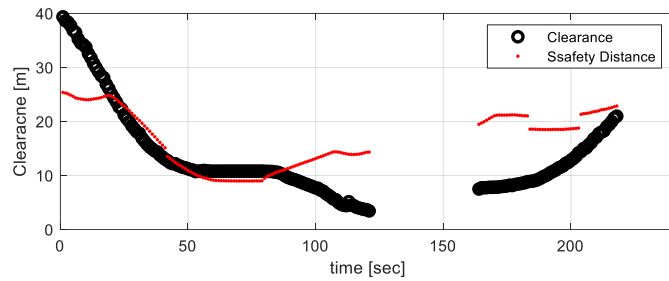
(b) Lateral position.



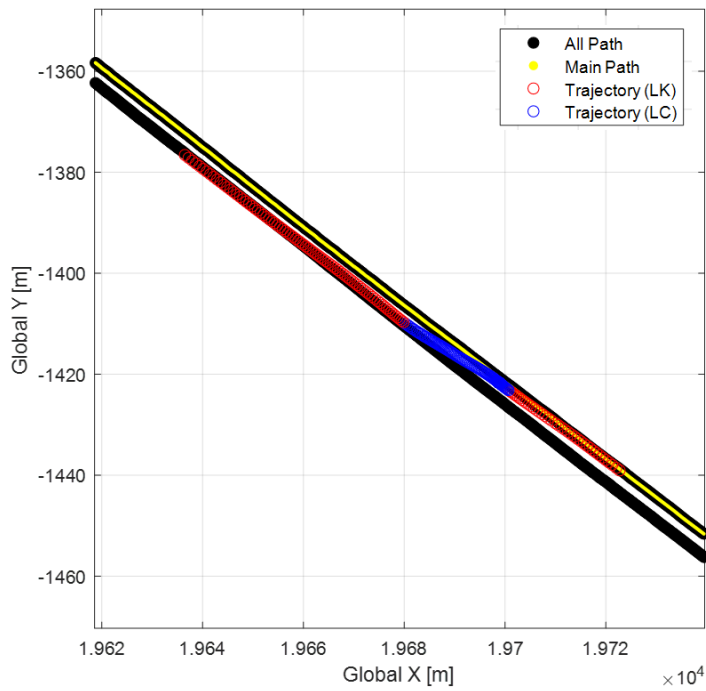
(c) Longitudinal acceleration.



(d) Longitudinal velocity.



(e) Clearance with the overtaken bus.



(f) Path and trajectory of the ego vehicle.

Figure 7.45. Vehicle test results: the DLC situation.

7.2.5. Self-directed Interactive Lane Change Test using Second Vehicle Platform

The proposed lane change algorithm has been evaluated through a real vehicle test. The test environment is the test bed located at Siheung Campus, Seoul National University in Korea. The test bed was established for the purpose of developing and verifying autonomous vehicles. Figure 7.46 shows the test bed.

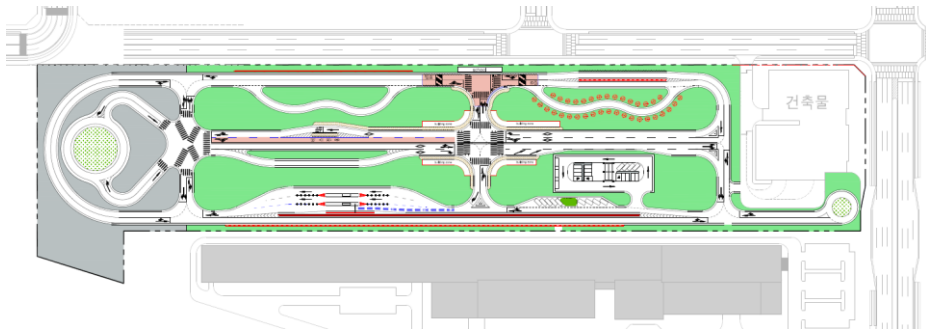


Figure 7.46. Test bed for autonomous vehicles at Siheung Campus, Seoul National University.

In this test bed, the interactive lane change test has been conducted. In this test, one autonomous vehicle and two vehicles that are actually driven by humans are used. The autonomous vehicle is second platform in the dissertation. In this test, it is necessary to simulate the lane change of the congestion traffic. It is practically impossible to use multiple vehicles for congested traffic situation. Therefore, it is implemented that there are virtual vehicles of congestion in front of and behind the two vehicles driven by humans. Figure 7.47 represents the test environments. The yield intention by surrounding

vehicles to change lanes of autonomous vehicles is important. Accordingly, the surrounding vehicles driven by humans take the behavior of yielding or not yielding.

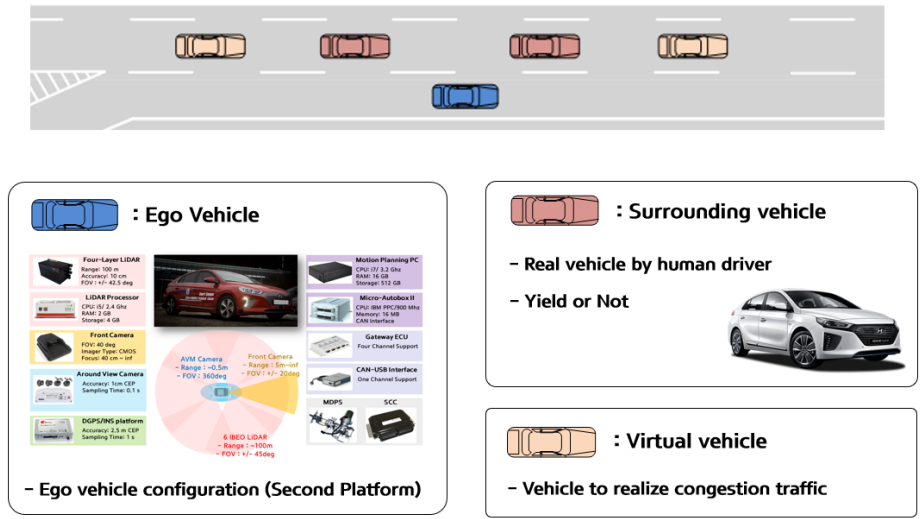


Figure 7.47. Interactive lane change vehicle test environment.

Autonomous vehicle attempts to change lanes between surrounding vehicles. The first situation is a situation in which the side-rear vehicle has yield intention. Therefore, the autonomous vehicle can change lanes immediately. The second situation is a situation in which the side-rear vehicle has no intention to yield. Therefore, the autonomous vehicle fails to change lanes and goes in front of the side-front vehicle. Since the side-front vehicle has yield intention, the autonomous vehicle changes lanes in front of the side-front vehicle. Figure 7.48 shows the two situations.

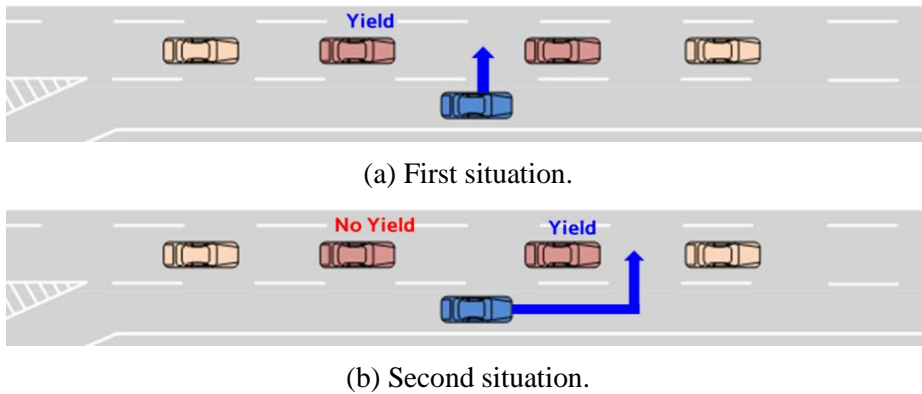
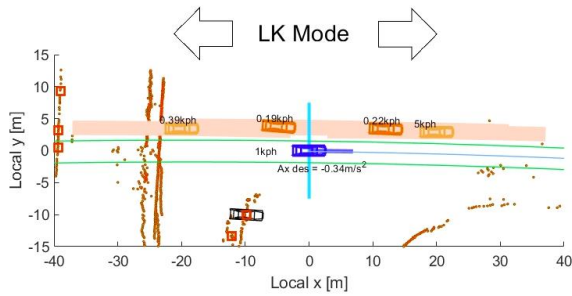


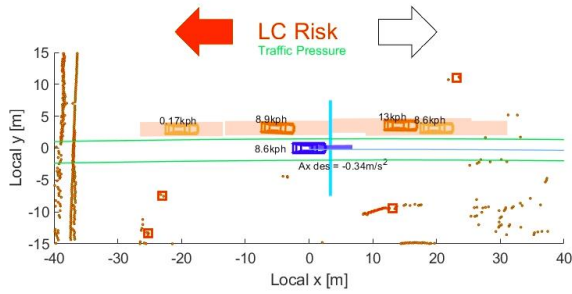
Figure 7.48. Two situation of interactive lane change vehicle test.

The test snapshots of first situation are represented in Figure 7.49. The test results of first situation are shown in Figure 7.50. The autonomous vehicle is well aware of the yield intention of the side-rear vehicle and immediately succeeds in changing lanes.

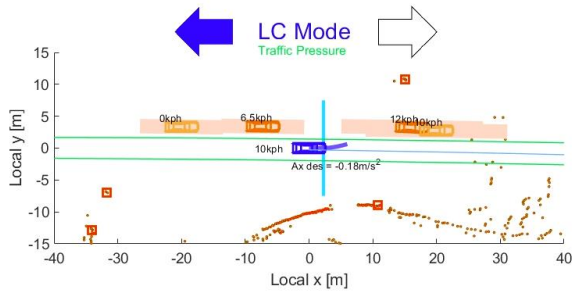
The test snapshots and results of second situation are represented in Figure 7.51 and Figure 7.52, respectively. The autonomous vehicle is well aware of the non-yield intention of side-rear and abandon the lane change. Then, the autonomous vehicle drives in front of the side-front vehicle. After moving to the front of the side-front vehicle, the autonomous vehicle figures out the yield intention of side-front vehicle and proceeds with the lane change.



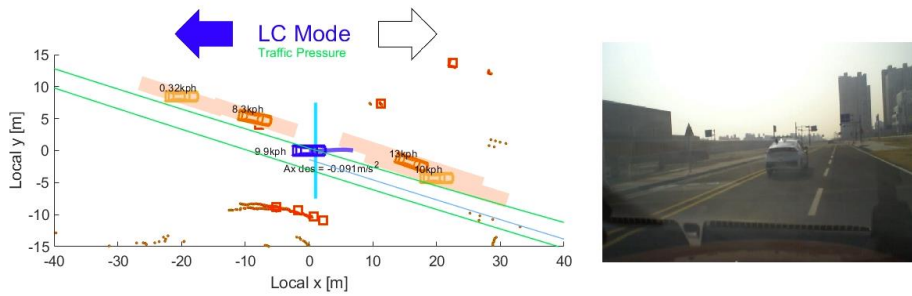
(a) First snapshot (Time: 0sec).



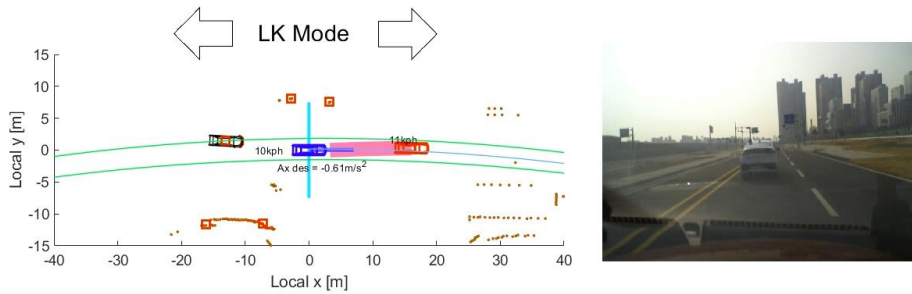
(b) Second snapshot (Time: 7sec).



(c) Third snapshot (Time: 10sec).

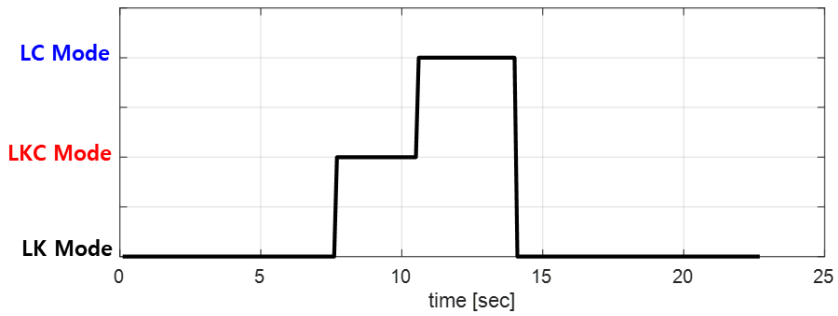


(d) Fourth snapshot (Time: 12sec).

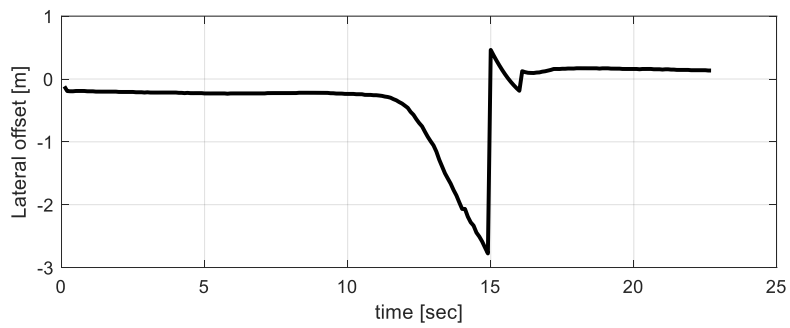


(e) Fifth snapshot (Time: 17sec).

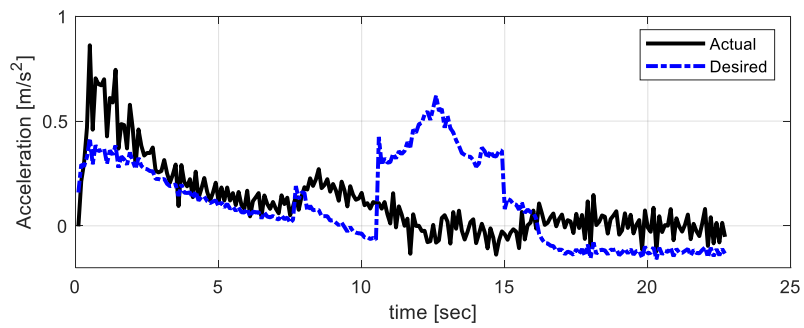
Figure 7.49. Vehicle test snapshots: the first situation.



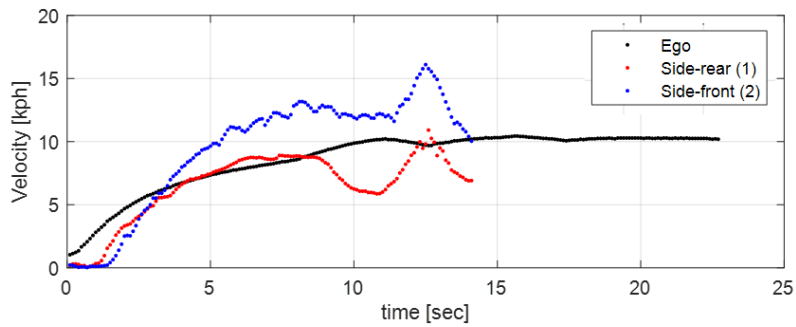
(a) Driving mode.



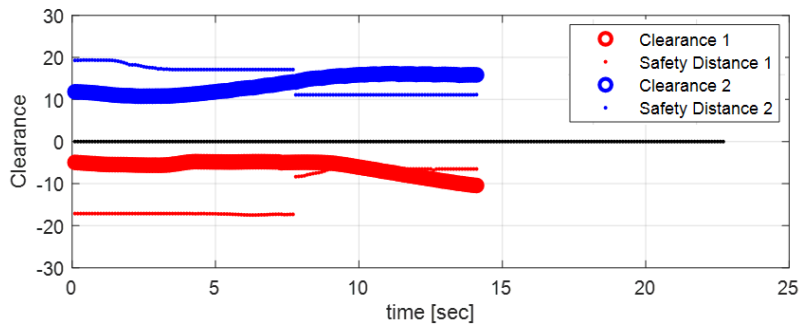
(b) Lateral position.



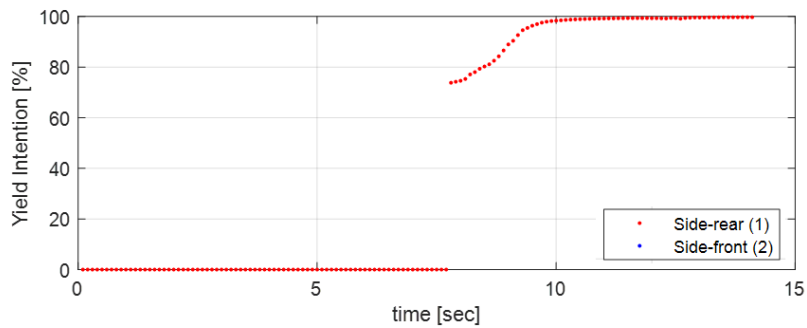
(c) Longitudinal acceleration.



(d) Longitudinal velocity.

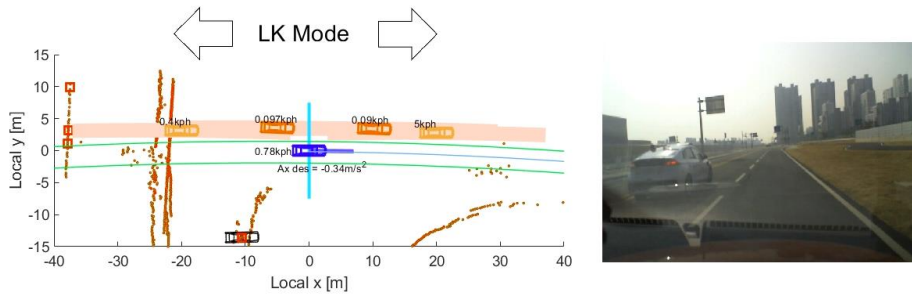


(e) Clearance with the two side vehicles.

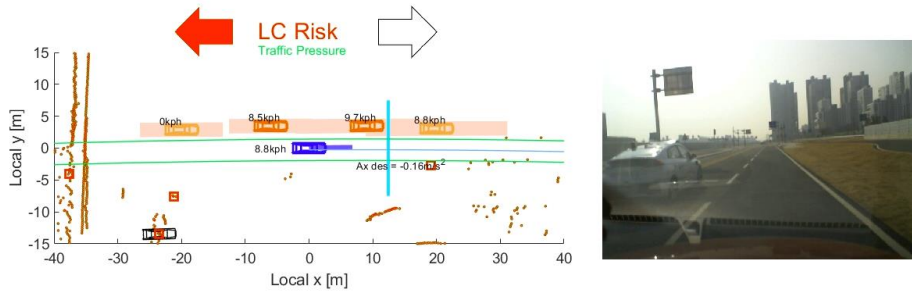


(f) Yield intention of the side-rear vehicle.

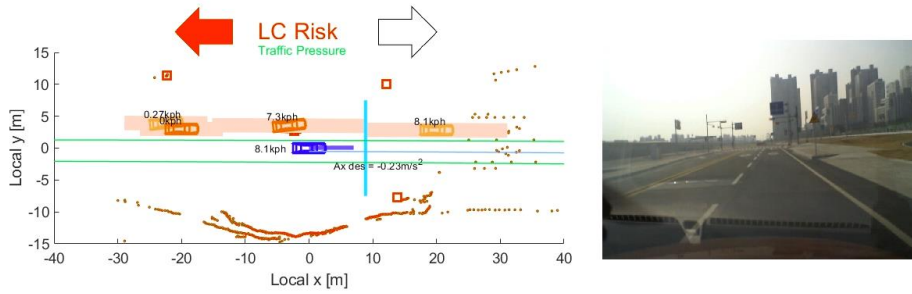
Figure 7.50. Vehicle test results: the first situation.



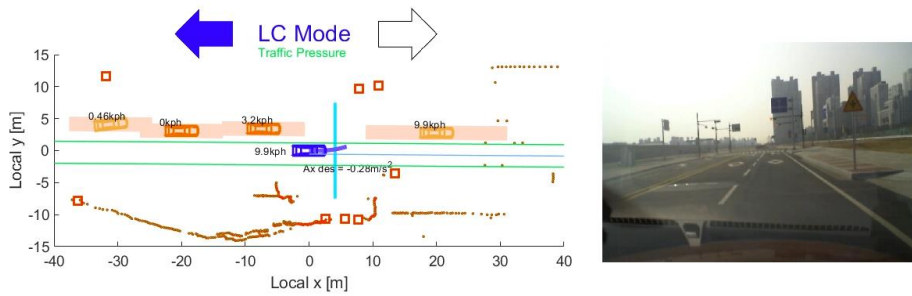
(a) First snapshot (Time: 0sec).



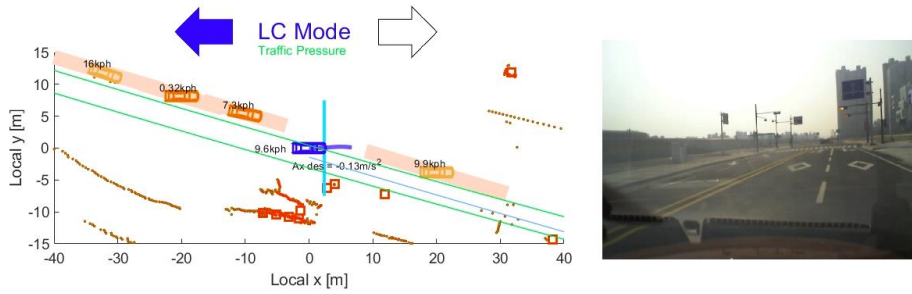
(b) Second snapshot (Time: 7sec).



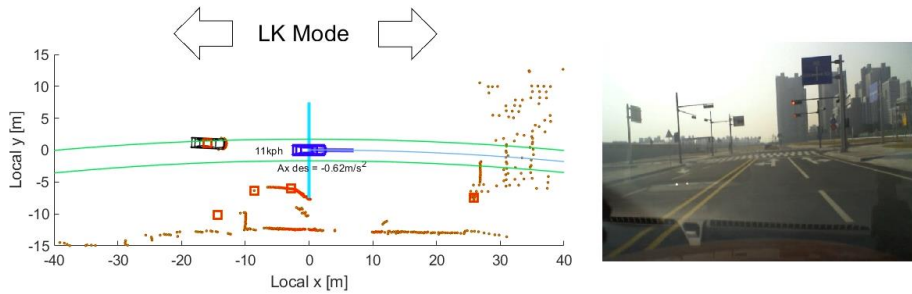
(c) Third snapshot (Time: 21sec).



(d) Fourth snapshot (Time: 24sec).

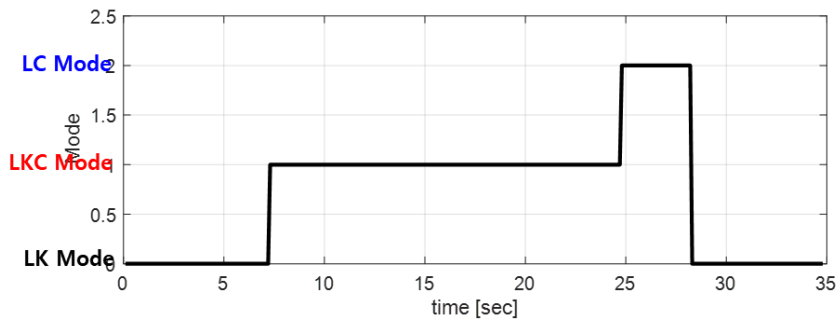


(e) Fifth snapshot (Time: 26sec).

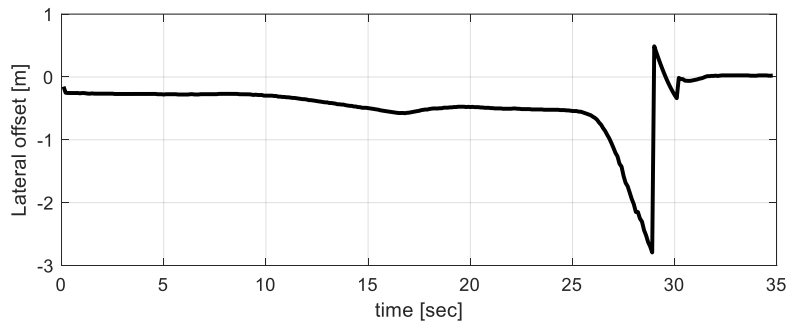


(f) Sixth snapshot (Time: 31sec).

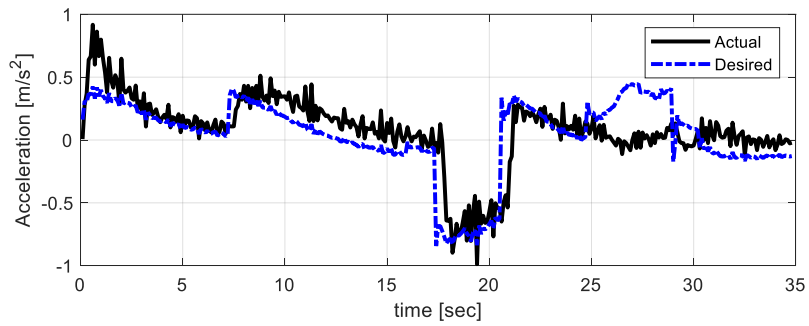
Figure 7.51. Vehicle test snapshots: the second situation.



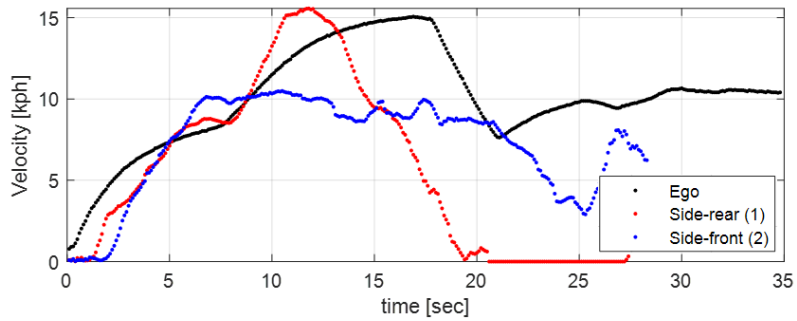
(a) Driving mode.



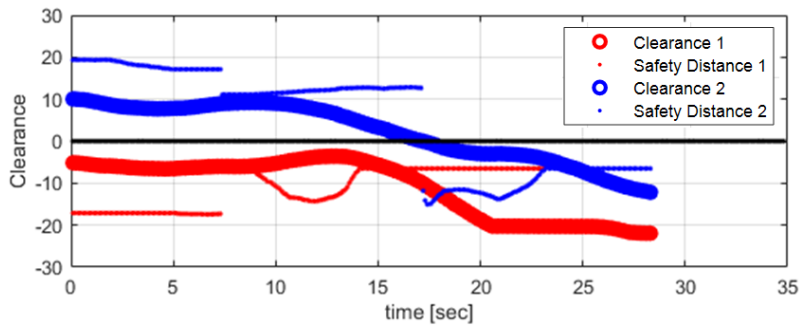
(b) Lateral position.



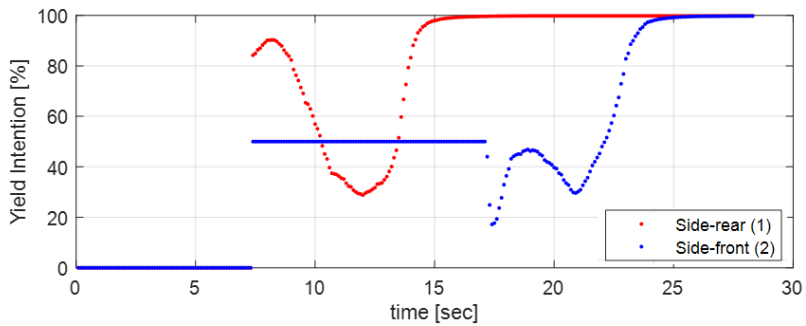
(c) Longitudinal acceleration.



(d) Longitudinal velocity.



(e) Clearance with the two side vehicles.



(f) Yield intention of the two side vehicles.

Figure 7.52. Vehicle test results: the second situation.

Chapter 8 Conclusion & Future Works

8.1. Conclusion

Human driver data based active lane change algorithm has been developed in this dissertation. Since most autonomous vehicles recognize the environment by the local sensor, there is a problem with the limitation of the cognitive range. Virtual targets have been devised to cope with this problem. Since proper prediction is helpful for autonomous driving, the stochastic prediction models of both ego vehicle and surrounding vehicle are presented. In terms of reflecting uncertainties, the stochastic prediction is conducted. Since autonomous driving systems must be acceptable to both drivers and passengers, the human driving data of lane change has been acquired to design the system to accurately simulate drivers. Based on the acquired driving data, safety indices are defined for the lane change situation. Rule based and learning based approaches are adopted for safety indices. Safety indices are supplemented with intention inference using LSTM based RNN, which can cope with various lane changes. To validate about safety performance, these indices are analyzed kinematically. Then, stochastic prediction-based safety distances are derived by safety indices and prediction models. Also, collision probability has been employed to consider various uncertainties. The active lane change algorithm has been developed based on these risk assessment. Decision and motion planning are

conducted based on the stochastic prediction-based safety distance, which is able to achieve safety performance without heavy computational burden. The algorithm has considered the decision rules that drivers adopt when performing lane change. For this purpose, the concepts of availability, target space, demand, and possibility for lane change have been devised. The desired driving mode is decided to handle both DLC and MLC. Intuitive and efficient motion planning has determined desired states and constraints according to the desired driving mode. Longitudinal and lateral motion planning proceed, respectively, in which references and constraints are defined in each of the states. The references are decided based on the stochastic prediction-based safety distances. The safe driving envelope is adopted as constraints. The envelope is defined as an area in which the ego vehicle can drive without collision with surrounding vehicles. Finally, in order to track the desired motion, a decoupled control architecture has been adopted solving the SMPC problem.

The effectiveness of the proposed automated driving algorithm has been evaluated via test-data based simulations and vehicle tests. In order to show various performances, a total of 5 types of simulations have been proceeded. Simulation tests show performance improvement compared to other algorithms. And they reveal repeated performance improvement through monte-calro simulation. The performance of the proposed algorithm has been investigated via a vehicle test on highways and urbans. The vehicle test results revealed that safe and comfortable lane changes have been achieved using our autonomous test vehicle. A number of test results have been compared with human driving data and shown the similar behavior pattern.

The main contributions of this work are as follows: 1) the virtual vehicle is devised to overcome perception limitation by local sensors and blind spots; 2) the safe distance with intention inference is defined for driver acceptance using rule based and learning based approaches; 3) the diverse uncertainties for safety improvement are considered using stochastic prediction based safety distance and the collision probability; 4) the efficient and intuitive decision-making and motion planning are achieved using driving mode and target space; 5) based on stochastic prediction and SMPC, the smooth and safe driving performance are accomplished with light computation for vehicle implementation; and 6) the efficacy of safe and repetitive driving performance are confirmed by simulation tests and actual vehicle tests.

8.2. Future Works

Future works aim at advancing the proposed algorithm, which could perform successful lane changes in congested traffic. Congestion occurs on both highways and urbans. Lane changes in congested traffic are especially important in urban driving. In congested situations, the only safety distances may be insufficient to conduct lane change decision and planning. It is important to infer yield intentions of surrounding vehicles. Intention inference of surrounding vehicles is currently studied for autonomous driving in highway on-ramp and urban intersection. In this dissertation, such intention inference has been applied to surrounding vehicles in congested lane change situations. Also, it is necessary to transmit the intent of the lane change. The intent could be conveyed to surrounding vehicles through turn signal or lateral motion of the ego vehicle. The proposed algorithm has been vailidated to carry out interactive lane changes through simulation study. Future works aims to validate advanced interactive lane change with real vehicle test on actual roads.

Future works also aim at advancing the proposed algorithm, which could perform biased driving. Biased driving is requied with diverse situations on both highways and urbans. Biased driving is needed to avoid side vehicles running in the lane or parked on the shoulder. There is a need for motion planning for vehicles that can be avoided without having to change lanes. In particular, it is essential when avoiding shoulder vehicles on the first lane.

Bibliography

- AFOLABI, O., DRIGGS–CAMPBELL, K., DONG, R., KOCHENDERFER, M. J. & SASTRY, S. S. People as sensors: Imputing maps from human actions. 2018 IEEE/RSJ International Conference on Intelligent Robots and Systems (IROS), 2018. IEEE, 2342-2348.
- AHMED, K. I. 1999. *Modeling drivers' acceleration and lane changing behavior*. Massachusetts Institute of Technology.
- ALESSANDRINI, A., CATTIVERA, A., HOLGUIN, C. & STAM, D. 2014. CityMobil2: challenges and opportunities of fully automated mobility. *Road Vehicle Automation*. Springer.
- ALTHOFF, M., STURSBURG, O. & BUSS, M. 2009. Model-based probabilistic collision detection in autonomous driving. *IEEE Transactions on Intelligent Transportation Systems*, 10, 299-310.
- ANDERSON, S. J., PETERS, S. C., PILUTTI, T. E. & IAGNEMMA, K. 2010. An optimal-control-based framework for trajectory planning, threat assessment, and semi-autonomous control of passenger vehicles in hazard avoidance scenarios. *International Journal of Vehicle Autonomous Systems*, 8, 190-216.
- BASJARUDDIN, N. C., SAEFUDIN, D., RAKHMAN, E. & RAMADLAN, A. M. 2015. Overtaking assistant system based on fuzzy logic. *Telkomnika*, 13, 76.
- BIBULI, M., CACCIA, M. & LAPIERRE, L. 2010. Virtual target based coordinated path-following for multi-vehicle systems. *IFAC Proceedings Volumes*, 43, 336-341.
- BISHOP, R. A survey of intelligent vehicle applications worldwide. Intelligent Vehicles Symposium, 2000. IV 2000. Proceedings of the IEEE, 2000. IEEE, 25-30.
- BRECHTEL, S., GINDELE, T. & DILLMANN, R. Probabilistic MDP-behavior planning for cars. 2011 14th International IEEE Conference on Intelligent Transportation Systems (ITSC), 2011. IEEE, 1537-1542.

- BUTAKOV, V. A. & IOANNOU, P. 2015. Personalized driver/vehicle lane change models for ADAS. *IEEE Transactions on Vehicular Technology*, 64, 4422-4431.
- CARVALHO, A., GAO, Y., LEFEVRE, S. & BORRELLI, F. Stochastic predictive control of autonomous vehicles in uncertain environments. 12th International Symposium on Advanced Vehicle Control, 2014. 712-719.
- CHAE, H., JEONG, Y., KIM, S., LEE, H., PARK, J. & YI, K. Design and vehicle implementation of autonomous lane change algorithm based on probabilistic prediction. 2018 21st International Conference on Intelligent Transportation Systems (ITSC), 2018. IEEE, 2845-2852.
- CHAE, H. & YI, K. Supervised Learning based Overtaking Decision Algorithm for Highway Autonomous Driving. Proceedings of the 5th International Symposium on Future Active Safety Technology toward Zero Accidents (FAST-zero '19), 2019 Blacksburg, VA, USA.
- CHAE, H. & YI, K. 2020. Virtual Target-Based Overtaking Decision, Motion Planning, and Control of Autonomous Vehicles. *IEEE Access*, 8, 51363-51376.
- DO, Q. H., TEHRANI, H., MITA, S., EGAWA, M., MUTO, K. & YONEDA, K. 2017. Human drivers based active-passive model for automated lane change. *IEEE Intelligent Transportation Systems Magazine*, 9, 42-56.
- DOMAHIDI, A. & JEREZ, J. 2014. Forces Professional. *embotech GmbH*.
- DONG, C., DOLAN, J. M. & LITKOUHI, B. Intention estimation for ramp merging control in autonomous driving. 2017 IEEE Intelligent Vehicles Symposium (IV), 2017. IEEE, 1584-1589.
- ENACHE, N. M., NETTO, M., MAMMAR, S. & LUSETTI, B. 2009. Driver steering assistance for lane departure avoidance. *Control engineering practice*, 17, 642-651.
- ESKANDARIAN, A. 2012. *Handbook of intelligent vehicles*, Springer.
- ETEMAD, A. 2017. AdaptIVe: Automated Driving Applications and Technologies for Intelligent Vehicles. *Automated Driving*. Springer.

- FALCONE, P., BORRELLI, F., ASGARI, J., TSENG, H. E. & HROVAT, D. 2007. Predictive active steering control for autonomous vehicle systems. *IEEE Transactions on control systems technology*, 15, 566-580.
- FENG, J., RUAN, J. & LI, Y. Study on intelligent vehicle lane change path planning and control simulation. 2006 IEEE international conference on information acquisition, 2006. IEEE, 683-688.
- FERGUSON, D., HOWARD, T. M. & LIKHACHEV, M. 2008. Motion planning in urban environments. *Journal of Field Robotics*, 25, 939-960.
- FINNEGAN, P. & GREEN, P. 1990. The time to change lanes: A literature review. University of Michigan, Transportation Research Institute.
- GAO, H., CHENG, B., WANG, J., LI, K., ZHAO, J. & LI, D. 2018. Object classification using CNN-based fusion of vision and LIDAR in autonomous vehicle environment. *IEEE Transactions on Industrial Informatics*, 14, 4224-4231.
- GOODFELLOW, I., BENGIO, Y. & COURVILLE, A. 2016. *Deep learning*, MIT press.
- GRAY, A., GAO, Y., LIN, T., HEDRICK, J. K. & BORRELLI, F. Stochastic predictive control for semi-autonomous vehicles with an uncertain driver model. Intelligent Transportation Systems-(ITSC), 2013 16th International IEEE Conference on, 2013. IEEE, 2329-2334.
- HOCHREITER, S. & SCHMIDHUBER, J. 1997. Long short-term memory. *Neural computation*, 9, 1735-1780.
- HPLNHAGEN, T., DENGLER, I., TAMKE, A., DANG, T. & BREUEL, G. Maneuver recognition using probabilistic finite-state machines and fuzzy logic. Intelligent vehicles symposium (IV), 2010 IEEE, 2010. IEEE, 65-70.
- HU, Y., ZHAN, W., SUN, L. & TOMIZUKA, M. Multi-modal probabilistic prediction of interactive behavior via an interpretable model. 2019 IEEE Intelligent Vehicles Symposium (IV), 2019. IEEE, 557-563.
- ISING, K. W., DROLL, J. A., KROEKER, S. G., D'ADDARIO, P. M. & GOULET, J.-F. Driver-related delay in emergency braking response to a laterally

- incurring hazard. Proceedings of the Human Factors and Ergonomics Society Annual Meeting, 2012. Sage Publications Sage CA: Los Angeles, CA, 705-709.
- JEONG, Y., KIM, S. & YI, K. 2020a. Surround vehicle motion prediction using LSTM-RNN for motion planning of autonomous vehicles at multi-lane turn intersections. *IEEE Open Journal of Intelligent Transportation Systems*, 1, 2-14.
- JEONG, Y. & YI, K. 2020b. Bidirectional Long Shot-Term Memory-Based Interactive Motion Prediction of Cut-In Vehicles in Urban Environments. *IEEE Access*, 8, 106183-106197.
- KESTING, A., TREIBER, M. & HELBING, D. 2007. General lane-changing model MOBIL for car-following models. *Transportation Research Record*, 1999, 86-94.
- KIM, B., PARK, K. & YI, K. 2017. Probabilistic threat assessment with environment description and rule-based multi-traffic prediction for integrated risk management system. *IEEE Intelligent Transportation Systems Magazine*, 9, 8-22.
- KIM, B. & YI, K. 2014. Probabilistic and holistic prediction of vehicle states using sensor fusion for application to integrated vehicle safety systems. *IEEE Transactions on Intelligent Transportation Systems*, 15, 2178-2190.
- KIM, D., KIM, B., CHUNG, T. & YI, K. 2016. Lane-level localization using an AVM camera for an automated driving vehicle in urban environments. *IEEE/ASME Transactions on Mechatronics*, 22, 280-290.
- KOSIS, K. S. I. S. 2018. Available: http://kosis.kr/statHtml/statHtml.do?orgId=101&tblId=DT_1SSSA113R&conn_path=I2.
- LEE, H., CHAE, H. & YI, K. 2019. A Geometric Model based 2D LiDAR/Radar Sensor Fusion for Tracking Surrounding Vehicles. *IFAC-PapersOnLine*, 52, 130-135.

- LEE, H., JEONG, Y., MIN, K., LEE, M., SHIN, J. K. & YI, K. 2016. Multi-Vehicle Environment Simulation Tool to Develop and Evaluate Automated Driving Systems in Motorway. *Journal of Auto-vehicle Safety Association*, 8, 31-37.
- LEE, H., YOON, J., JEONG, Y. & YI, K. 2020. Moving Object Detection and Tracking Based on Interaction of Static Obstacle Map and Geometric Model-Free Approach for Urban Autonomous Driving. *IEEE Transactions on Intelligent Transportation Systems*.
- LEE, T. 2015. *Robust Autonomous Emergency Braking Algorithm using the Tire-road Friction Estimation and the Sensor Uncertainties*. Doctoral degree, Seoul National University.
- LI, J., ZHAN, W. & TOMIZUKA, M. Generic vehicle tracking framework capable of handling occlusions based on modified mixture particle filter. 2018 IEEE Intelligent Vehicles Symposium (IV), 2018. IEEE, 936-942.
- LI, K. & IOANNOU, P. 2004. Modeling of traffic flow of automated vehicles. *IEEE Transactions on Intelligent Transportation Systems*, 5, 99-113.
- LI, X., XU, X. & ZUO, L. Reinforcement learning based overtaking decision-making for highway autonomous driving. 2015 Sixth International Conference on Intelligent Control and Information Processing (ICICIP), 2015. IEEE, 336-342.
- LINDGREN, A. & CHEN, F. 2006. State of the art analysis: An overview of advanced driver assistance systems (adas) and possible human factors issues. *Human factors and economics aspects on safety*, 38-50.
- MAYNE, D. Q., RAWLINGS, J. B., RAO, C. V. & SCOKAERT, P. O. 2000. Constrained model predictive control: Stability and optimality. *Automatica*, 36, 789-814.
- MAYNE, D. Q., SERON, M. M. & RAKOVIĆ, S. 2005. Robust model predictive control of constrained linear systems with bounded disturbances. *Automatica*, 41, 219-224.
- MCNAUGHTON, M., URMSON, C., DOLAN, J. M. & LEE, J.-W. Motion planning for autonomous driving with a conformal spatiotemporal lattice. 2011 IEEE

- International Conference on Robotics and Automation, 2011. IEEE, 4889-4895.
- MOON, S. & YI, K. 2008. Human driving data-based design of a vehicle adaptive cruise control algorithm. *Vehicle System Dynamics*, 46, 661-690.
- NARANJO, J. E., GONZALEZ, C., GARCIA, R. & DE PEDRO, T. 2008. Lane-change fuzzy control in autonomous vehicles for the overtaking maneuver. *IEEE Transactions on Intelligent Transportation Systems*, 9, 438-450.
- NGAI, D. C. K. & YUNG, N. H. C. 2011. A multiple-goal reinforcement learning method for complex vehicle overtaking maneuvers. *IEEE Transactions on Intelligent Transportation Systems*, 12, 509-522.
- NISHIWAKI, Y., MIYAJIMA, C., KITAOKA, N., TERASHIMA, R., WAKITA, T. & TAKEDA, K. Generating lane-change trajectories of individual drivers. *Vehicular Electronics and Safety*, 2008. ICVES 2008. IEEE International Conference on, 2008. IEEE, 271-275.
- OKUDA, R., KAJIWARA, Y. & TERASHIMA, K. A survey of technical trend of ADAS and autonomous driving. *VLSI Technology, Systems and Application (VLSI-TSA)*, Proceedings of Technical Program-2014 International Symposium on, 2014. IEEE, 1-4.
- OTTO, C. & LEON, F. P. Long-term trajectory classification and prediction of commercial vehicles for the application in advanced driver assistance systems. *American Control Conference (ACC)*, 2012, 2012. IEEE, 2904-2909.
- PEREZ, J., MILANES, V., ONIEVA, E., GODOY, J. & ALONSO, J. Longitudinal fuzzy control for autonomous overtaking. *2011 IEEE International Conference on Mechatronics*, 2011. IEEE, 188-193.
- PETRIDOU, E. & MOUSTAKI, M. 2000. Human factors in the causation of road traffic crashes. *European journal of epidemiology*, 16, 819-826.
- RAJAMANI, R. 2011. *Vehicle dynamics and control*, Springer Science & Business Media.

- RUCCO, A., AGUIAR, A. P. & HAUSER, J. Trajectory optimization for constrained UAVs: a virtual target vehicle approach. 2015 International Conference on Unmanned Aircraft Systems (ICUAS), 2015. IEEE, 236-245.
- SAYER, J., MEFFORD, M., FANCHER, P., ERVIN, R. & BOGARD, S. An experimental design for studying how driver characteristics influence headway control. Intelligent Transportation System, 1997. ITSC'97., IEEE Conference on, 1997. IEEE, 870-875.
- SCHILDBACH, G. & BORRELLI, F. Scenario model predictive control for lane change assistance on highways. Intelligent Vehicles Symposium (IV), 2015 IEEE, 2015. IEEE, 611-616.
- SHILLER, Z. & SUNDAR, S. 1998. Emergency lane-change maneuvers of autonomous vehicles. *Journal of Dynamic Systems, Measurement, and Control*, 120, 37-44.
- SUGANUMA, N. & HAYASHI, Y. Development of autonomous vehicle-Overview of autonomous driving demonstration in ITS world Congress 2013. 2014 11th International Conference on Informatics in Control, Automation and Robotics (ICINCO), 2014. IEEE, 545-549.
- SUGANUMA, N. & UOZUMI, T. Development of an autonomous vehicle—System overview of test ride vehicle in the Tokyo motor show 2011. 2012 Proceedings of SICE Annual Conference (SICE), 2012. IEEE, 215-218.
- SUH, J. 2016. *Design and Evaluation of Lane Change Decision for Automated Driving Vehicle Using Stochastic Predictive Control*. Doctoral degree, Seoul National University.
- SUH, J., CHAE, H. & YI, K. 2018. Stochastic model-predictive control for lane change decision of automated driving vehicles. *IEEE Transactions on Vehicular Technology*, 67, 4771-4782.
- SUH, J. & YI, K. A new adaptive uncertainty propagation method based Stochastic Model Predictive Control for automated driving vehicles. 2017 American Control Conference (ACC), 2017. IEEE, 5660-5665.

- SUN, L., ZHAN, W., CHAN, C.-Y. & TOMIZUKA, M. Behavior planning of autonomous cars with social perception. 2019 IEEE Intelligent Vehicles Symposium (IV), 2019. IEEE, 207-213.
- SUN, L., ZHAN, W. & TOMIZUKA, M. Probabilistic prediction of interactive driving behavior via hierarchical inverse reinforcement learning. 2018 21st International Conference on Intelligent Transportation Systems (ITSC), 2018. IEEE, 2111-2117.
- TOLEDO, T., KOUTSOPOULOS, H. & BEN-AKIVA, M. 2003. Modeling integrated lane-changing behavior. *Transportation Research Record: Journal of the Transportation Research Board*, 30-38.
- TOLEDO, T., KOUTSOPOULOS, H. N. & BEN-AKIVA, M. 2007a. Integrated driving behavior modeling. *Transportation Research Part C: Emerging Technologies*, 15, 96-112.
- TOLEDO, T. & ZOHAR, D. 2007b. Modeling duration of lane changes. *Transportation Research Record*, 1999, 71-78.
- TRUCKS, V. 2013. EUROPEAN ACCIDENT RESEARCH AND SAFETY REPORT 2MI3.
- ULBRICH, S. & MAURER, M. Probabilistic online POMDP decision making for lane changes in fully automated driving. 16th International IEEE Conference on Intelligent Transportation Systems (ITSC 2013), 2013. IEEE, 2063-2067.
- ULBRICH, S. & MAURER, M. Towards tactical lane change behavior planning for automated vehicles. 2015 IEEE 18th International Conference on Intelligent Transportation Systems, 2015. IEEE, 989-995.
- VAN WATERSCHOOT, B. & VAN DER VOORT, M. Implementing human factors within the design process of advanced driver assistance systems (ADAS). International Conference on Engineering Psychology and Cognitive Ergonomics, 2009. Springer, 461-470.
- WAN, L., RAKSINCHAROENSAK, P., MAEDA, K. & NAGAI, M. 2011. Lane change behavior modeling for autonomous vehicles based on surroundings recognition. *International Journal of Automotive Engineering*, 2, 7-12.

- WEI, J., DOLAN, J. M. & LITKOUHI, B. Autonomous vehicle social behavior for highway entrance ramp management. 2013 IEEE Intelligent Vehicles Symposium (IV), 2013. IEEE, 201-207.
- YAMAMOTO, T. 2015. Automated Driving Activities in Japan. *Road Vehicle Automation 2*. Springer.
- YAO, W., ZHAO, H., BONNIFAIT, P. & ZHA, H. Lane change trajectory prediction by using recorded human driving data. Intelligent Vehicles Symposium (IV), 2013 IEEE, 2013. IEEE, 430-436.

초 록

데이터 기반 안전 영역 및 충돌 확률을 이용한 능동형 차로 변경 판단 및 제어 알고리즘 개발

지난 수십 년 동안 주의 산만, 졸음 또는 실수와 같은 인적 오류로 인한 교통 사고는 전체의 94 %를 차지한다. 안전 운전은 도로 교통 차량 분야들의 목표이기 때문에 주요 자동차 제조업체는 운전자 지원 및 능동형 안전 시스템을 개발해왔다. 최근 대부분의 자동차 제조업체는 이미 능동형 안전 시스템을 상용화했다. 자율 주행 시스템 개발을 위한 개별 능동형 안전 시스템들을 통합하여 안전성을 높이고 사망자 줄이려는 수많은 연구가 진행되고 있다. 더욱이 최근 자동차 산업의 관심은 능동적 안전 개발에서 주변 환경을 감지하고 스스로 운전할 수 있는 자율 주행 시스템으로 확장되고있다. 환경, 인구 통계, 사회 및 경제적 측면에서 자율 주행의 영향을 평가하기 위해 많은 프로젝트가 진행되었다.

많은 문헌을 통해, 자율 주행 시스템이 교통 사용자의 안전을 높이고 교통 혼잡을 줄이며 운전자 편의를 향상시키는 것으로 입증되었다. 자율 주행 차량의 핵심 기술인 인지, 거동 계획, 제어 등을 위한 다양한 방법론이 개발되었다. 그러나 현재의 자율 주행 알고리즘은 각 기술의 개별 개발에 초점을 맞추고 있다. 결과적으로 통합 관점에서 자율 주행 시스템을 개발하는 것이 필요하다.

이 논문에서는 운전자 특성을 고려한 자율 주행 차량용 능동형 차로 변경 제어 알고리즘의 설계, 구현 및 평가에 대해 기술한다. 운전자와 주변 차량의 안전을 모두 고려하여 차로 변경이 수행되어야 한다. 따라서 자율 주행 시스템은 사람의 운전 특성을 기반으로 설계되어야 한다. 주행 데이터를 바탕으로 규칙 기반 및 학습 기반 접근 방식을 사용하여 안전 지수를 정의하였다. 또한 충돌 확률을 통해 다양한 불확실성을 고려한다. 이를 바탕으로 확률론적 위험 판단 기반 차로 변경 결정 및 제어 알고리즘이 개발되었다. 주행 모드 결정은 모든 차로 변경 상황을 대처한다. 주행 데이터 기반의 안전 지수를 고려하여 차로 변경을 위한 목표 거동이 계획된다. 확률론적 모델 예측 제어 기법을 통해 차량의 최종 제어 입력이 결정된다. 제안된 알고리즘은 실제 차량에 구현하기 위해 다양한 불확실성, 계산 부하 및 센서 한계를 고려하였다.

제안된 자율 주행 알고리즘의 효과는 시뮬레이션 및 차량 테스트를 통해 평가되었다. 다른 알고리즘에 비해 성능 향상을 보여주기 위해 다양한 시뮬레이션을 진행하였다. 제안된 능동형 차로 변경 알고리즘은 다양한 주행 도로에서 안전하고 편안한 차로 변경을 차량에 성공적으로 구현했다.

주요어: 자율 주행 자동차, 운전자 주행 데이터, 확률론적 예측, 위험 판단, 의도 추론, 회귀 뉴럴 네트워크, 의사 결정, 차로 변경 판단, 거동 계획, 가상 차량, 모델 예측 제어, 능동형 차로 변경.

학 번: 2015-20754